-Ocean Salinity With SMOS-

N.REUL

French Research Institute for the Exploration of the Sea

Oceanography from Space Laboratory

Outline

- How does it work in practice with SMOS?
- An overview of the first oceanographic applications of SMOS data

How in Practice ?

Brightness Temperature

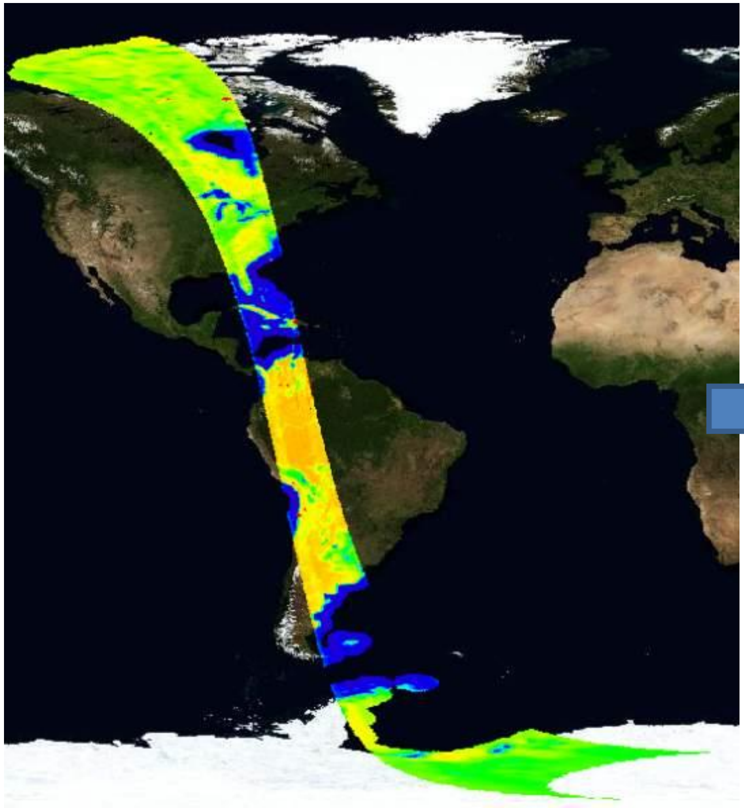

Sea Surface Salinity (SSS) Maps

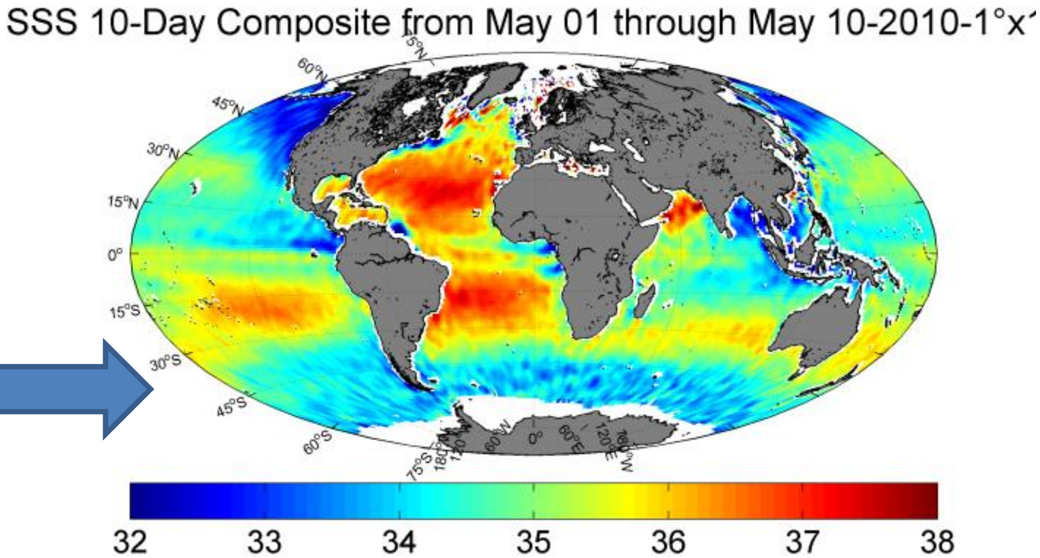

A change of state in the Hydrogen atom energy generates
micro-wave electromagnetic radiations at a frequency of 1420 MHz
(L band) ≡length 21 cm known as the « Hydrogen line »

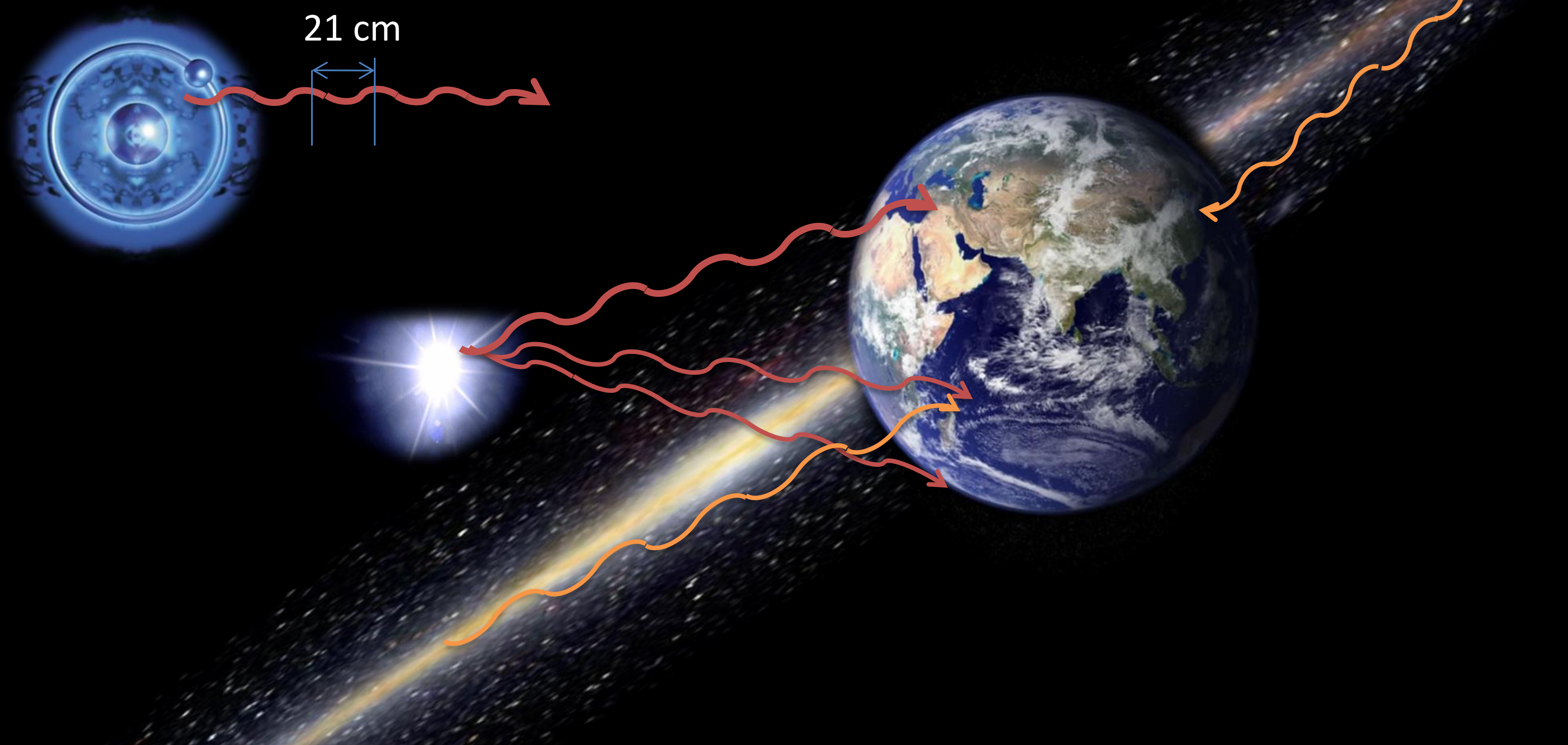

Hydrogen being one of the first constituent of the sun
And of most of the stars, Earth is constantly illuminated
by L-band radiations

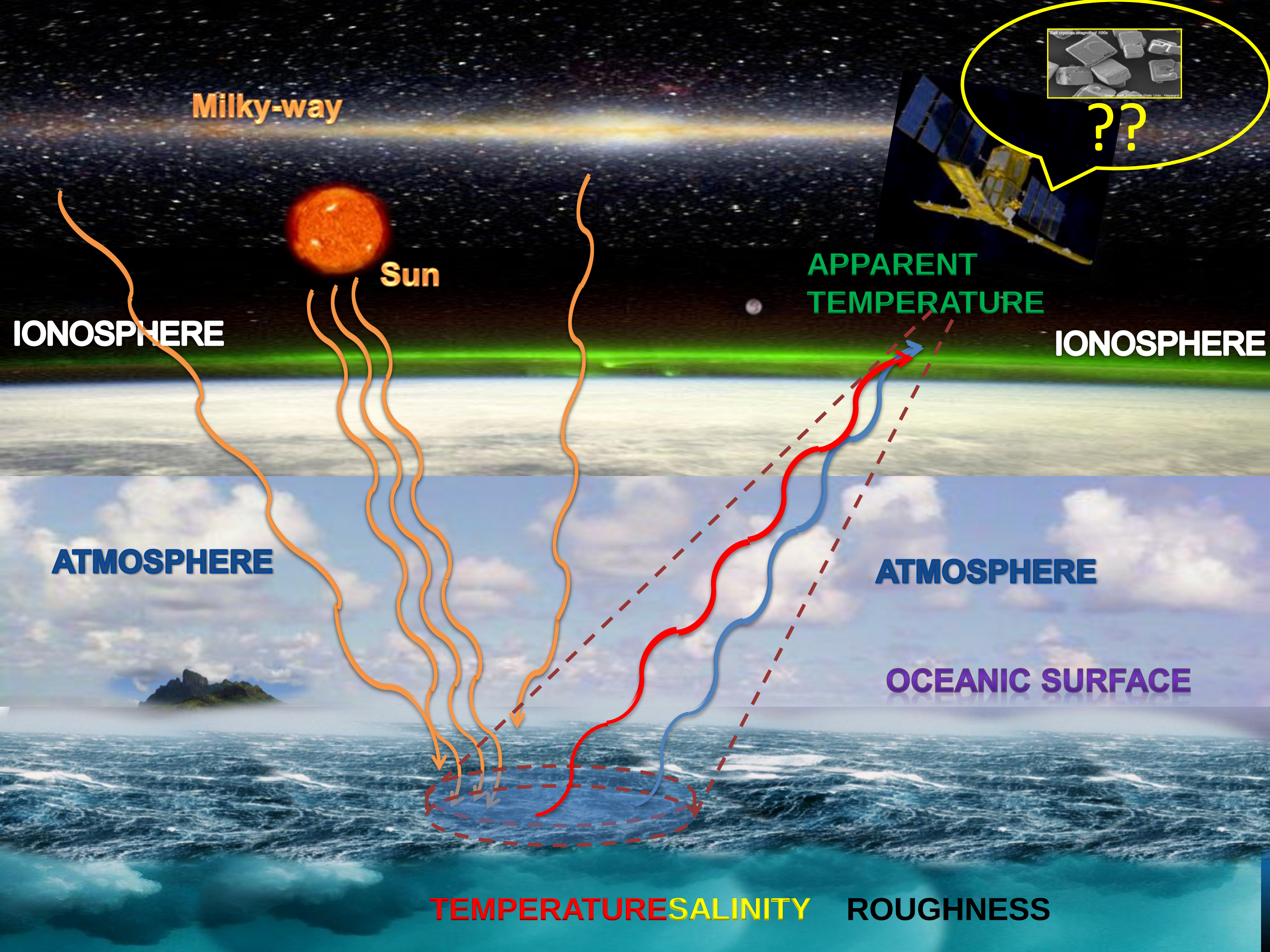

Milky-way
??
Sun
APPARENT
TEMPERATURE
IONOSPHERE
IONOSPHERE
ATMOSPHERE
ATMOSPHERE
OCEANIC SURFACE
TEMPERATURE SALINITY ROUGHNESS

Penetration Depth of Electromagnetic Radiation at 1.4 GHz in sea water

$$\delta_p \simeq \sqrt{\epsilon'}/(k_o\epsilon'')$$

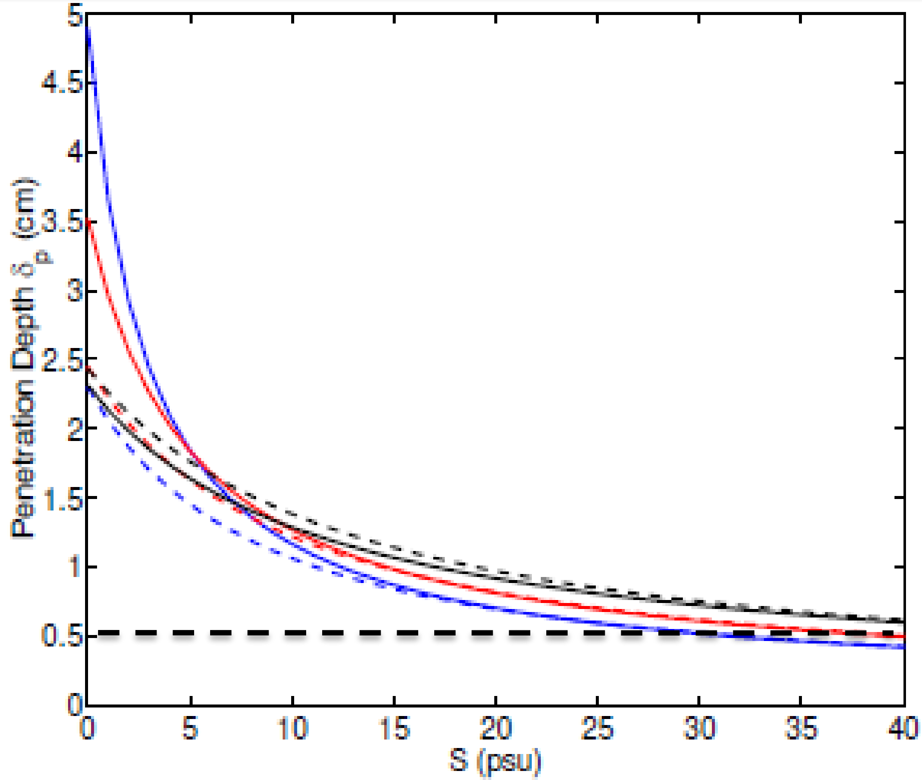

SMOS is sensing the first half-centimeter below the sea surface

Retrieving SSS from Space: a challenge !

SMOS data

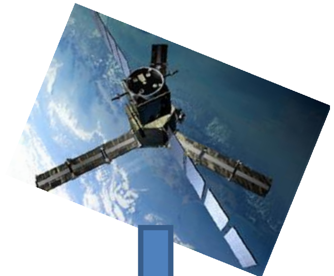

Ionosphere

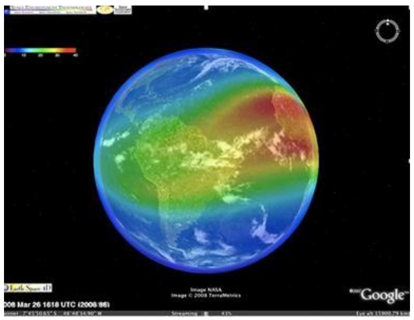

Sky Brightness

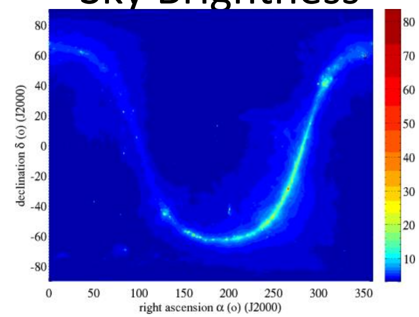

Electromagnetic Modelling

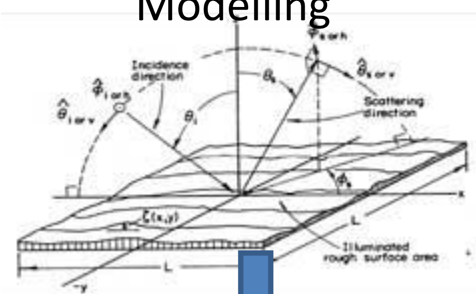

Atmosphere

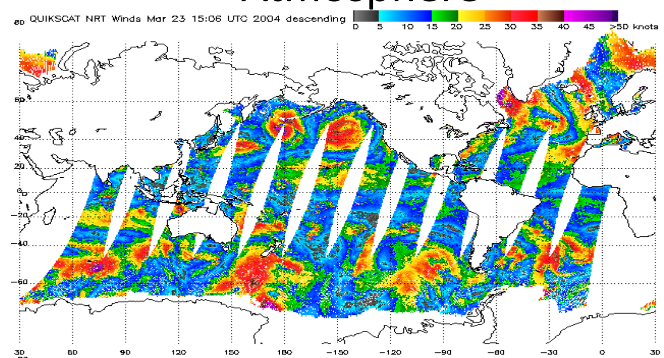

Sea Surface Temperature

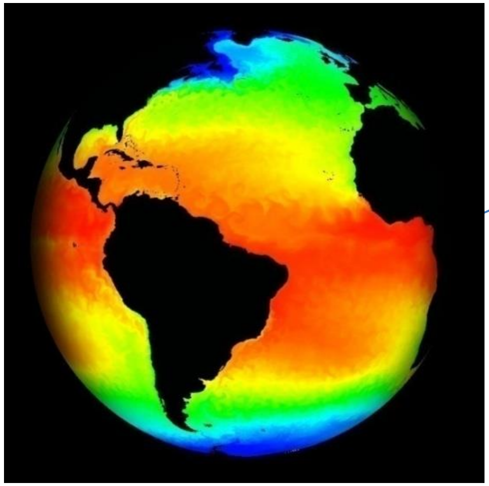

Salts

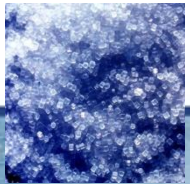

Sea States & winds

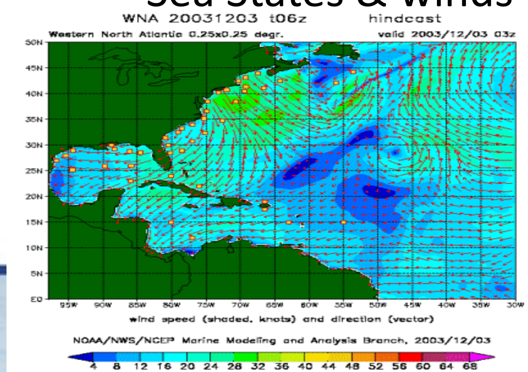

SSS from Space: a low sensitivity measurement

Flat sea (*Klein and Swift model)*

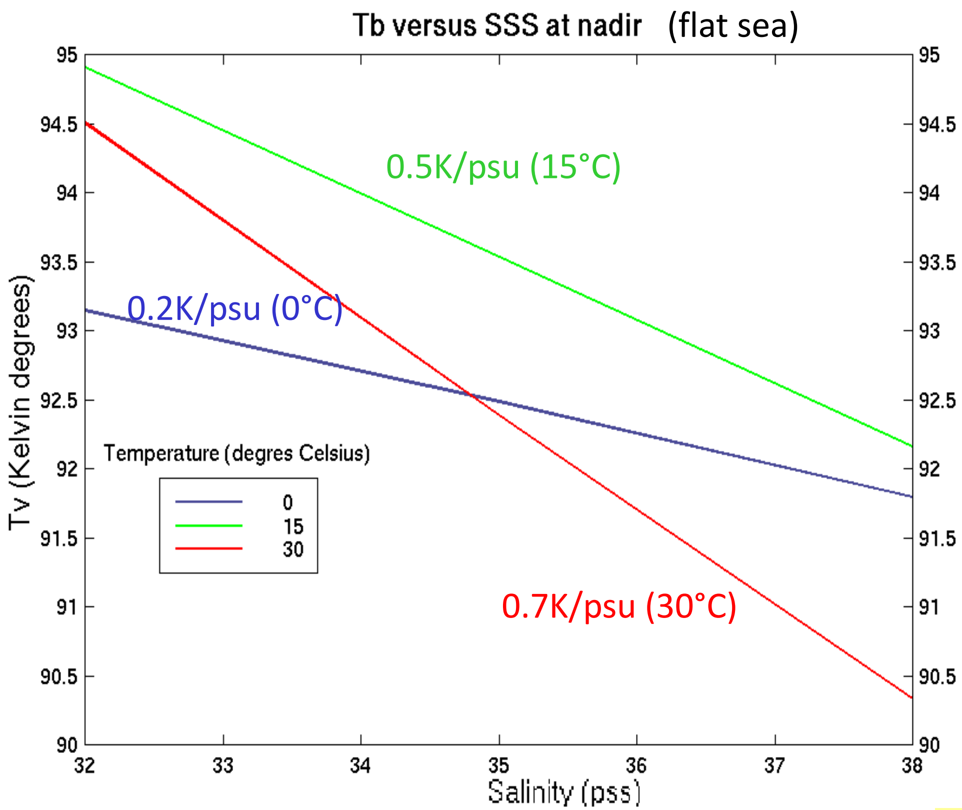

Sensitivity of Tb to SSS is:

-small: always less than 1K/psu (SMOS radiometric precision of 1 Tb: several K)

-Higher in warm water

NB: L-band radiometer measurements are representative of top 1cm surface ocean

Dielectric Constant Model

- At electromagnetic frequency f < 20 GHz, sea water dielectric constant ε is a function of Salinity S, temperature T and electromagnetic Frequency f. **ε = ε(S,T,f).**

$$\epsilon = \epsilon' - j\epsilon''$$

Fig. 2. Seawater dielectric measurement setup.

$$\epsilon_{sw}(T,S,f) = \epsilon_{sw\infty}(T,S) + \frac{\epsilon_{swo}(T,S) - \epsilon_{sw\infty}(T,S)}{1 - j2\pi f \tau_{sw}(T,S)} + j\frac{\sigma_i(T,S)}{2\pi\epsilon_o f}$$

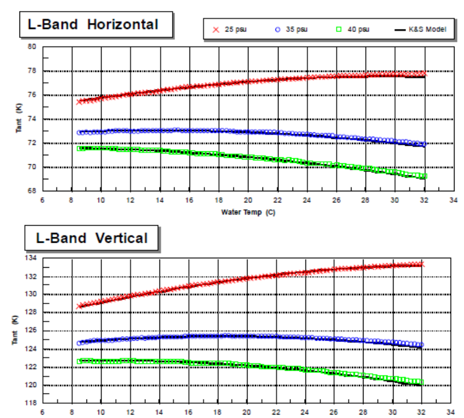

Fig. 2. L-band saltwater pond brightness temperature measurements at 25, 35 and 40 psu over a temperature range of 9° C to 32° C. The colored curves represent average data from 5 different days. The width of the data curves represents the peak-to-peak variation (0.25 K) of the different days of the data. The solid black curves are from the Klein and Swift model [2], showing excellent agreement between the L-band PALS's data and the model. The RMS difference between the measured data and the Klein and Swift model is ~0.1 K.

For SMOS:
=>Klein and Swift, 1977 analysis

Radiative transfer forward model Developments for SMOS

Contributions from Roughness & Breaking waves

N. Reul & B. Chapron (2003). **A model of sea-foam thickness distribution for passive microwave remote sensing applications**. *Journal Of Geophysical Research Oceans*, 108(C10),

S. Zine, J. Boutin 1, J.Font, N. Reul, P.Waldteufel, C.Gabarró, J. Tenerelli, F. Petitcolin, J.-L. Vergely, M. Talone, **Overview of the SMOS sea surface salinity prototype processor**, *IEEE Transactions on Geoscience and Remote Sensing,* vol 46, 3, doi:10.1109/TGRS.2007.915543, 2008.

A. Camps, M. Vall-llossera, R. Villarino, N. Reul, B. Chapron, I. Corbella, N. Duff, F. Torres, J. Miranda, R. Sabia, A. Monerris, R. Rodríguez, "***The Emissivity Of Foam-Covered Water Surface at L-Band: Theoretical Modeling And Experimental Results From The Frog 2003 Field Experiment***", *IEEE Transactions on Geoscience and Remote Sensing*, vol 43, No 5, pp 925-937, 2005.

Interprétation et modélisation de mesures à distance de la surface marine dans le domaine micro−onde» Thèse Sébastien Guimbard,

Solar Reflections

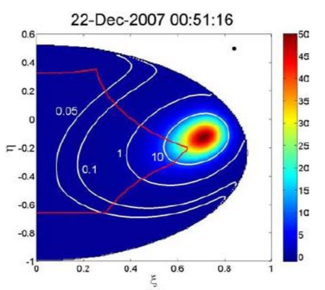

N. Reul, J. Tenerelli, B. Chapron and P. Waldteufel, "**Modelling Sun glitter at L-band for the Sea Surface Salinity remote sensing with SMOS**", *IEEE Transactions on Geoscience and Remote Sensing*, vol 45, No 7, pp 2073-2087, 2007.

Galactic Reflections

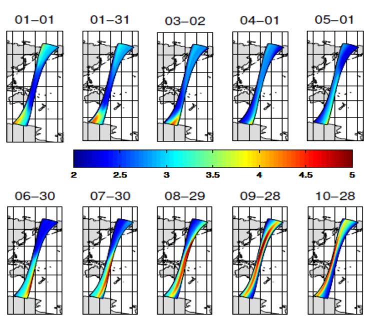

(a) Descending node.

J. Tenerelli, N. Reul, A. A. Mouche and B. Chapron, "**Earth Viewing L-Band Radiometer sensing of Sea Surface Scattered Celestial Sky Radiation. Part I: General characteristics**", *IEEE Transactions on Geoscience and Remote Sensing*, vol 46, 3, DOI:10.1109/TGRS.2007.914803, 2008.

N. Reul, J. Tenerelli, N. Floury and B. Chapron, "**Earth Viewing L-Band Radiometer sensing of Sea Surface Scattered Celestial Sky Radiation. Part II: Application to SMOS**", *IEEE Transactions on Geoscience and Remote Sensing*, vol 46, 3, doi:10.1109/TGRS.2007.914804, 2008.

Dedicated Campaigns

The WISE 2000 and 2001 Field Experiments

(c)

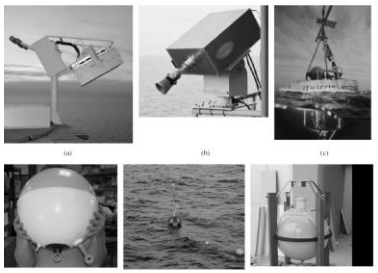

FROG, 2004

CoSMOS, 2006

CAROLS, 2009-2012

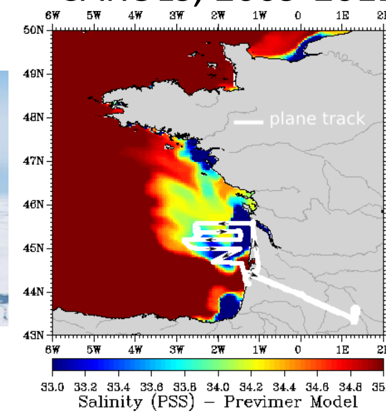

Measure Wind, Wave and foam Impacts

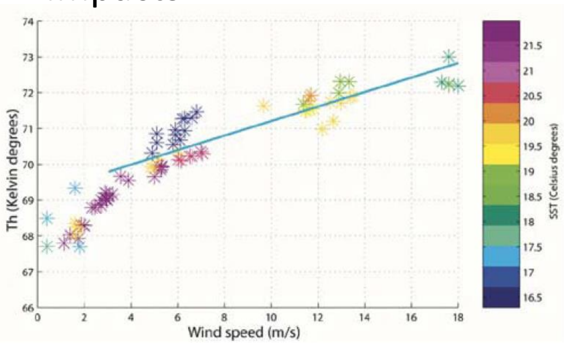

Validation of Electromagnetic models

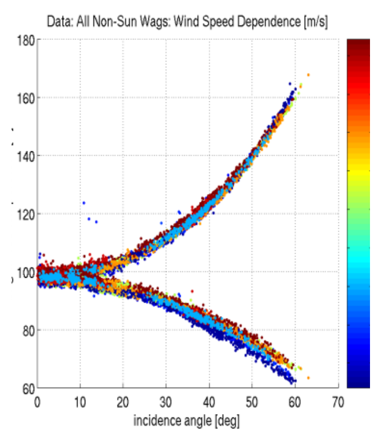

Data

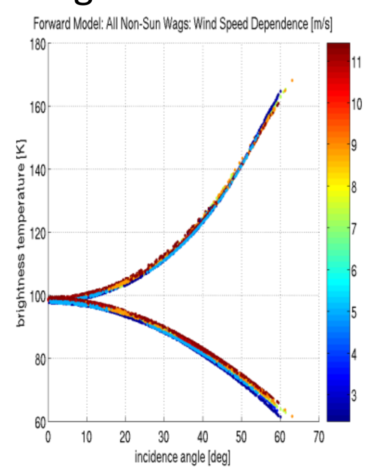

Models

Test SSS retrieval algorithms

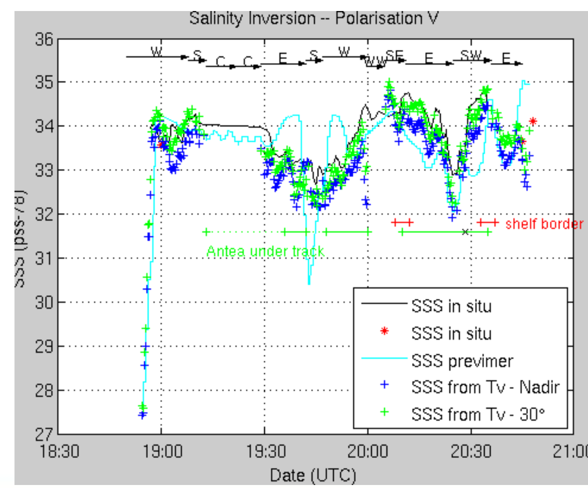

SMOS Sea Surface Salinity retrieval

- Direct model

$$Tb(pol, \theta, \ldots) = Tb_{atm}\uparrow + R_{sea}\,(Tb_{atm}\downarrow + Tb_{sky})\,\exp(-\tau_{atm}) + \mathbf{Tb_{sea}\,(SSS, SST, WS)}\,\exp(-\tau_{atm})$$

Dielectric constant of sea water (Klein and Swift, 1977)
Roughness models empirically deduced from SMOS data (Guimbard et al. , Yin et al. 2012)
Atmosphere: tropospheric model from Liebe (Liebe, 1993) + Faraday rotation
Scattering of sky radiation (Reul et al. , 2007 then empirical fits to SMOS (Tenerelli et al.)

- Auxiliary parameters (wind speed, atmospheric parameters, SST...) taken from ECMWF forecasts
- SSS-only retrieval (IFREMER-CATDS-CEC)
- Retrieval of SSS, wind speed by minimizing difference between measured & simulated Tbs (about 200 Tb along a dwell line) (ESA L2 OS processor)
- RFI sorting & bias adjustments different in the two processings

SMOS L2 OS retrieval method

SMOS SSS is retrieved through a least square minimisation of the difference between SMOS and modeled Tb along a dwell line:

Retrieval of SSS (σ=100pss), SST (σ=1°C), WS(σ=2m/s on wind components (model 1), σ=2m/s on wind modulus (model 2 & 3)), TEC (σ=10TecU) through the minimisation of:

$$\chi^2 = \sum_{i=0}^{Nm-1} \frac{\left[T_{bi}^{meas} - T_{bi}^{mod}(\theta, P)\right]^2}{\sigma_{T_{bi}}^{2}} + \sum_{j=0}^{Np-1} \frac{\left[P_j - P_{j,\,prior}\right]^2}{\sigma_{P_j}^{2}}$$

(iterative Levenberg & Marquard algorithm)

Tb^{meas} corrected for systematic biases in the FOV (Ocean Target Transformation)

ECMWF: WS & SST priors; atmospheric parameters

WOA2009 : SSS prior (σ=100psu =>does not influence SSS retrieval)

Advantage of iterative retrieval; in addition to SSS retrieval:

- retrieval (=adjustment) of WS, TEC and SST and
- Error on SSS (given errors on Tb, dTb/dparam, number of Tb)
- Xi2 = success of the retieval (consistency between measured and simulated Tbs)

Disadvantage: complexity

SMOS Level 2 SSS products

½ orbit

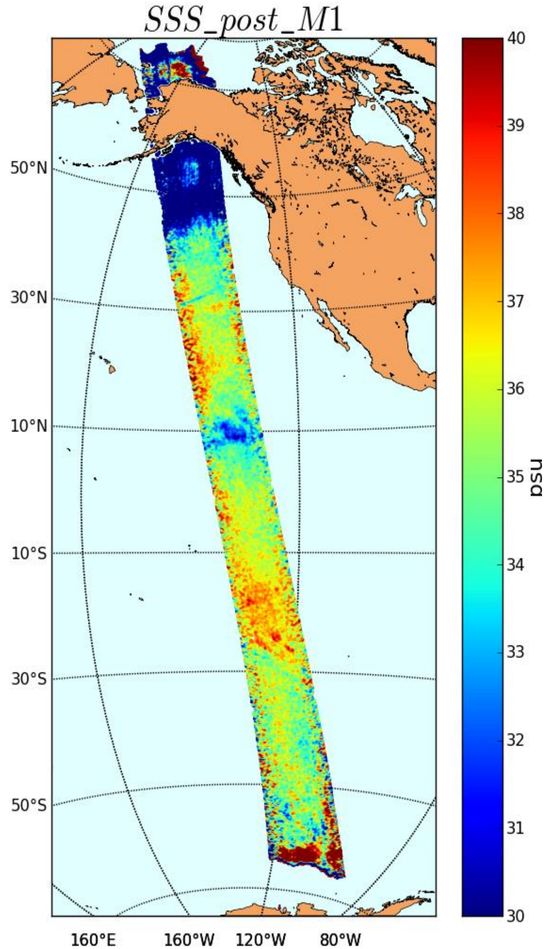

1 day

Passes ascendantes

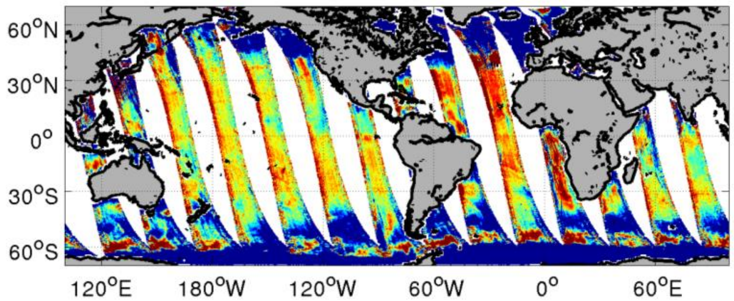

Passes descendantes

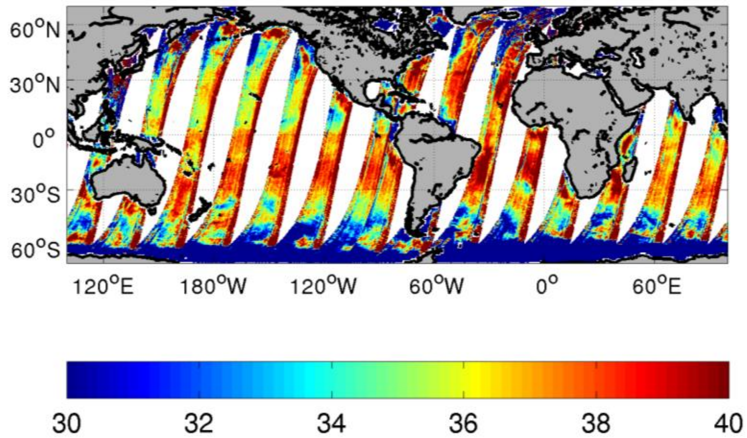

SMOS simple averaging L3 products

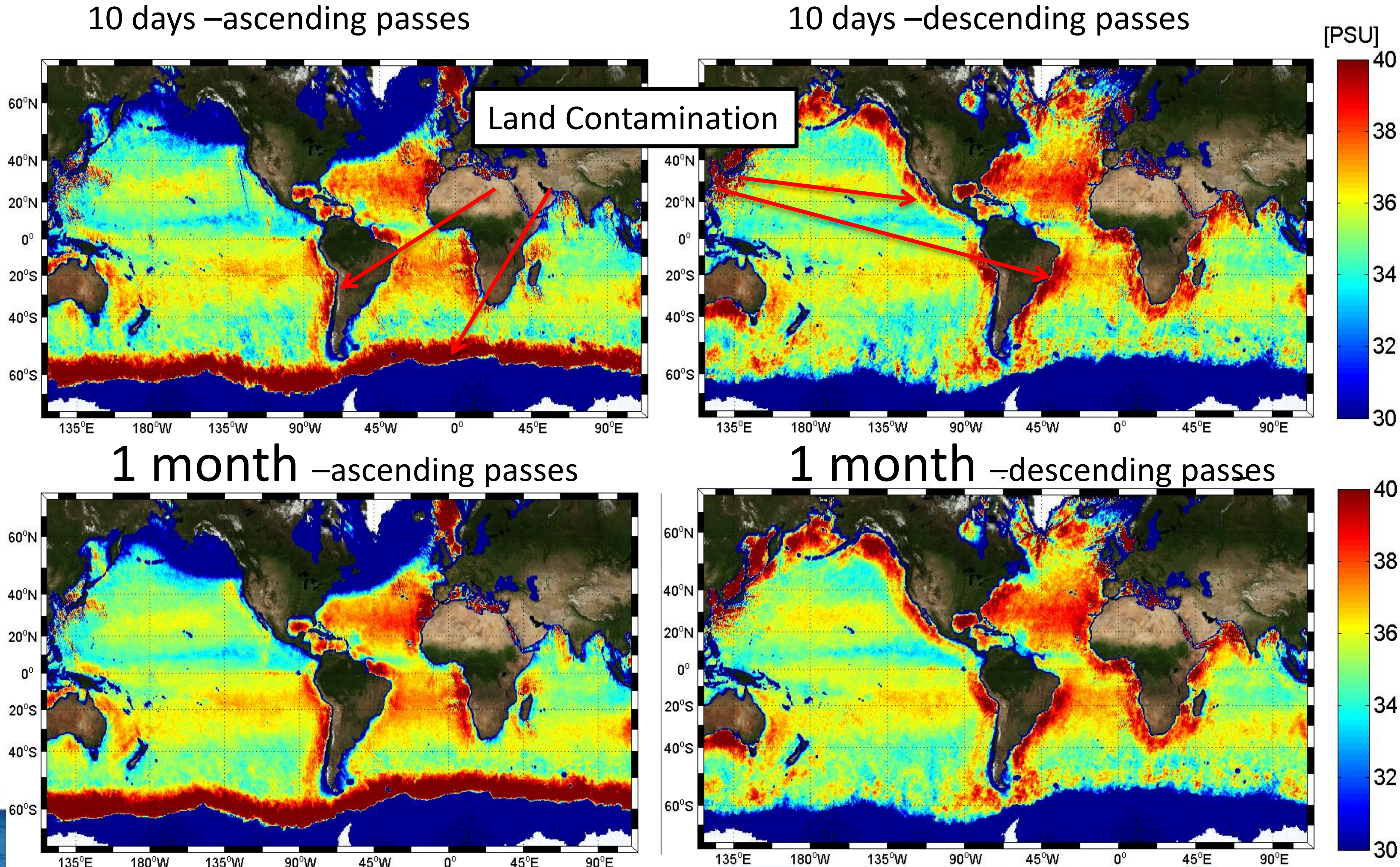

RADIO FREQUENCY INTERFERENCE

Many people have been working on this problem and at this time there is not a satisfactory correction methodology. Most of the effort is directed towards filtering out contaminated brightness temperature.

However, much (but not all) of the RFI impact over the ocean is related to sources over land, and the impact in the usable portion of the field of view can be difficult to detect by simple thresholds on brightness temperatures.

RFI for SMOS is most of the time a non-local issue thanks to the interferometric principle

RADIO FREQUENCY INTERFERENCES

RFI continues to plague both salinity and soil moisture retrievals, and no solution proposed thus far can eliminate its impact in all cases. Here is one example showing intermittent contamination from radars in Alaska. The RFI induces large spatial ripples in the images far from the sources, and the impact extends into the alias-free field of view.

J. Tenerelli
CLS

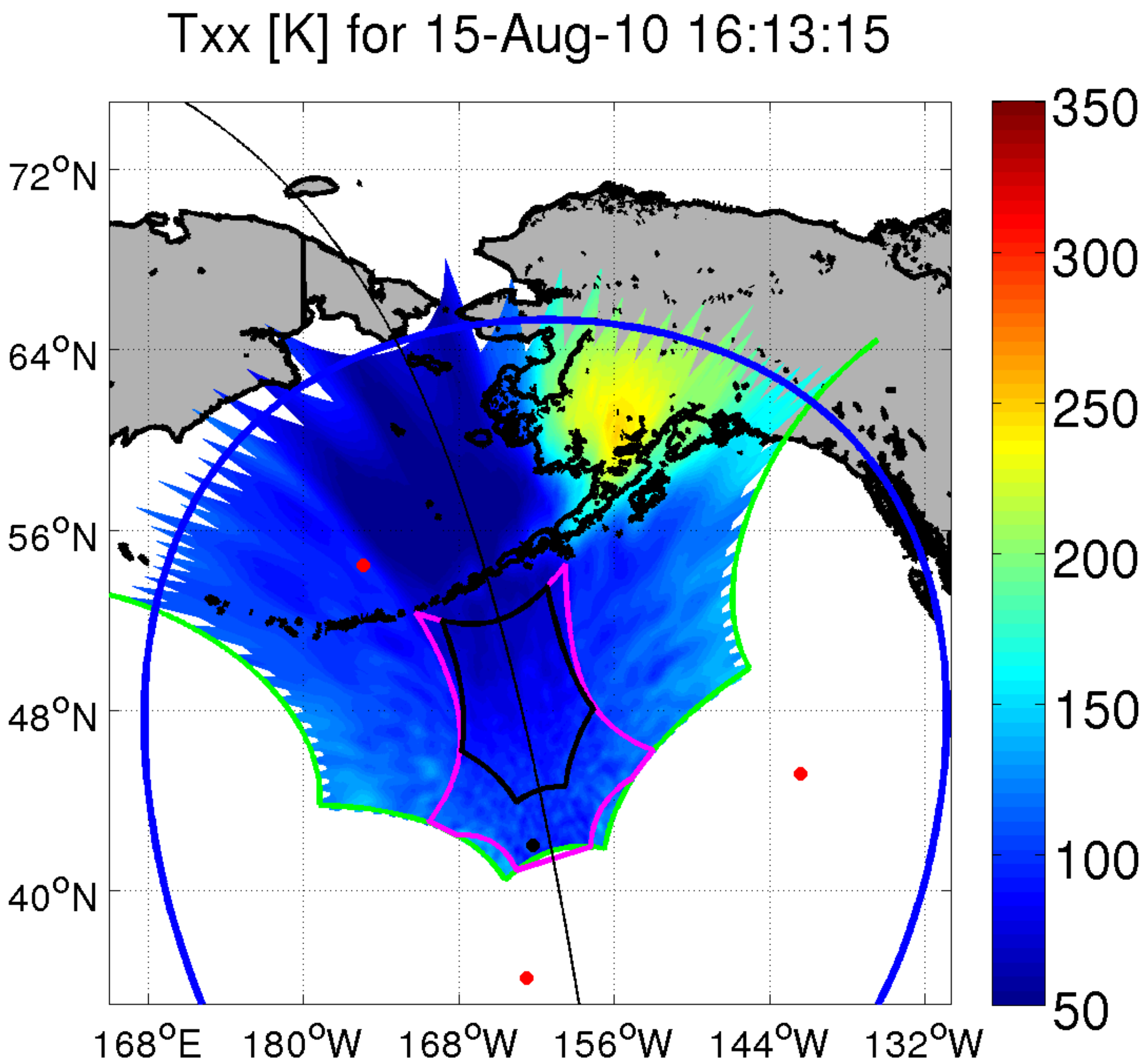

RADIO FREQUENCY INTERFERENCE

RFI continues to plague both salinity and soil moisture retrievals, and no solution proposed thus far can eliminate its impact in all cases. Here is one example showing intermittent contamination from radars in Alaska. The RFI induces large spatial ripples in the images far from the sources, and the impact extends into the alias-free field of view.

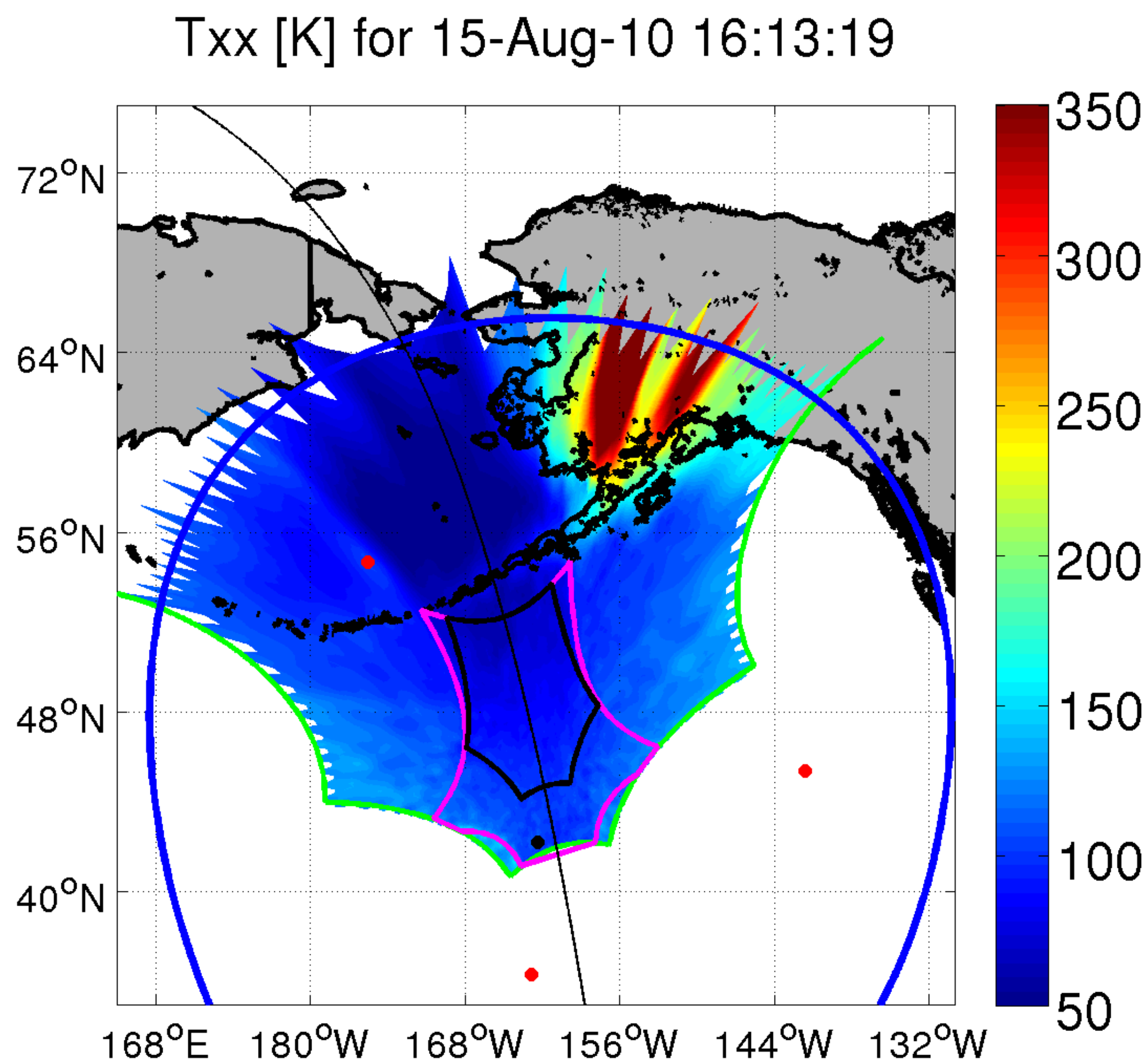

RADIO FREQUENCY INTERFERENCE

RFI continues to plague both salinity and soil moisture retrievals, and no solution proposed thus far can eliminate its impact in all cases. Here is one example showing intermittent contamination from radars in Alaska. The RFI induces large spatial ripples in the images far from the sources, and the impact extends into the alias-free field of view.

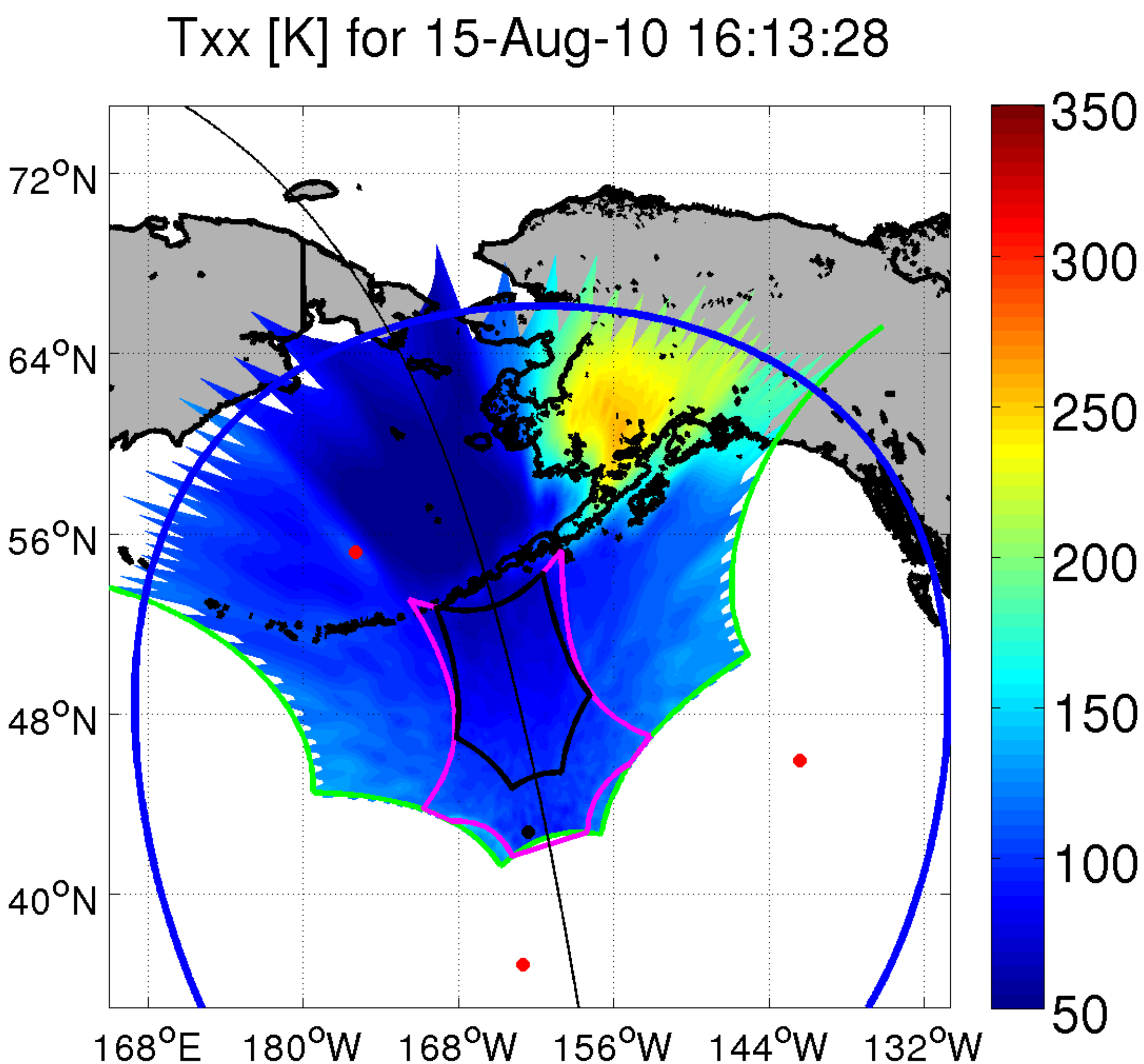

RADIO FREQUENCY INTERFERENCE

RFI continues to plague both salinity and soil moisture retrievals, and no solution proposed thus far can eliminate its impact in all cases. Here is one example showing intermittent contamination from radars in Alaska. The RFI induces large spatial ripples in the images far from the sources, and the impact extends into the alias-free field of view.

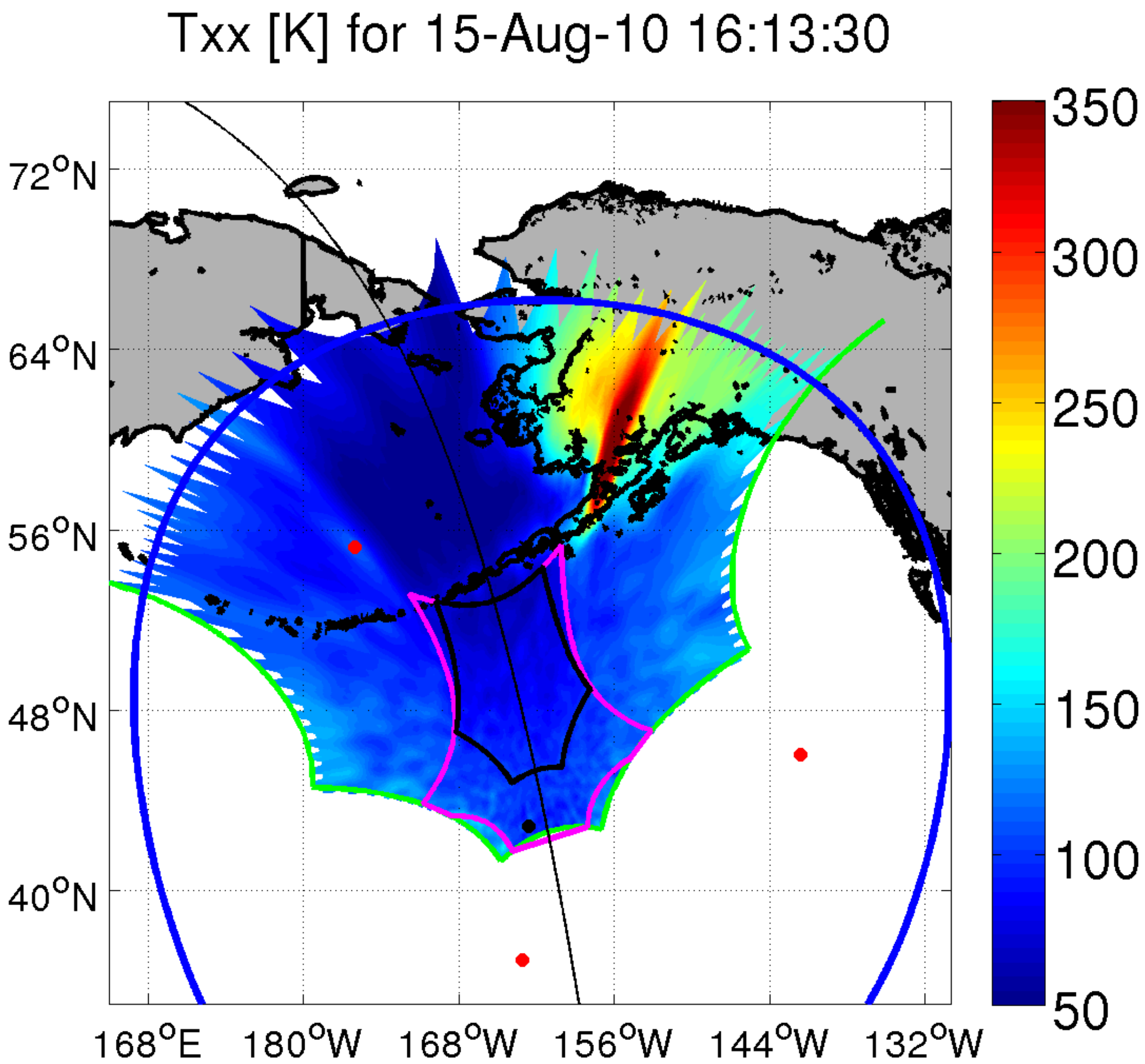

RADIO FREQUENCY INTERFERENCE

RFI continues to plague both salinity and soil moisture retrievals, and no solution proposed thus far can eliminate its impact in all cases. Here is one example showing intermittent contamination from radars in Alaska. The RFI induces large spatial ripples in the images far from the sources, and the impact extends into the alias-free field of view.

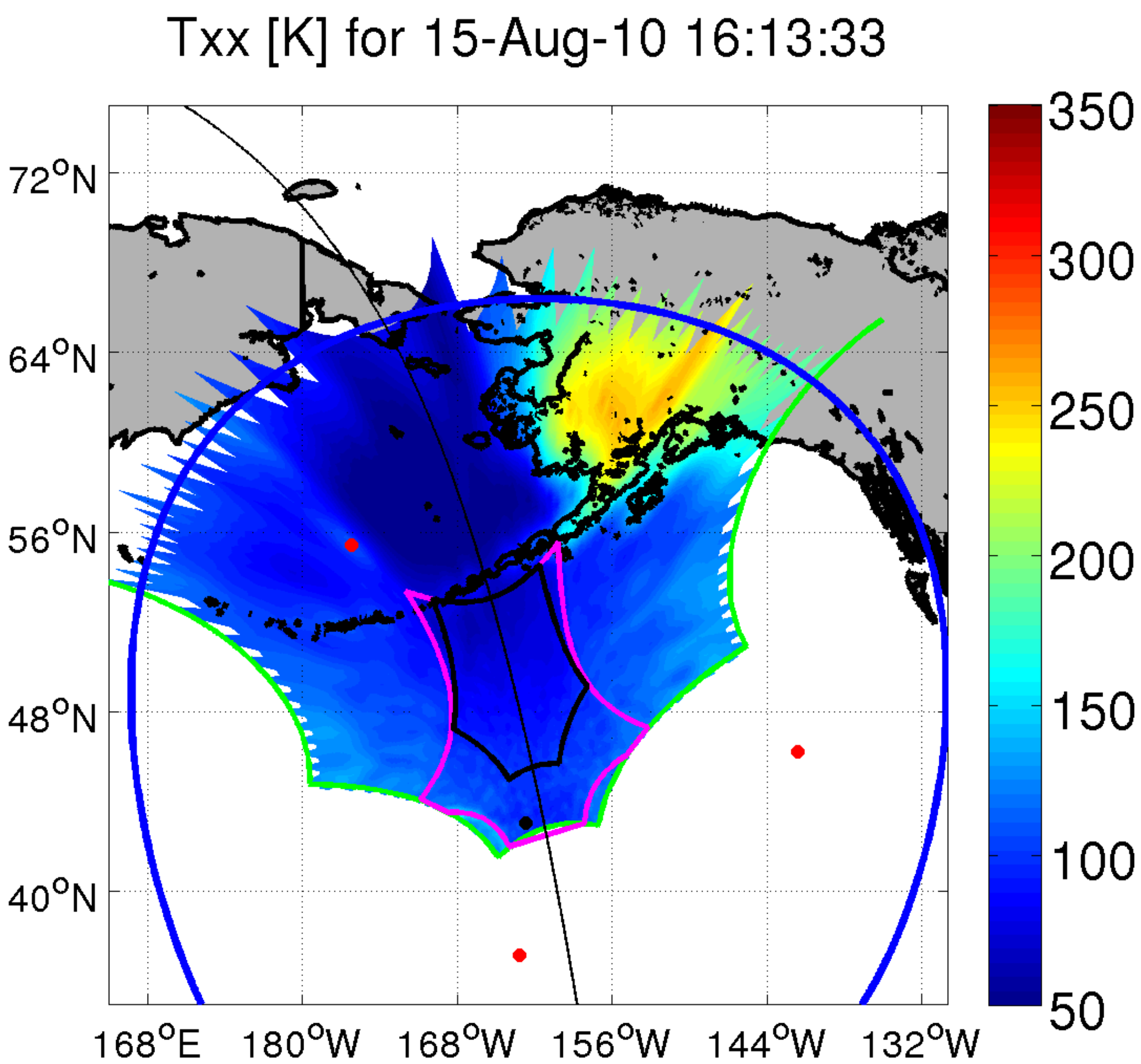

RADIO FREQUENCY INTERFERENCE

RFI continues to plague both salinity and soil moisture retrievals, and no solution proposed thus far can eliminate its impact in all cases. Here is one example showing intermittent contamination from radars in Alaska. The RFI induces large spatial ripples in the images far from the sources, and the impact extends into the alias-free field of view.

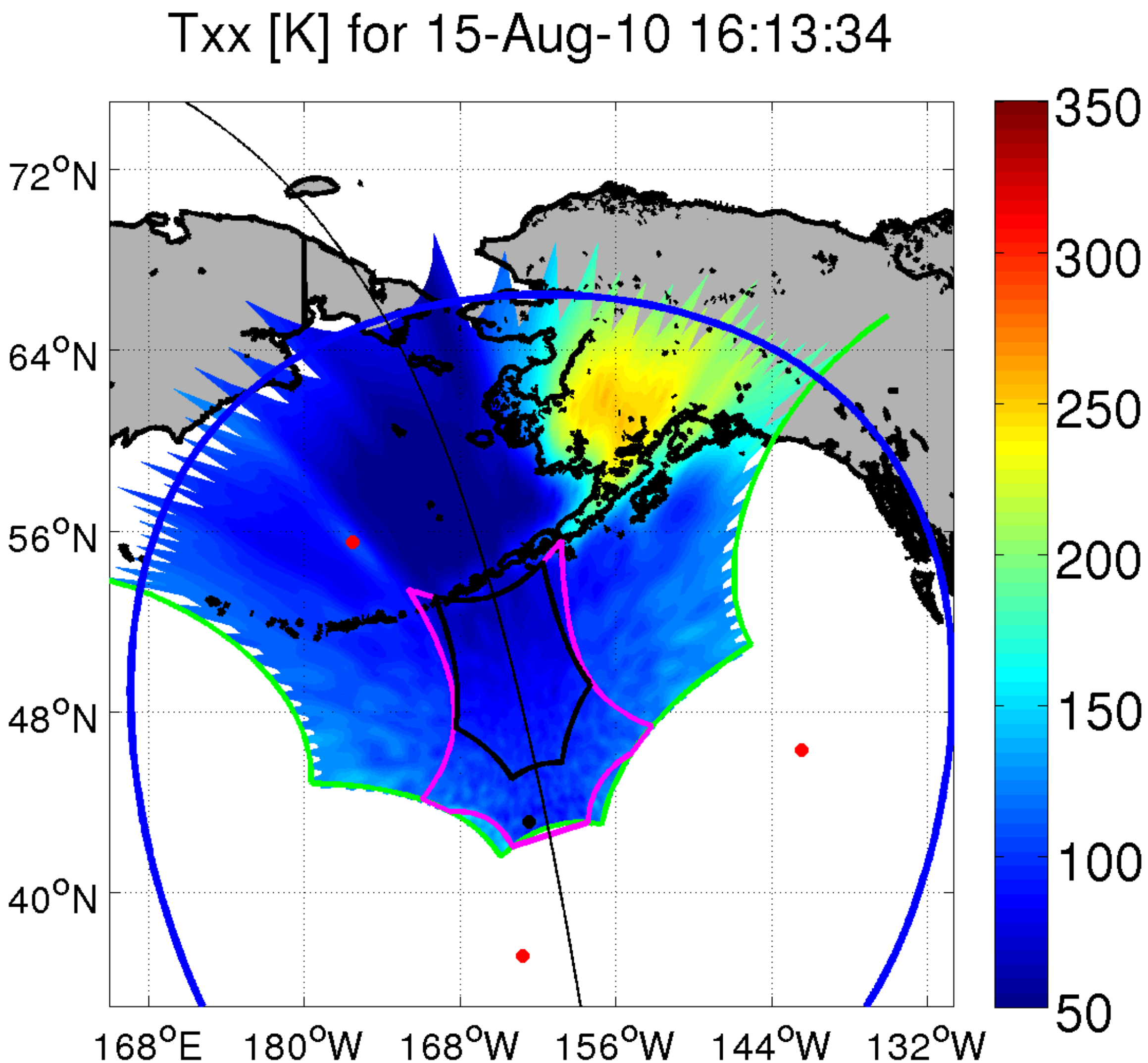

RADIO FREQUENCY INTERFERENCE

RFI continues to plague both salinity and soil moisture retrievals, and no solution proposed thus far can eliminate its impact in all cases. Here is one example showing intermittent contamination from radars in Alaska. The RFI induces large spatial ripples in the images far from the sources, and the impact extends into the alias-free field of view.

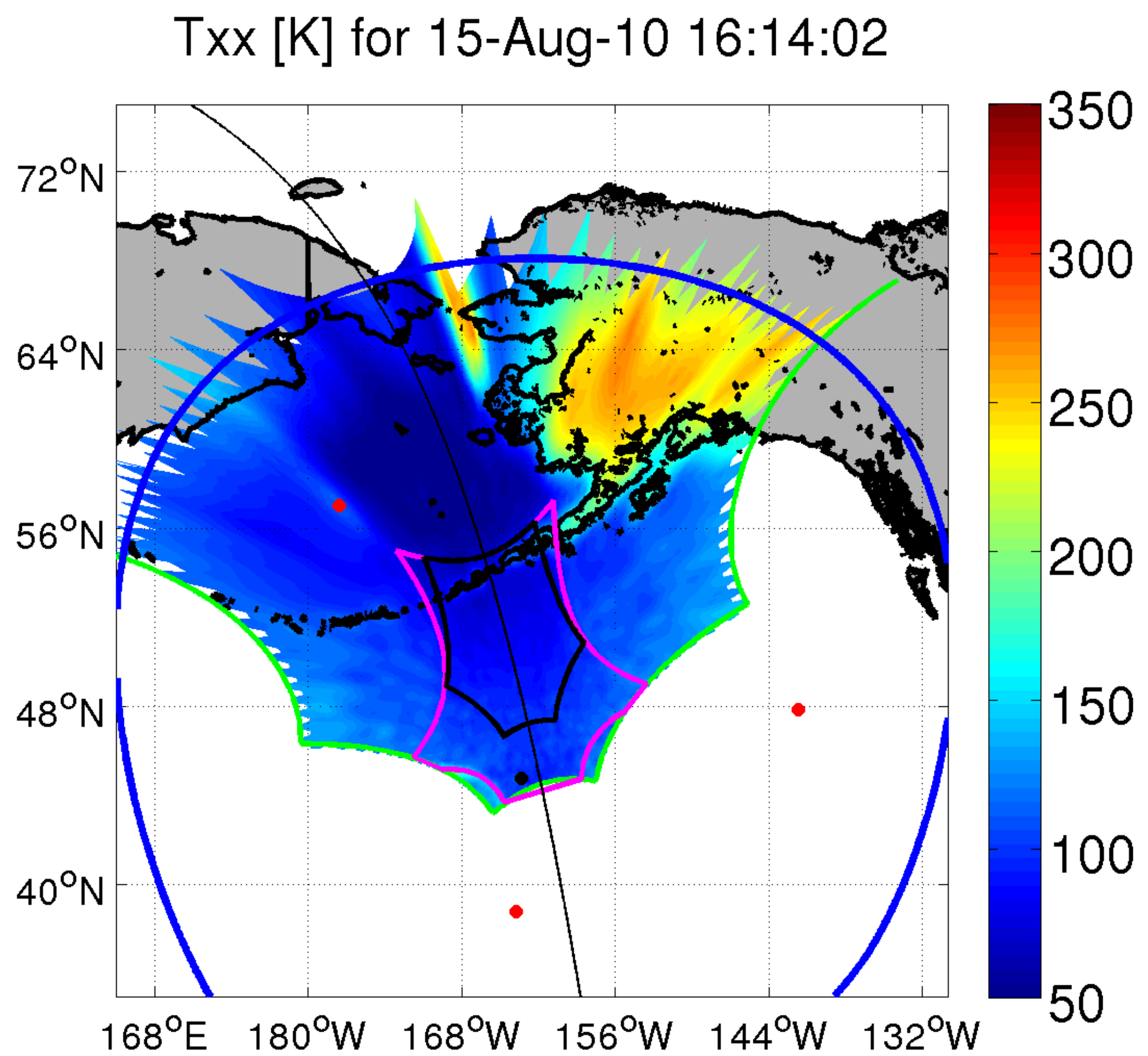

RADIO FREQUENCY INTERFERENCE

RFI continues to plague both salinity and soil moisture retrievals, and no solution proposed thus far can eliminate its impact in all cases. Here is one example showing intermittent contamination from radars in Alaska. The RFI induces large spatial ripples in the images far from the sources, and the impact extends into the alias-free field of view.

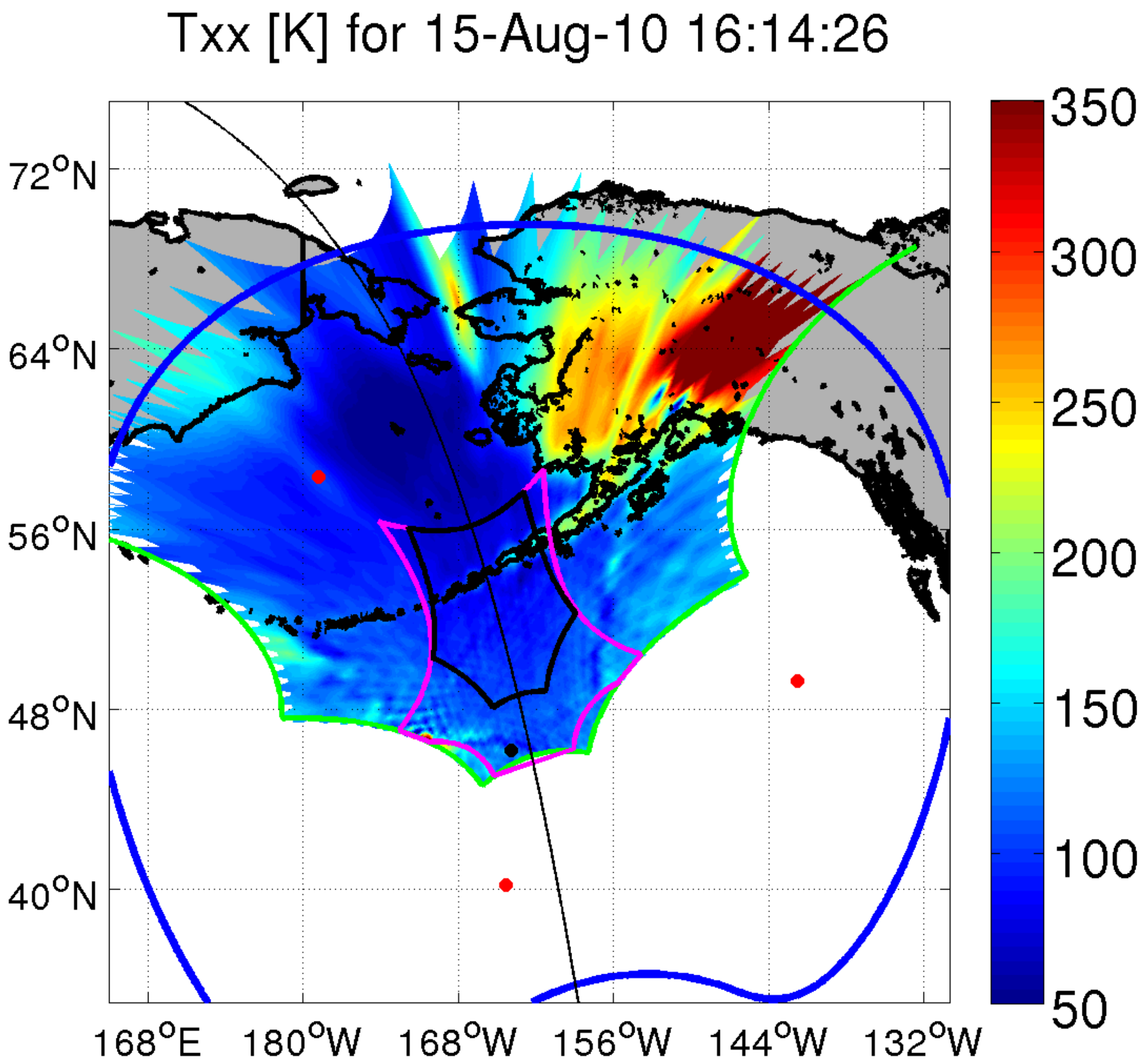

RADIO FREQUENCY INTERFERENCE

RFI continues to plague both salinity and soil moisture retrievals, and no solution proposed thus far can eliminate its impact in all cases. Here is one example showing intermittent contamination from radars in Alaska. The RFI induces large spatial ripples in the images far from the sources, and the impact extends into the alias-free field of view.

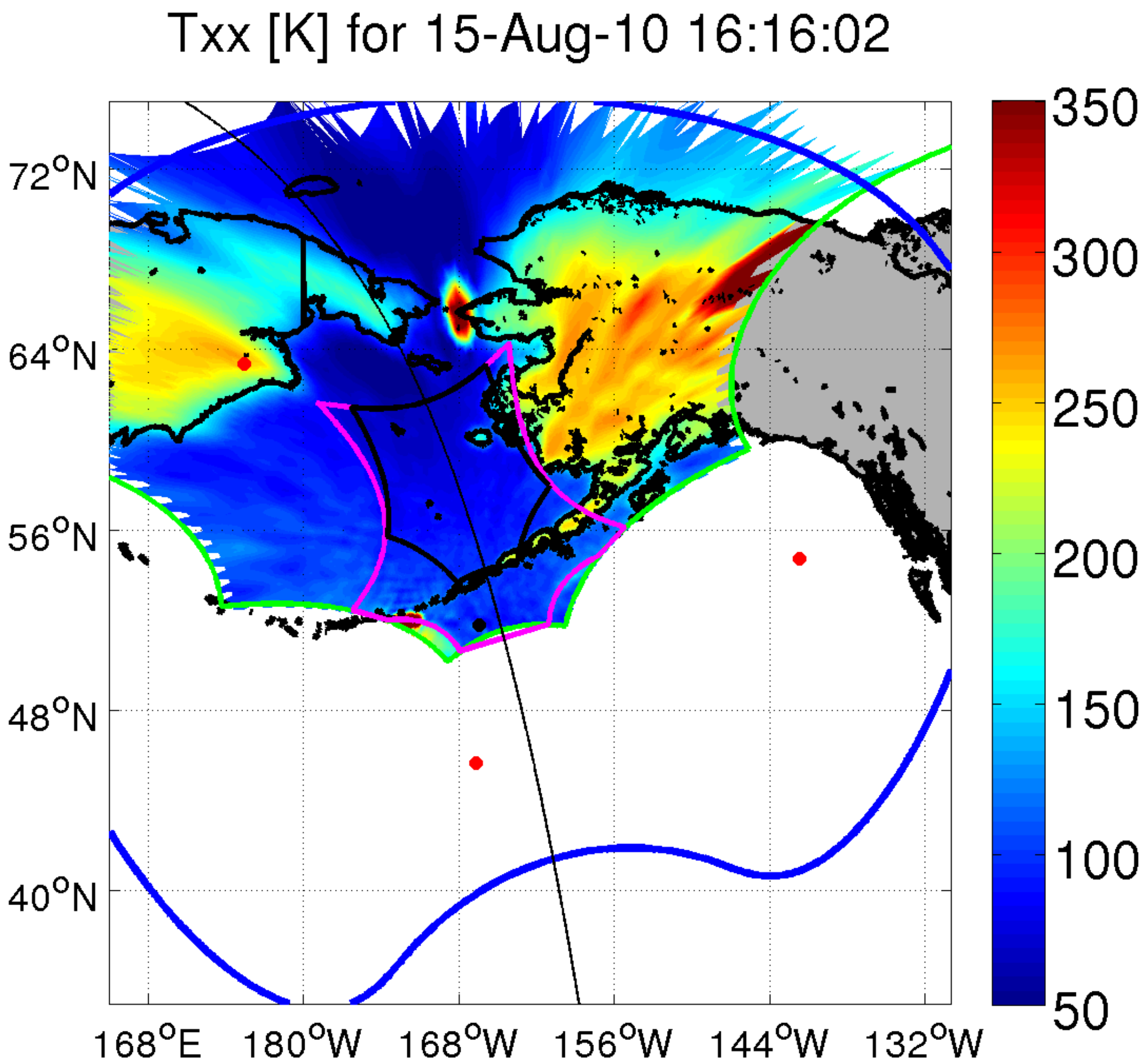

RADIO FREQUENCY INTERFERENCE

RFI continues to plague both salinity and soil moisture retrievals, and no solution proposed thus far can eliminate its impact in all cases. Here is one example showing intermittent contamination from radars in Alaska. The RFI induces large spatial ripples in the images far from the sources, and the impact extends into the alias-free field of view.

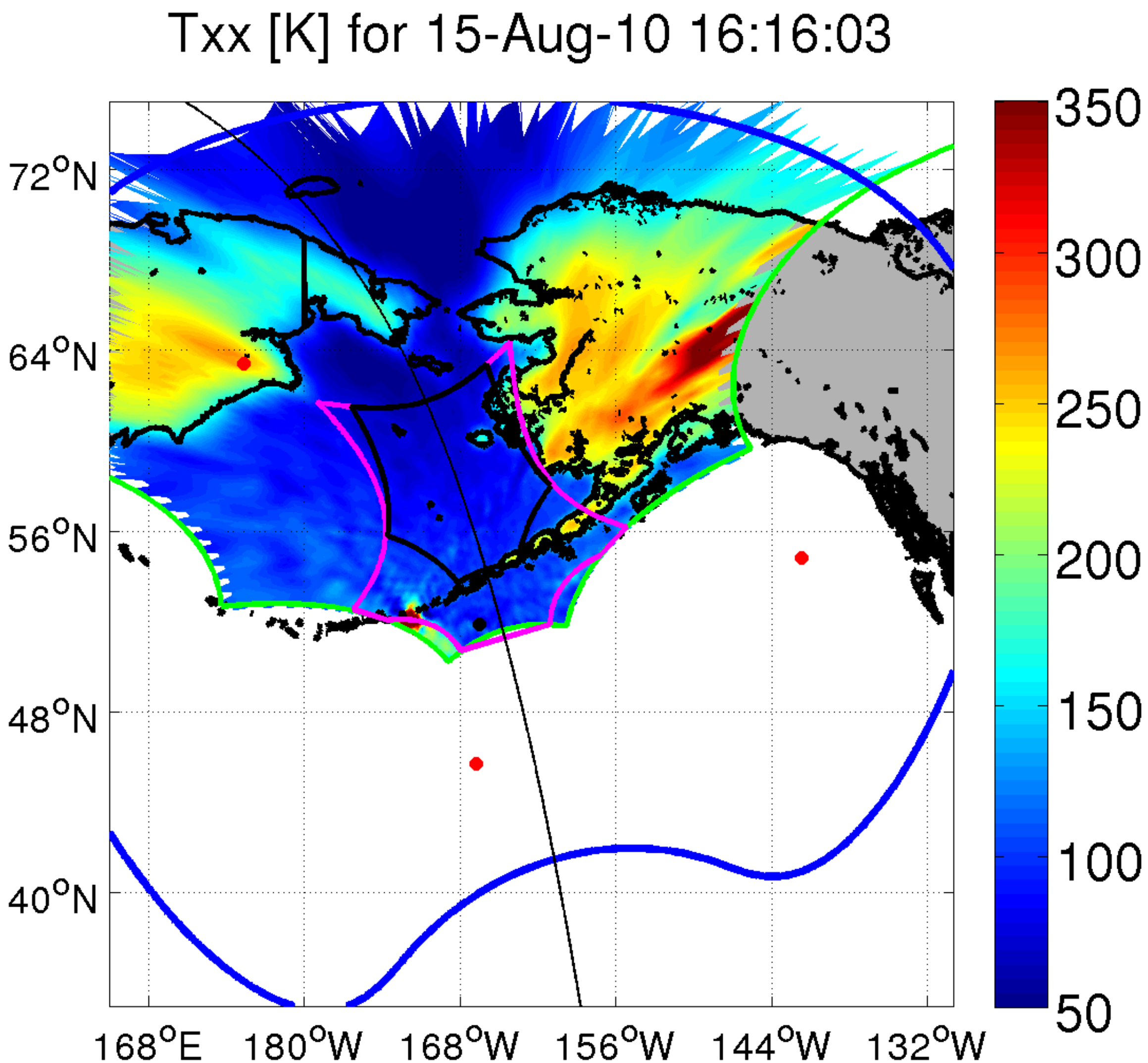

RADIO FREQUENCY INTERFERENCE

RFI continues to plague both salinity and soil moisture retrievals, and no solution proposed thus far can eliminate its impact in all cases. Here is one example showing intermittent contamination from radars in Alaska. The RFI induces large spatial ripples in the images far from the sources, and the impact extends into the alias-free field of view.

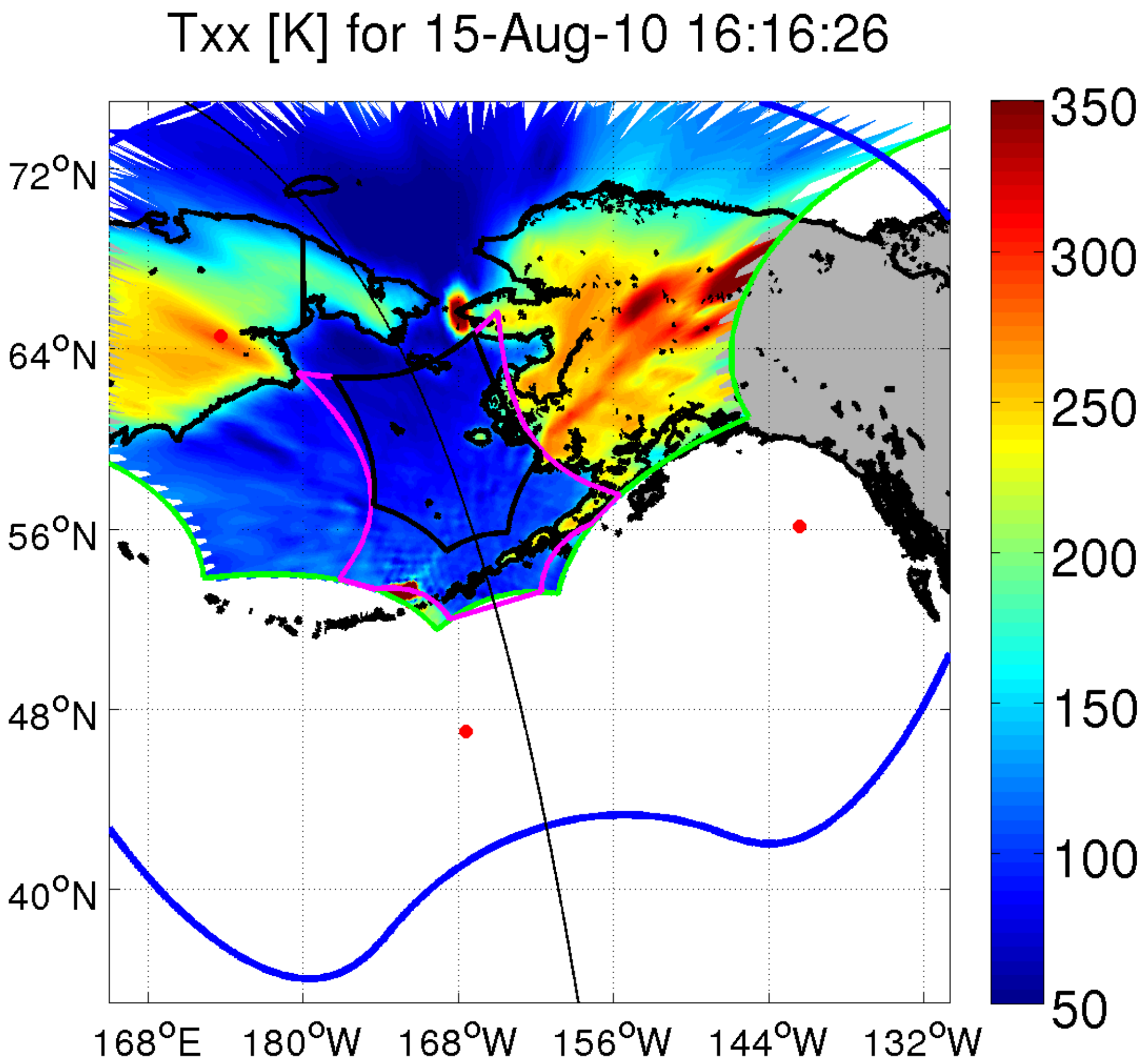

RADIO FREQUENCY INTERFERENCE

RFI continues to plague both salinity and soil moisture retrievals, and no solution proposed thus far can eliminate its impact in all cases. Here is one example showing intermittent contamination from radars in Alaska. The RFI induces large spatial ripples in the images far from the sources, and the impact extends into the alias-free field of view.

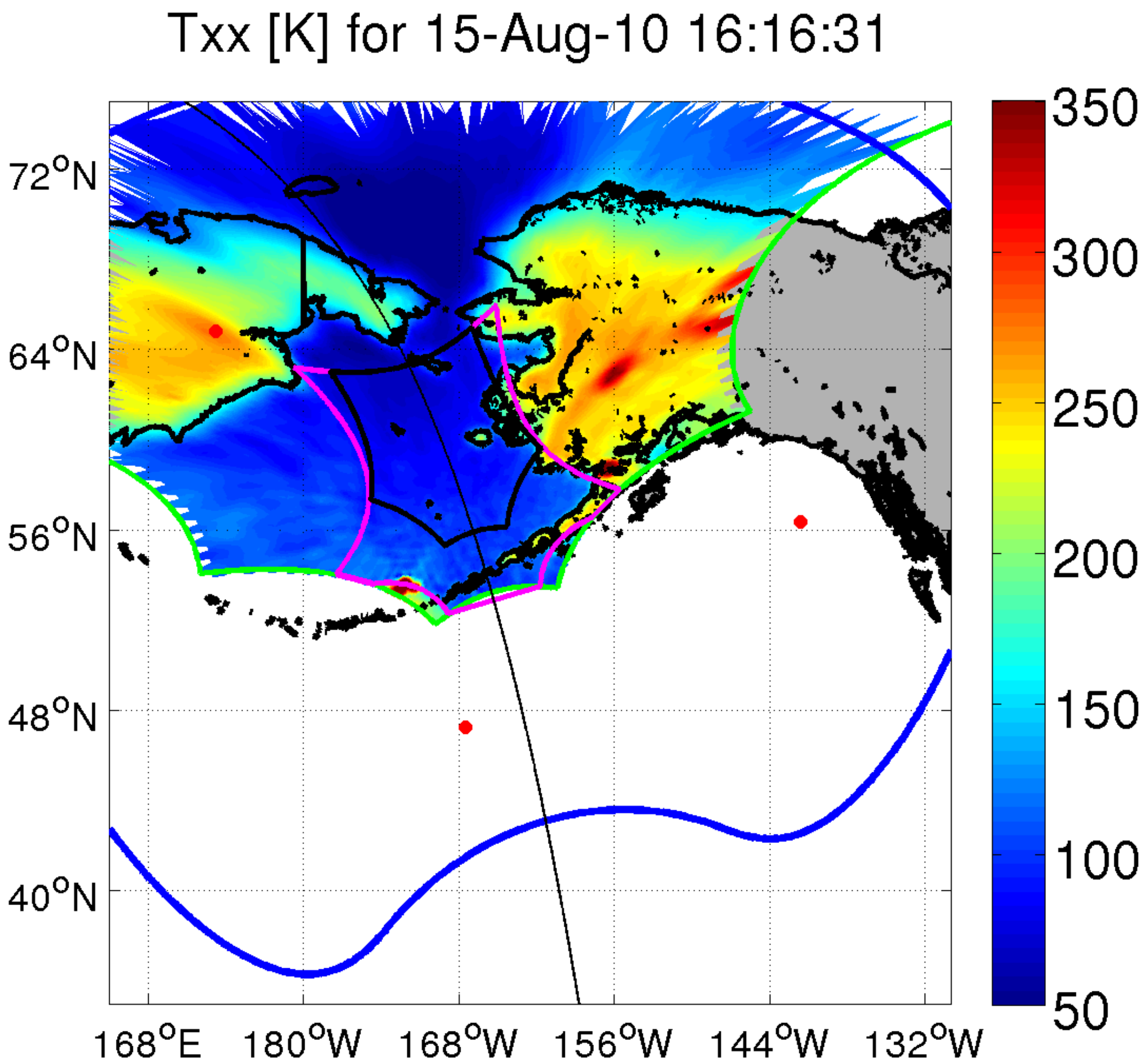

Radio Frequency Interference Contamination Probability

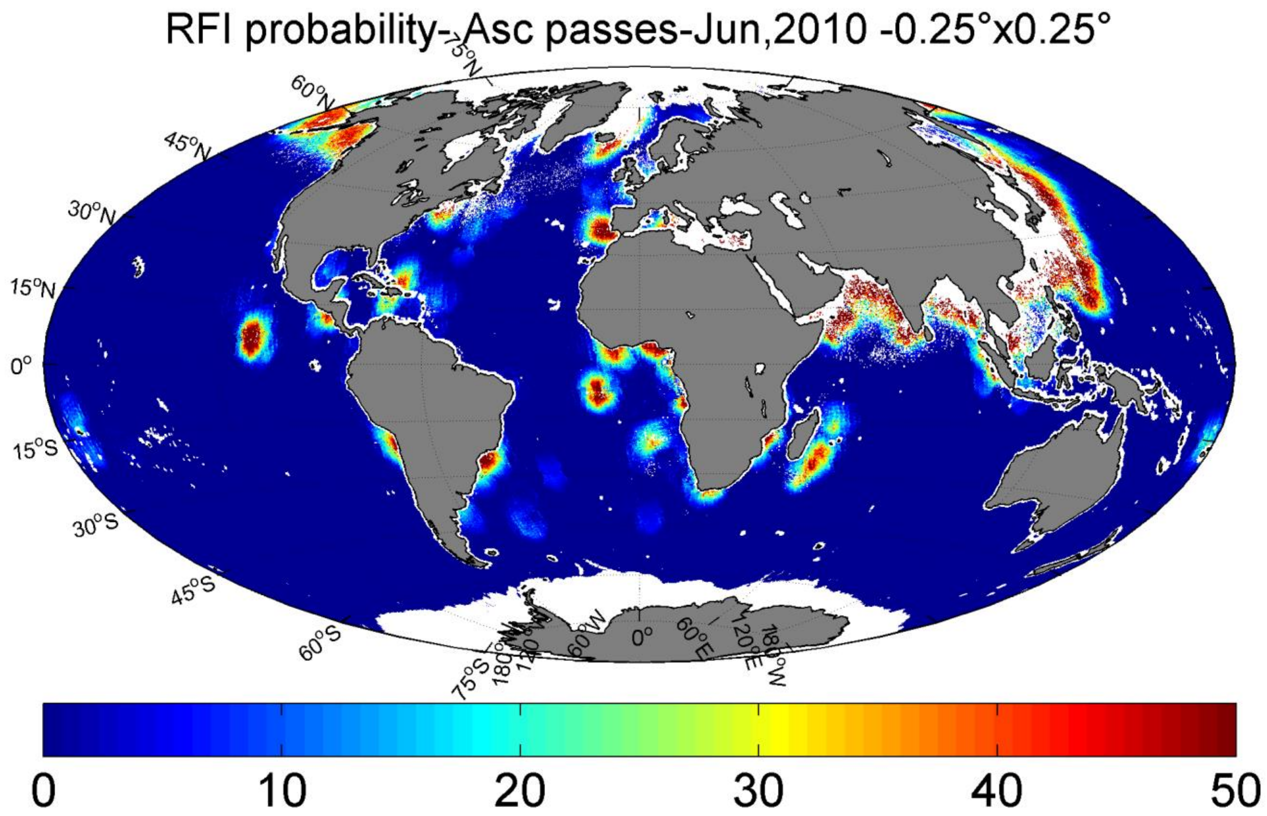

Strong data contamination in many oceanic areas

SOME CURRENT PROBLEMS WITH THE SMOS DATA

Radio frequency interference

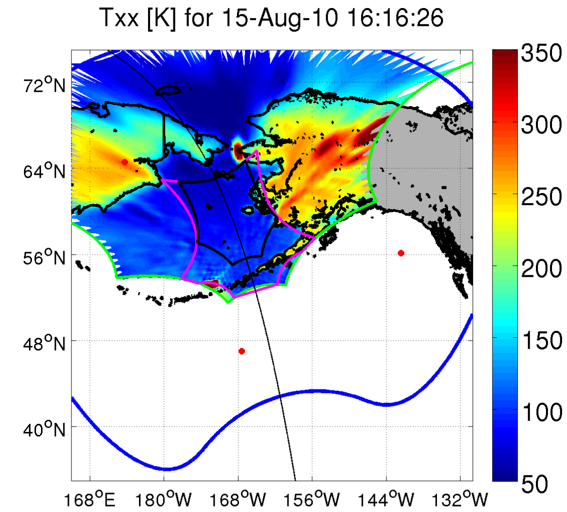

Drift on both short (orbital, latitudinal, and descending-ascending) and long (from weeks to months) time scales

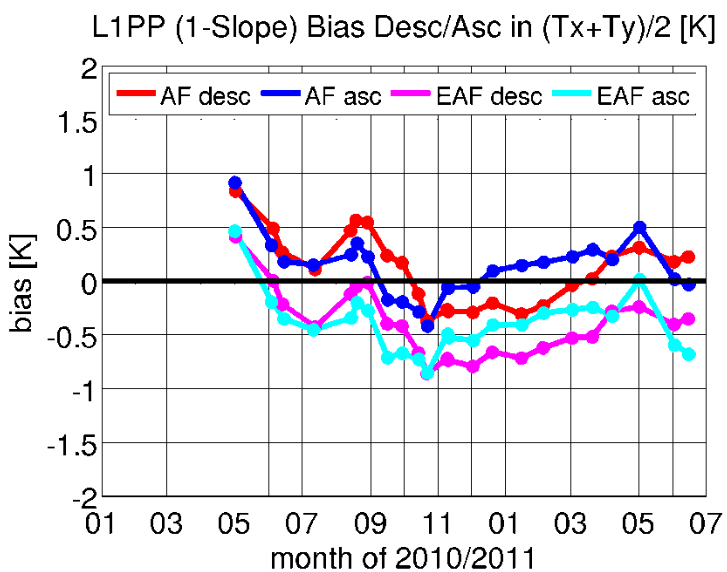

Scattering of galactic radiation (mostly synchrotron radiation) by the wind-roughened ocean surface

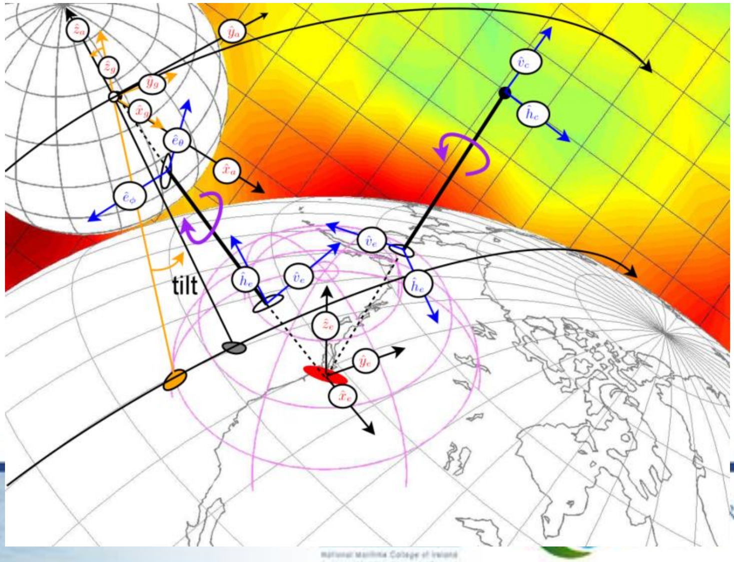

SMOS refined Level 3 SSS products

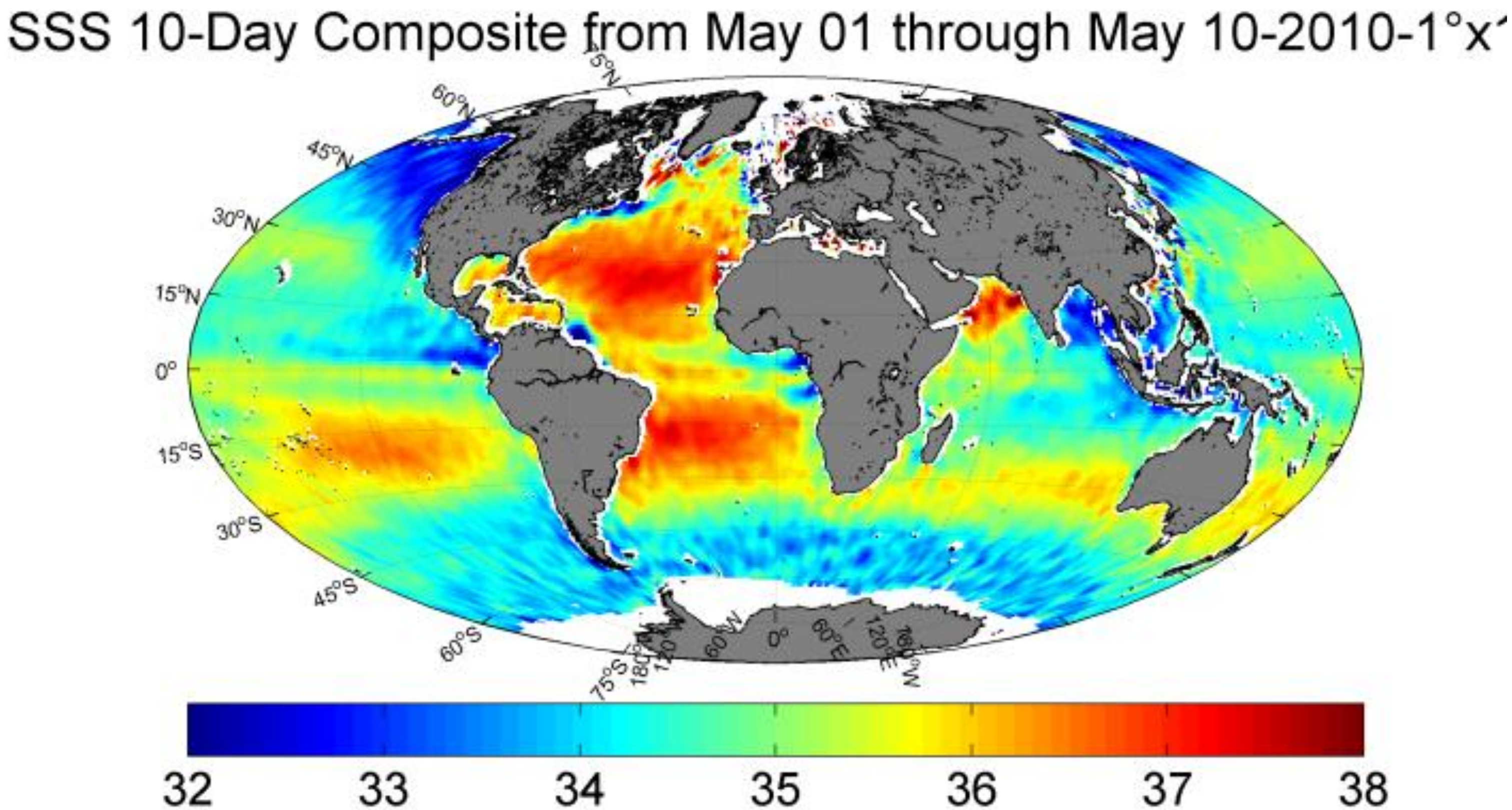

CATDS research CEC products

Global SMOS salinity maps: CATDS products

SMOS-CATDS-CEC Level 3 product (see http://www.catds.fr/): Monthly Composite

CATDS
Centre Aval de Traitement des Données SMOS

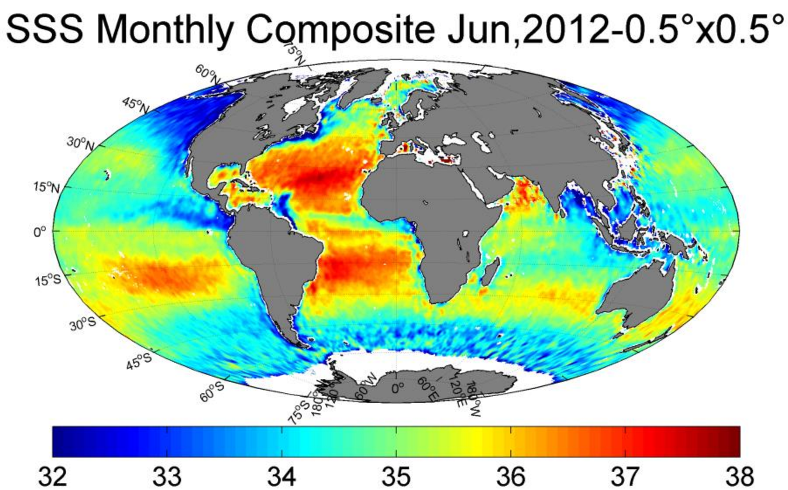

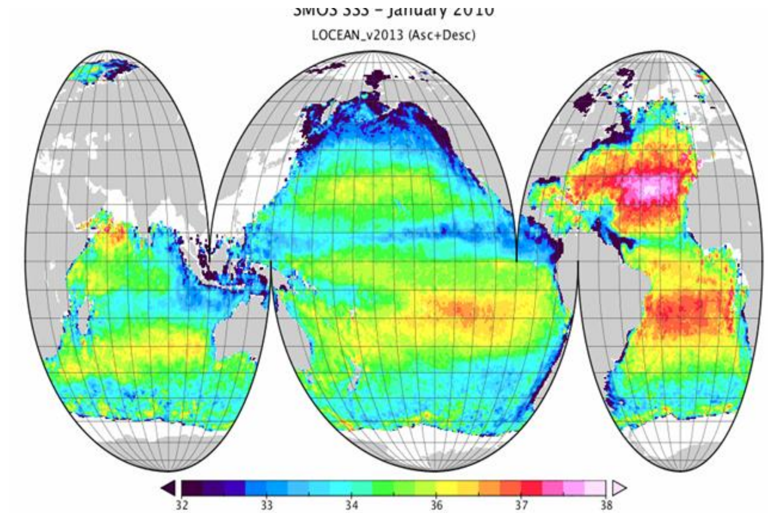

IFREMER-CEC
Stronger RFI filtering than ESA L2
Strong constraints wrt SSS climatology

LOCEAN (ESA L2 binned SMOS SSS)

So, several SSS products exists but needed because none of them is perfect
and parallel efforts & progresses are required

Global SMOS salinity maps: BEC products

SMOS Level 3 product: 10 days / 1º optimally interpolated ocean salinity map for 15 – 24 January 2012

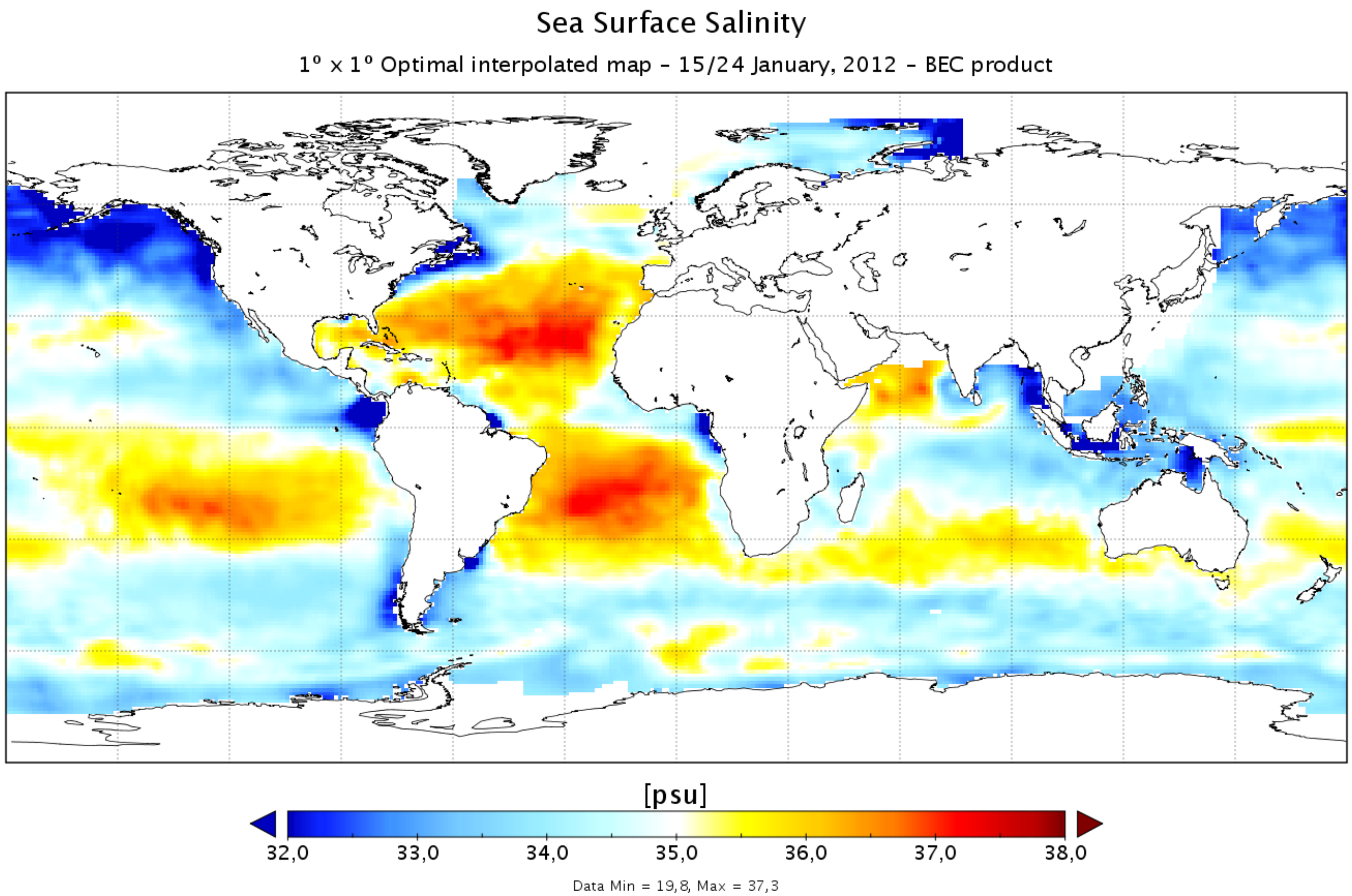

operationally generated by the SMOS Barcelona Expert Centre

SMOS SSS accuracy: in situ validation

Comparison SMOS-Argo:

Proxy for absolute accuracy (with care due to Argo not sampling SSS). Only data set available for global analysis. More precise local comparisons possible (moored buoys, surface drifters)

Diagnostic sites defined in Product Performance Evaluation Plan

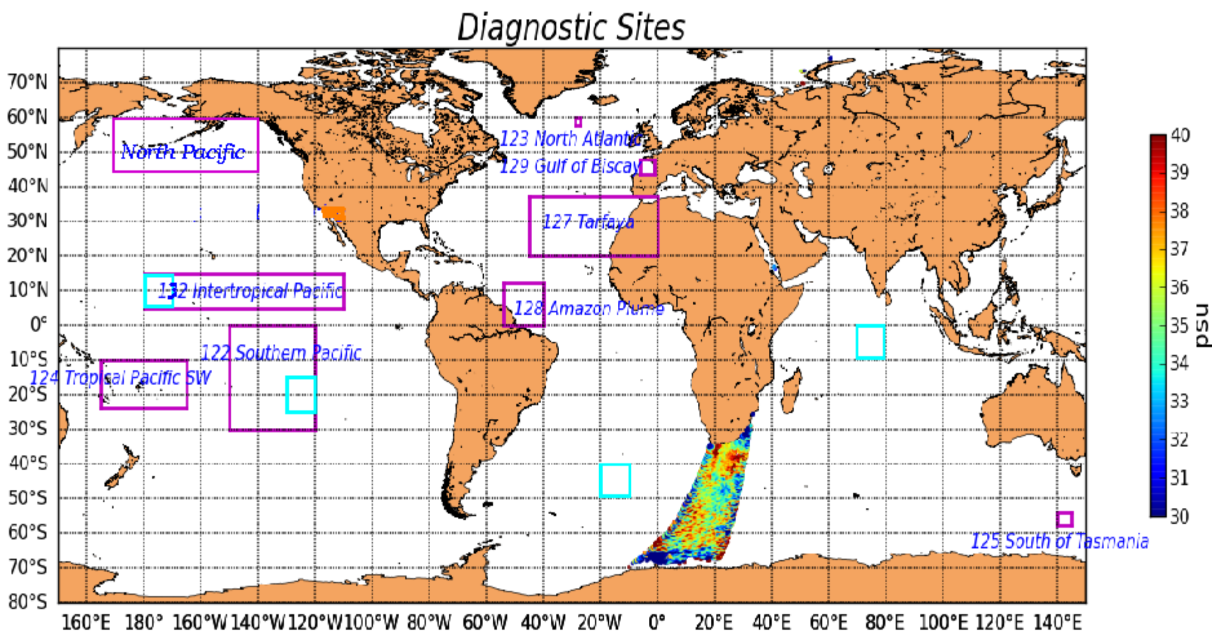

- Interesting ocean situations
- In situ sampling programs
- Expected problems

SMOS SSS accuracy: in situ validation

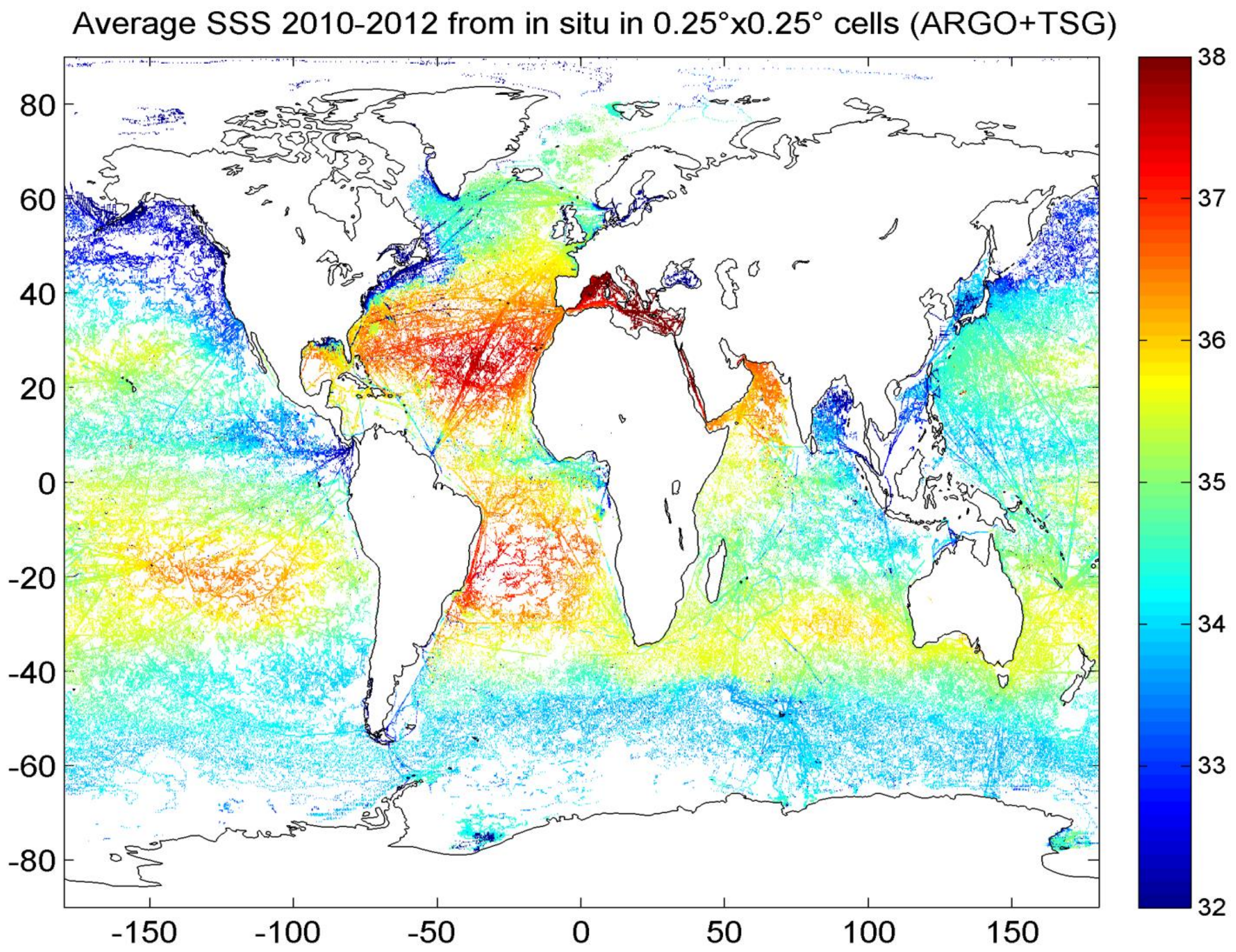

Temporal evolution of the error standard deviation

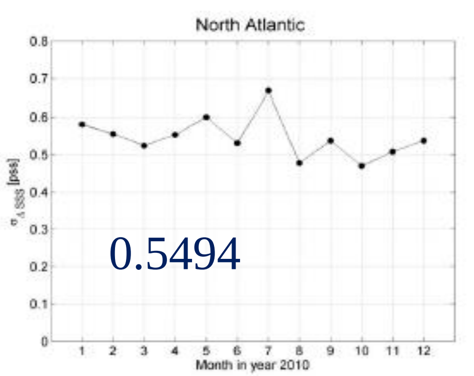

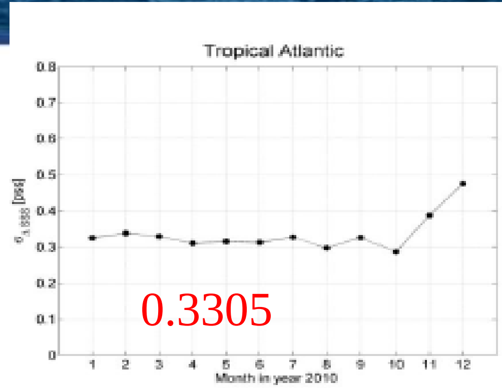

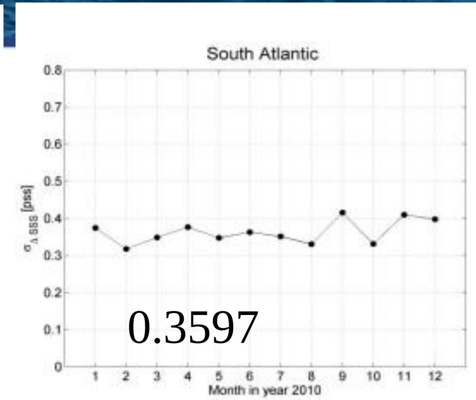

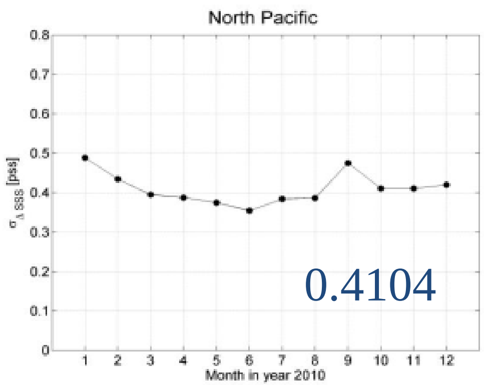

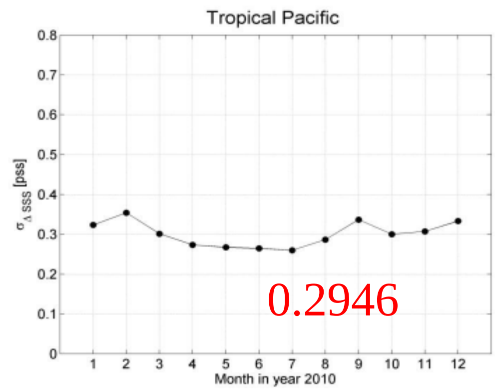

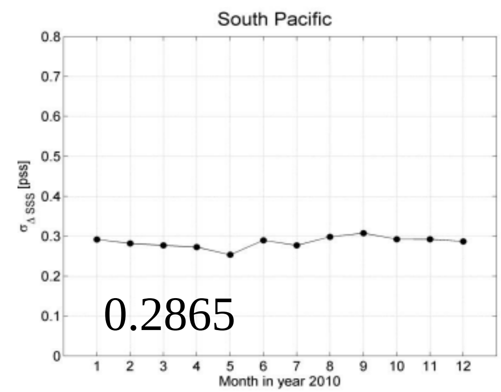

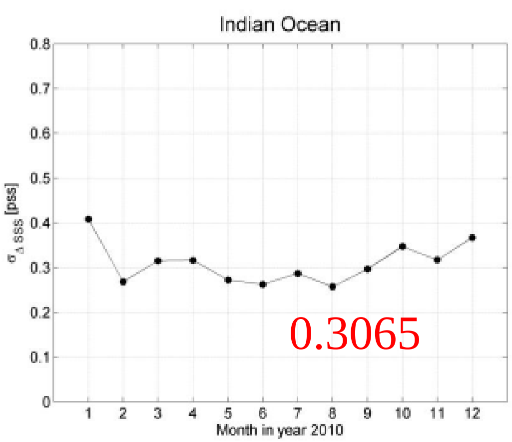

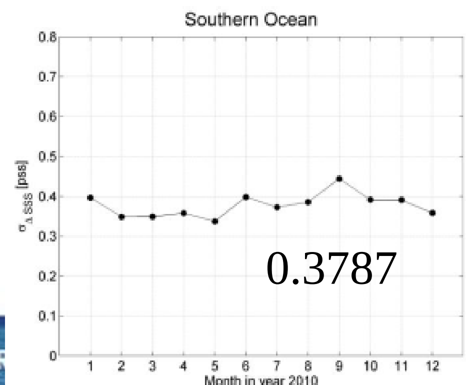

SMOS SSS accuracy: in situ validation

- CATDS Monthly Level 3 products

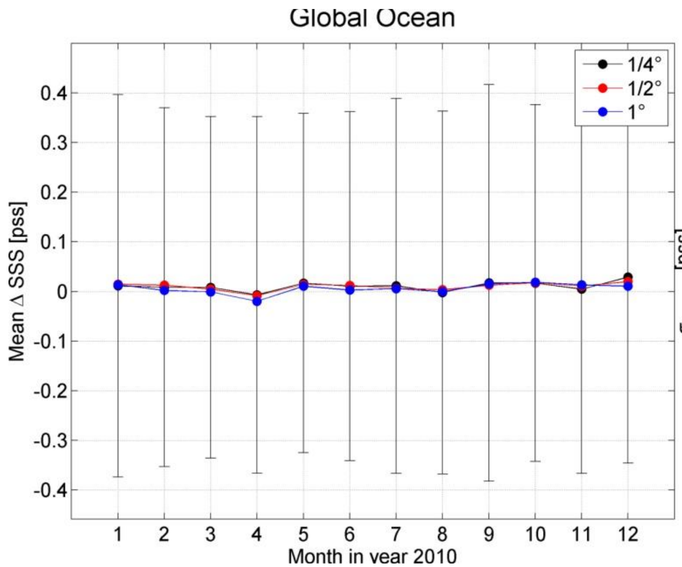

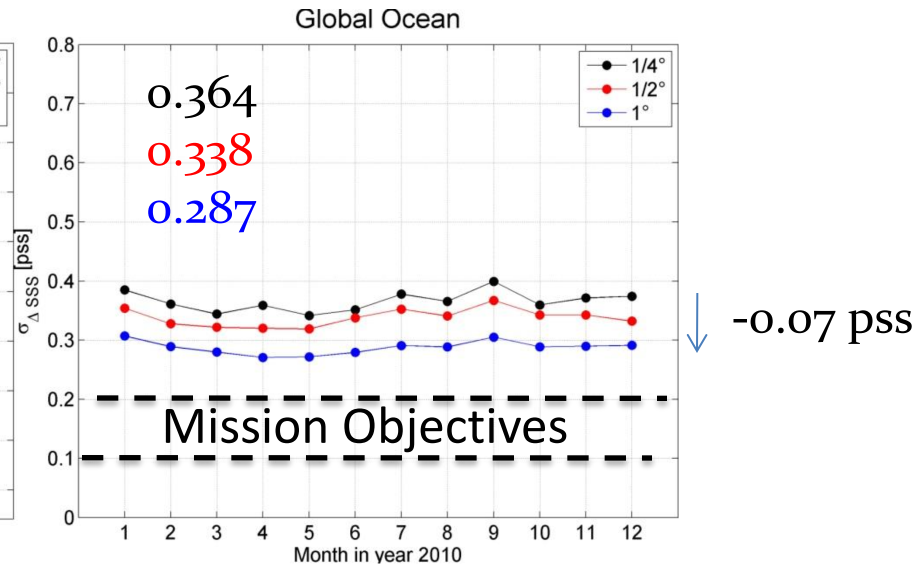

Applications of SMOS ocean

Global seasonal and interannual variability

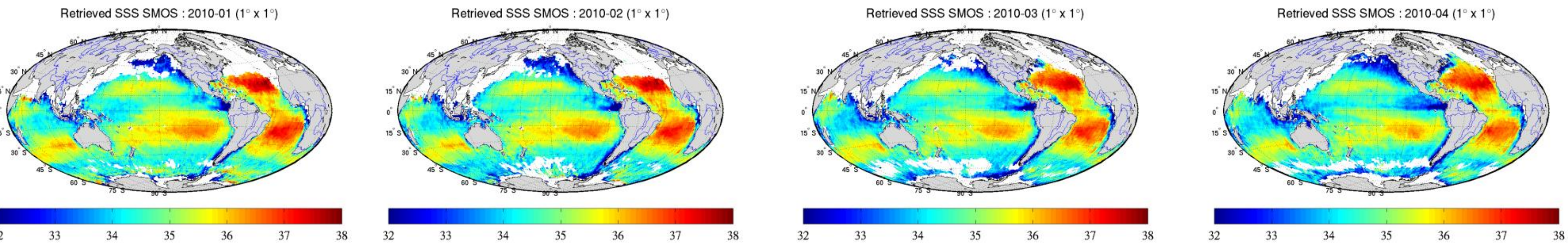

Tracking salinity variability at seasonal scale

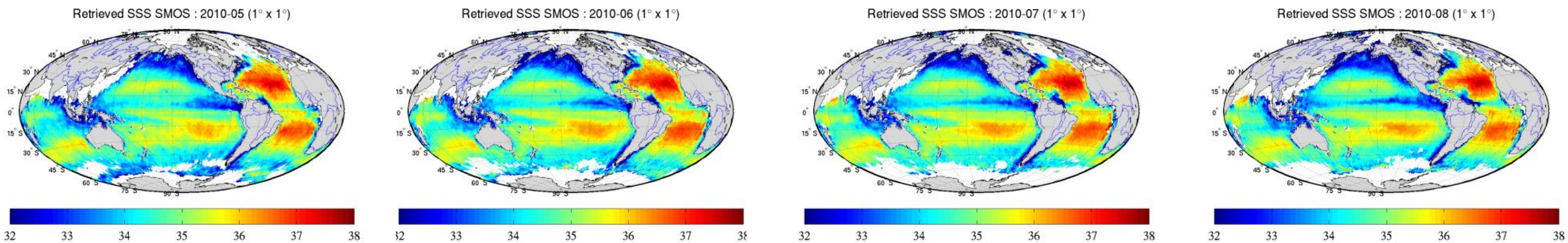

Monthly 1º x 1º bin averaged ocean salinity maps for **2010**

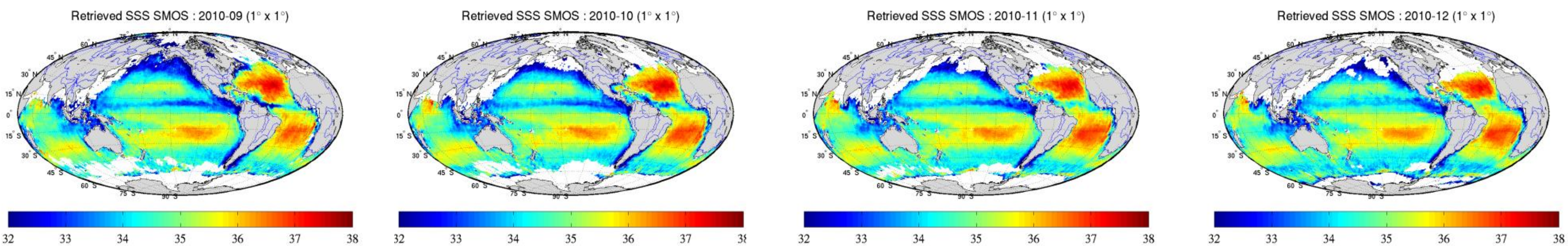

Global seasonal and interannual variability

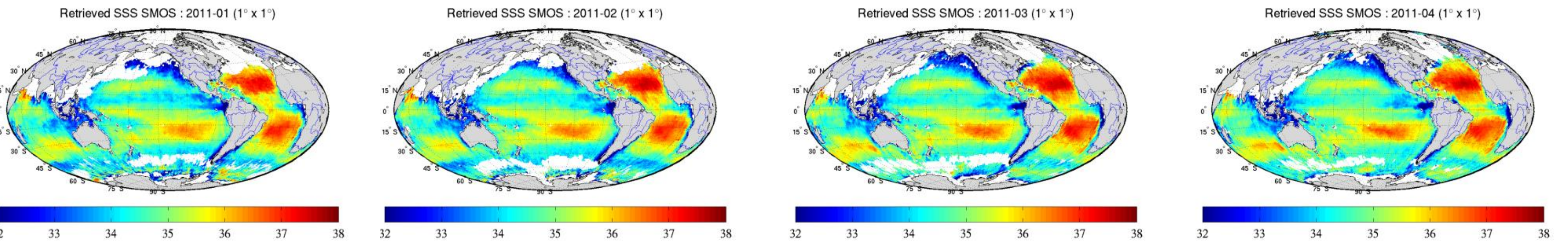

Tracking salinity variability at seasonal scale

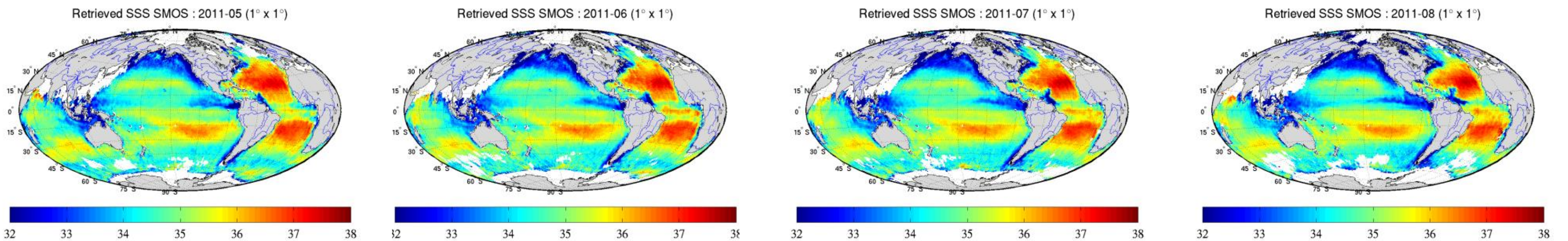

Monthly 1º x 1º bin averaged ocean salinity maps for **2011**

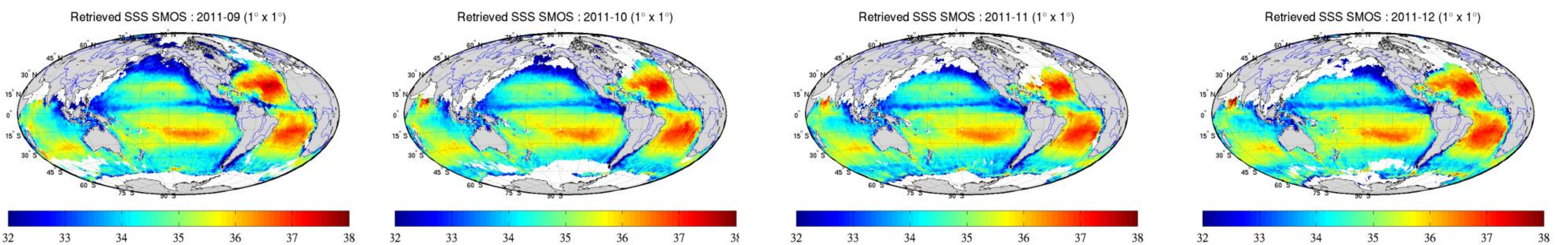

Large Tropical River Plume Monitoring

- SMOS SSS quality assessment in the Amazon-Orinoco River Plume region
- Monitoring advection pathways of the freshwater Amazon and Orinoco river plume along surface currents
- Spatio-temporal coherence between SSS and Ocean Colour properties over the Amazon-Orinoco river Plume & applications

Quality assessment

Thermo-salinograph

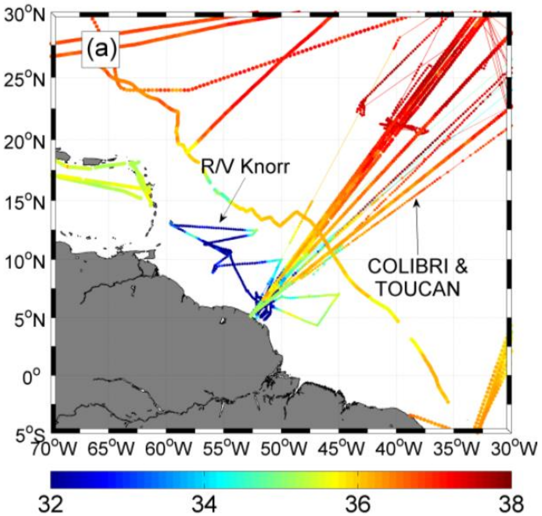

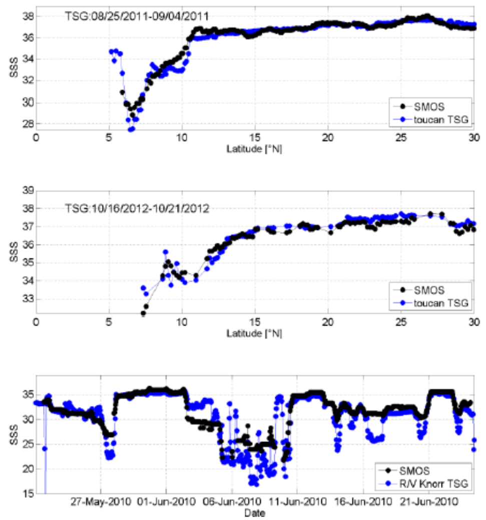

ARGO floats & Piratta moorings

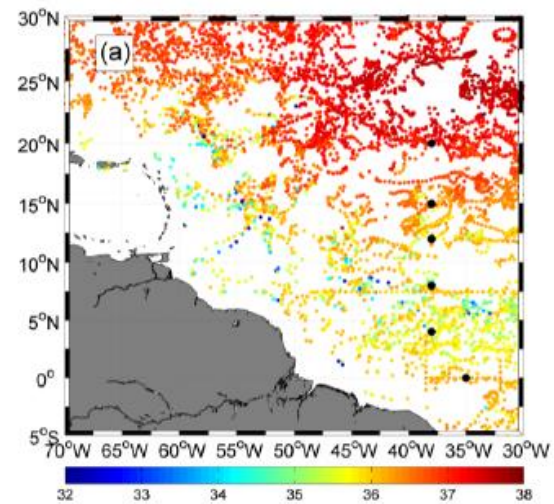

CTD profiles

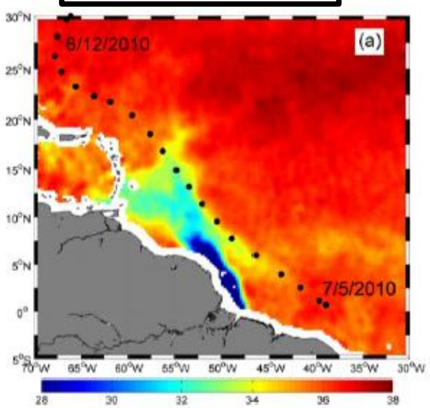

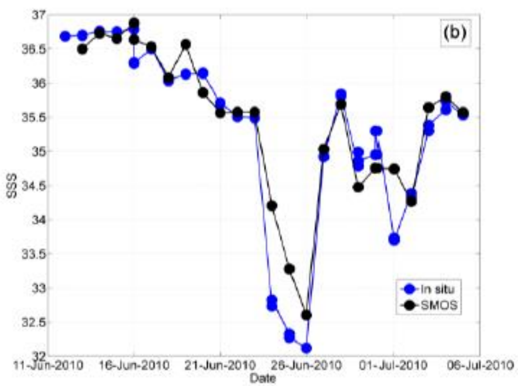

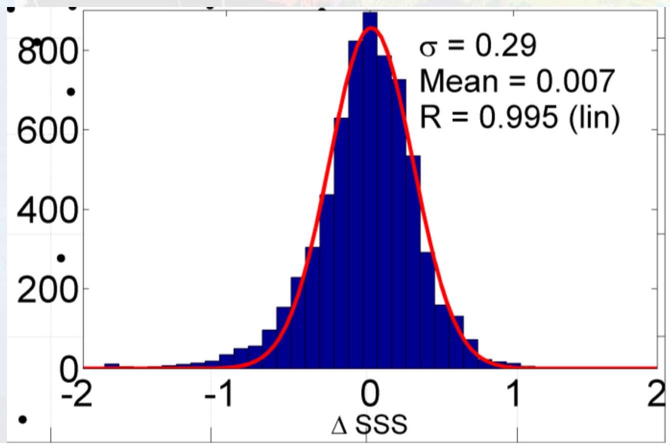

standard deviation of the differences $\Delta SSS = SSS_{SMOS} - SSS_{In\ Situ}$ is on the order of ~0.3-0.5, considering 10 days averaged satellite products at 50 km resolution. This is at least a factor 10 smaller than the SSS signal spatio-temporal variability encountered in this region.

Monitoring advection pathways of the freshwater Amazon and Orinoco river plume along surface currents

Synergy with Altimetry

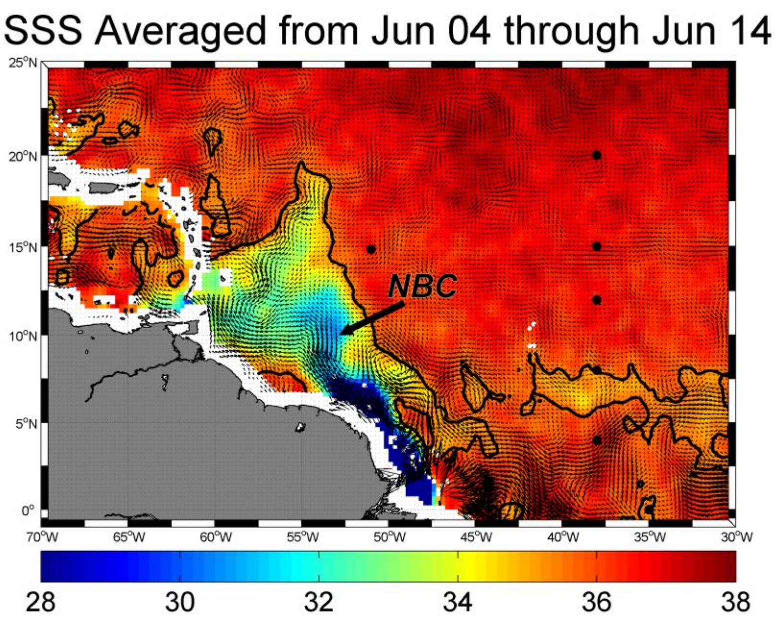

North Westward path

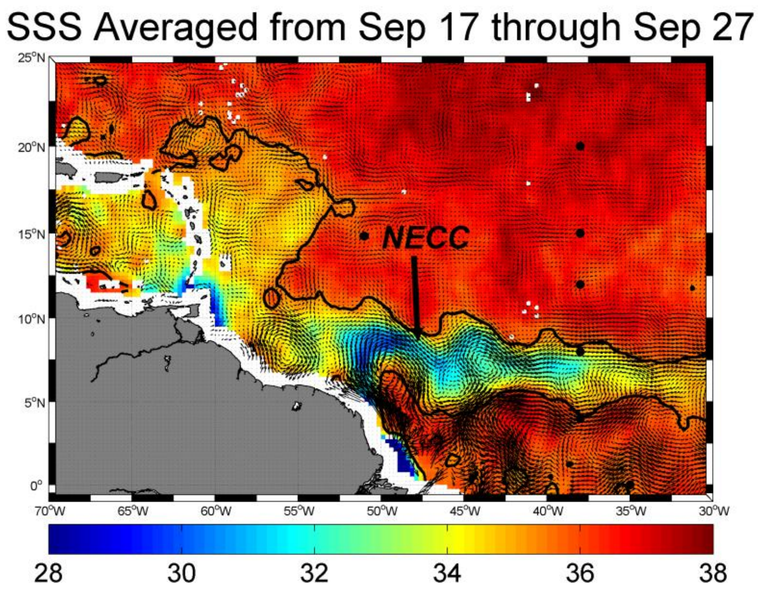

Eastward path

Monitoring advection pathways of the freshwater Amazon and Orinoco river plume along surface currents

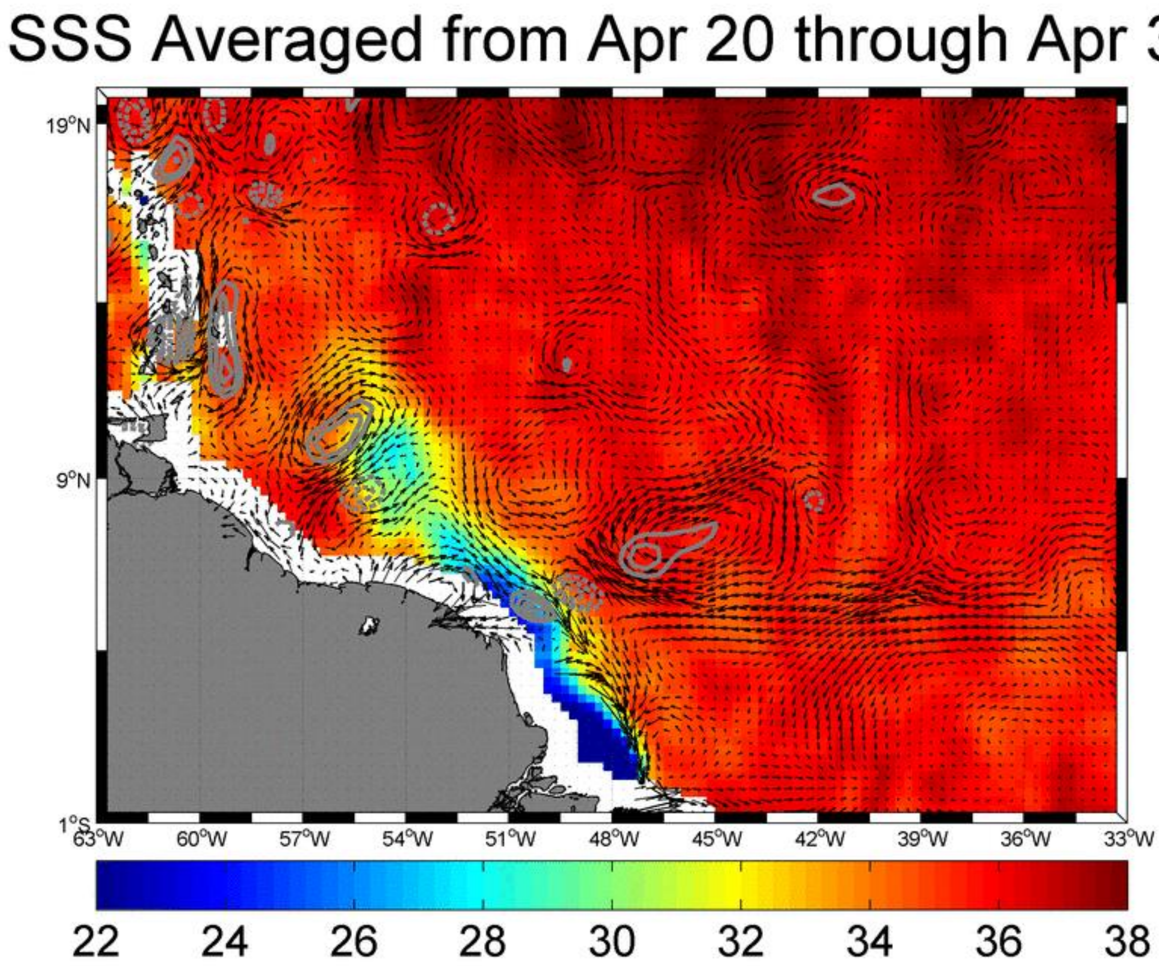

Seasonal cycle
of the freshwater pool extent
& its relashionships
with bio-optical properties

Salisbury et al., JGR 2011

River discharge cycle

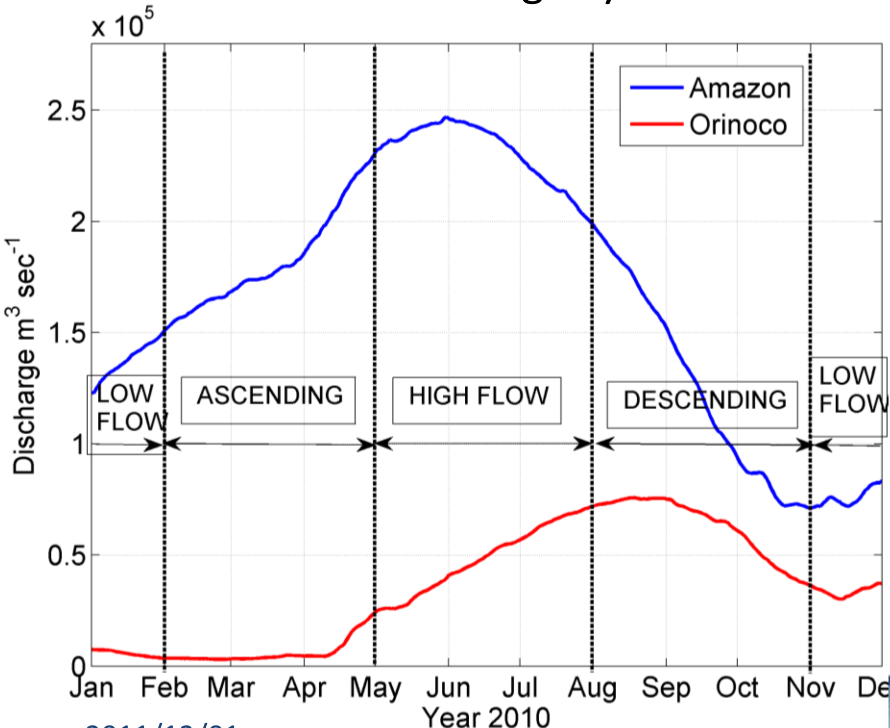

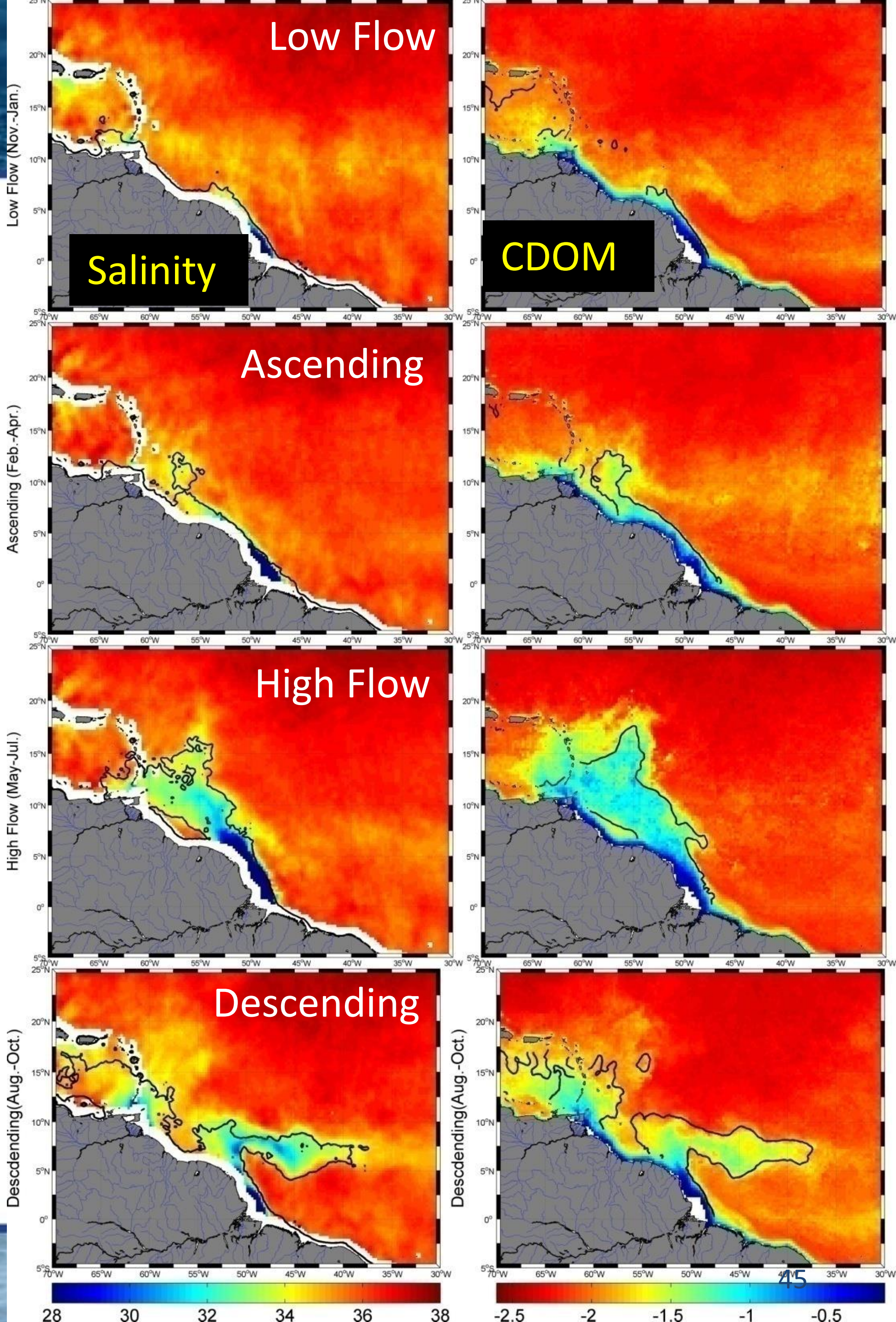

2011/12/01

Conservative Mixing between river constituents & open sea

Yearly average

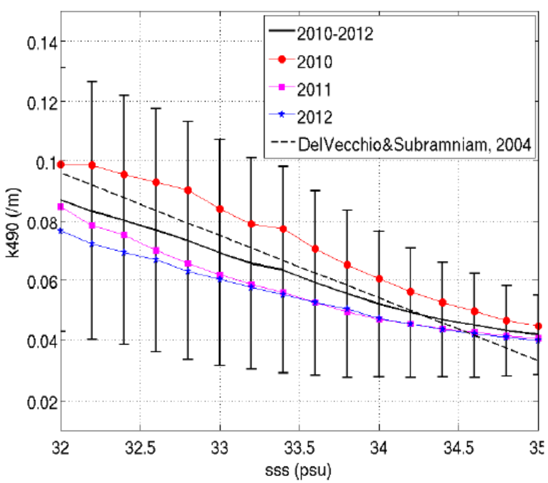

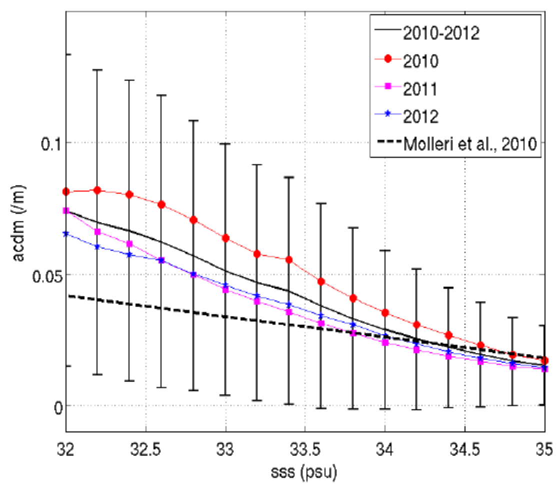

Seasonnal variability

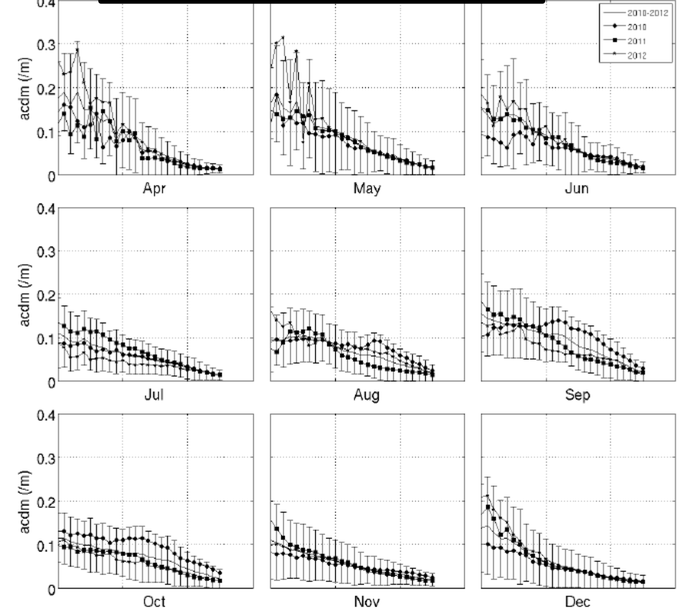

Applications:

1) From SMOS SSS=> reconstruct synthetic optical parameter maps & analyze departure from conservative mixing (photo-bleaching, primary productivity,..)

2) From Ocean Color=> reconstruct High resolution SSS

Identification of intense Net primary productivity Zones

Syn

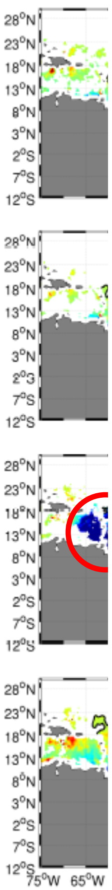

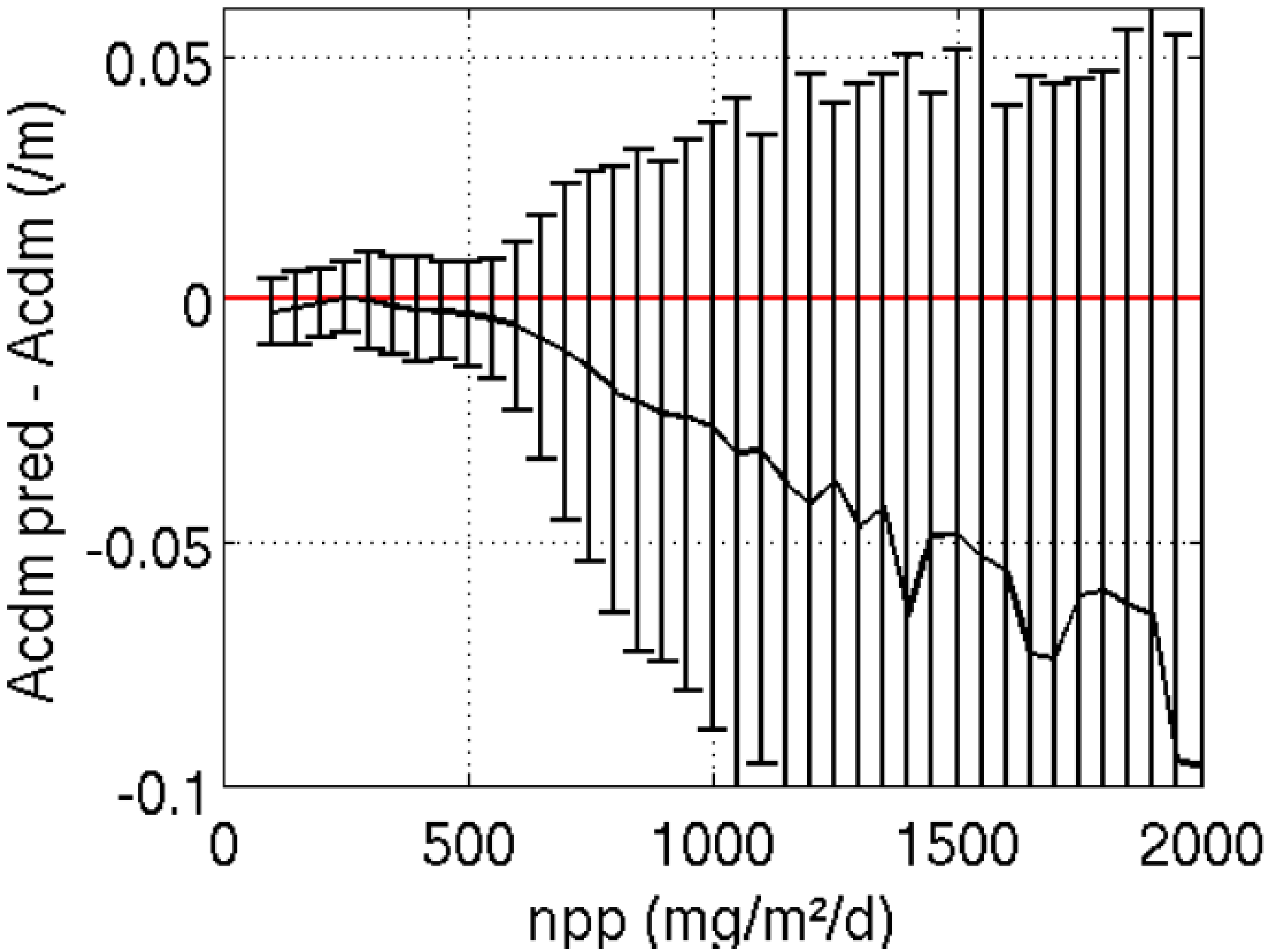

Figure 4.19: 2010 r ... ivity
Globcolour.

High Resolution SSS from Ocean Color estimated from SMOS derived conservative mixing

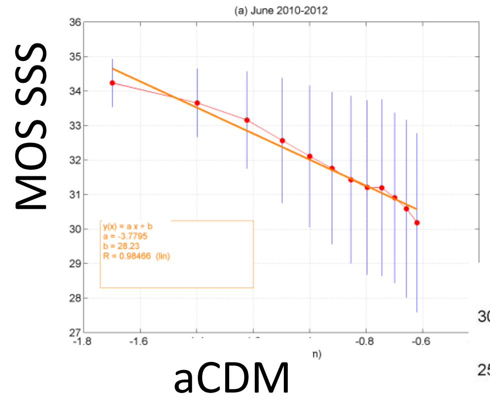

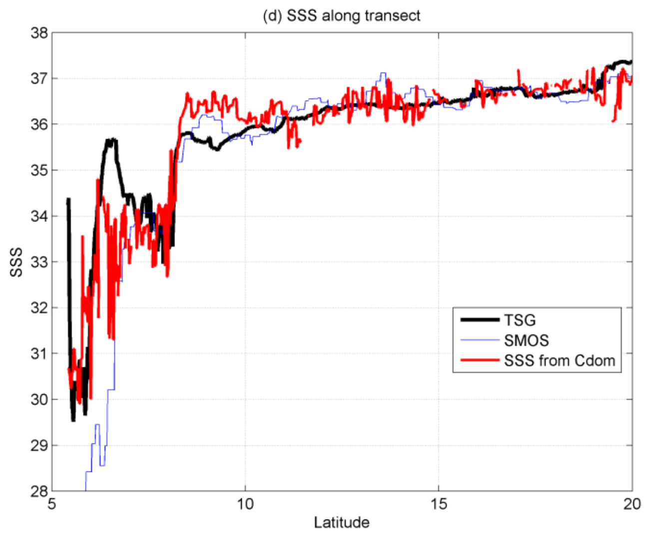

10 days aCDM composite at 4 km res

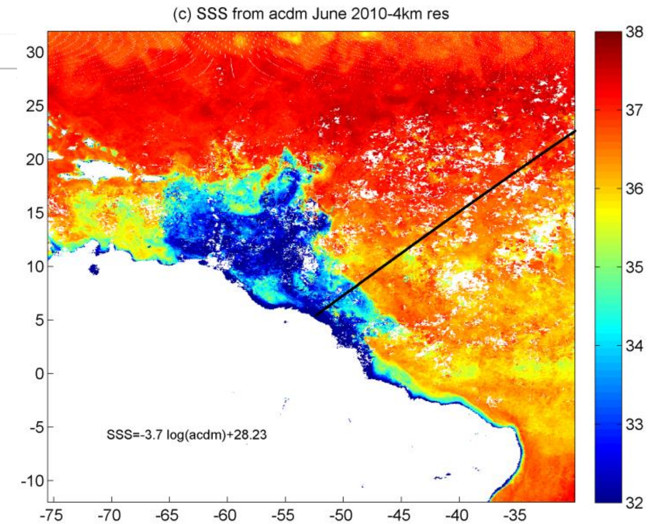

10 days « optical SSS » composite at 4 km res

Seasonal Cycles of the Congo and Niger River plumes

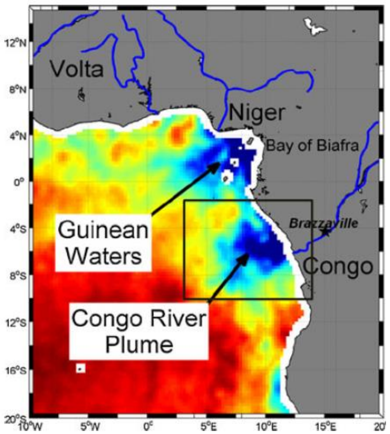

Seasonnal Cycle from 3 years of SMOS data

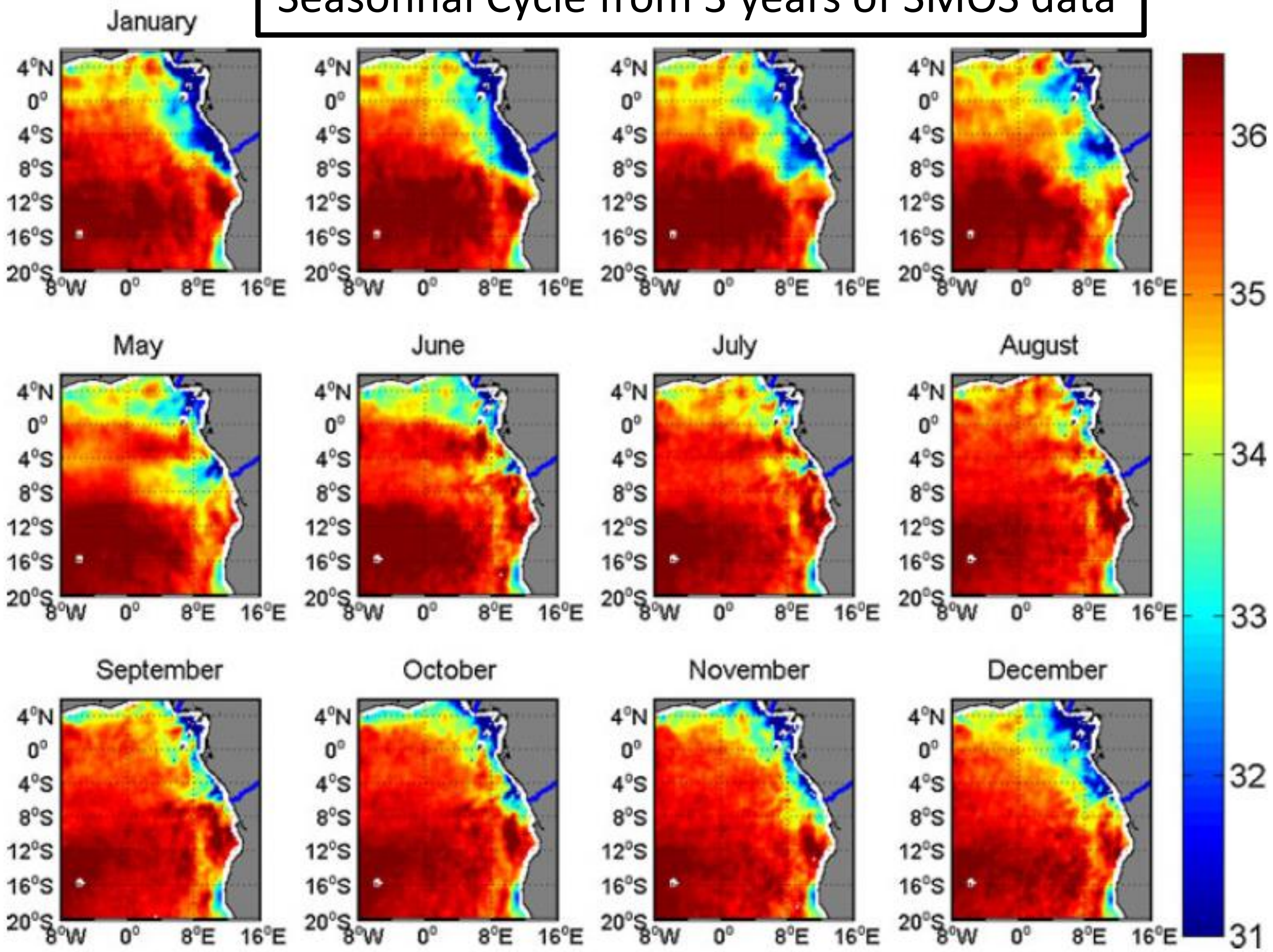

Fig. 10 2010–2012 Monthly averaged seasonal cycle of surface salinity in the eastern tropical Atlantic derived from SMOS observations

Impact of precipitation on salinity stratification in the upper ocean

J. Boutin, G. Reverdin, N. Martin, X. Yin, S. Morrisset

LOCEAN, UMR CNRS/UPMC/IRD, Paris, France

+ collaborations with French GLOSCAL SMOS Cal/Val participants
(IFREMER, Meteo-France, LEGOS)
and SMOS ESA Expert Support laboratories
(ICM/CSIC, LOS/IFREMER, ARGANS-st, CLS, ACRI-st)

Precipitation events are responsible for large temporal variability in the tropical ocean and for sea surface stratification effects

Rain events are responsible for large and sudden sea surface freshenings
Autonomous SVP drifter measurements (~45cm depth)

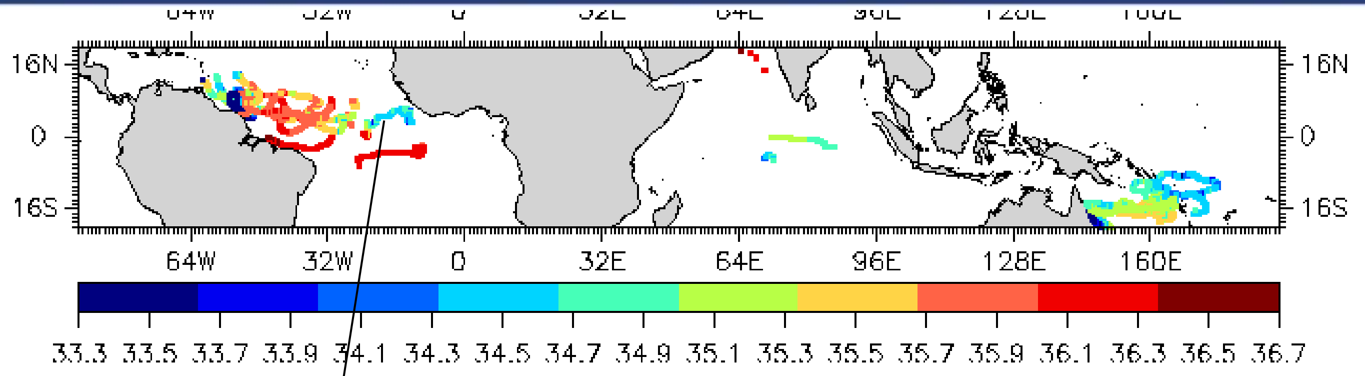

http://www.locean-ipsl.upmc.fr/smos/drifters/

Large SSS freshenings in rainy Atlantic ITCZ region

Reverdin et al. JGR 2012

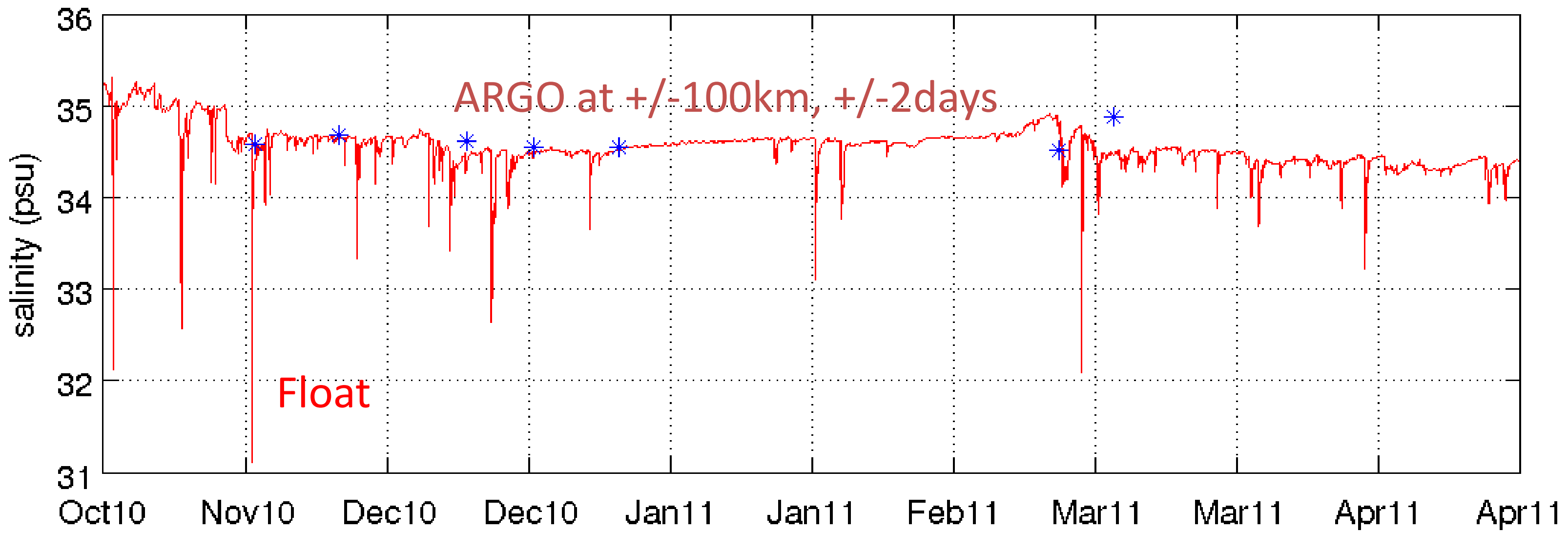

Study of SMOS & ARGO salinity variability in tropical Pacific region

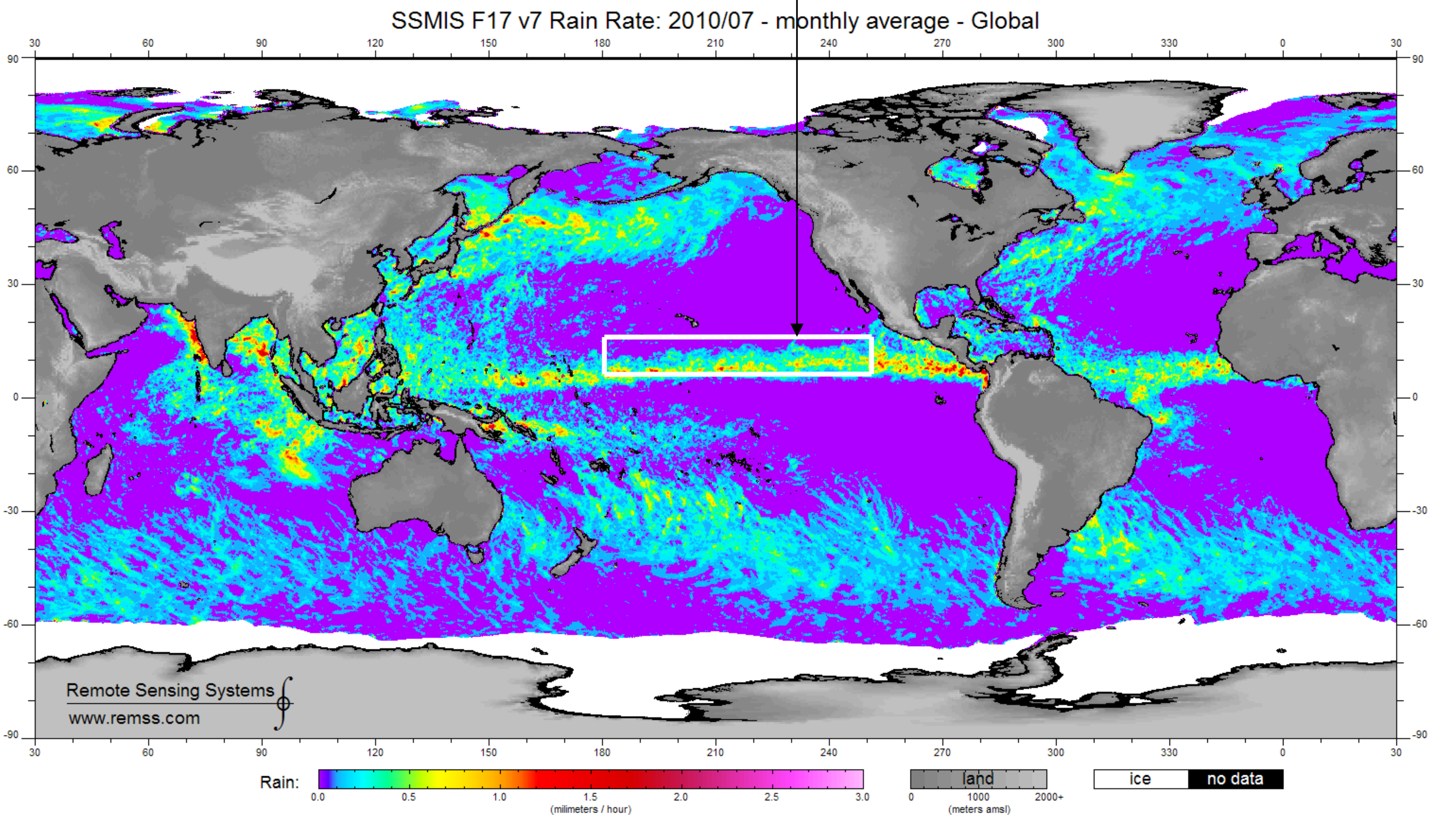

Rain induced sea surface freshenings

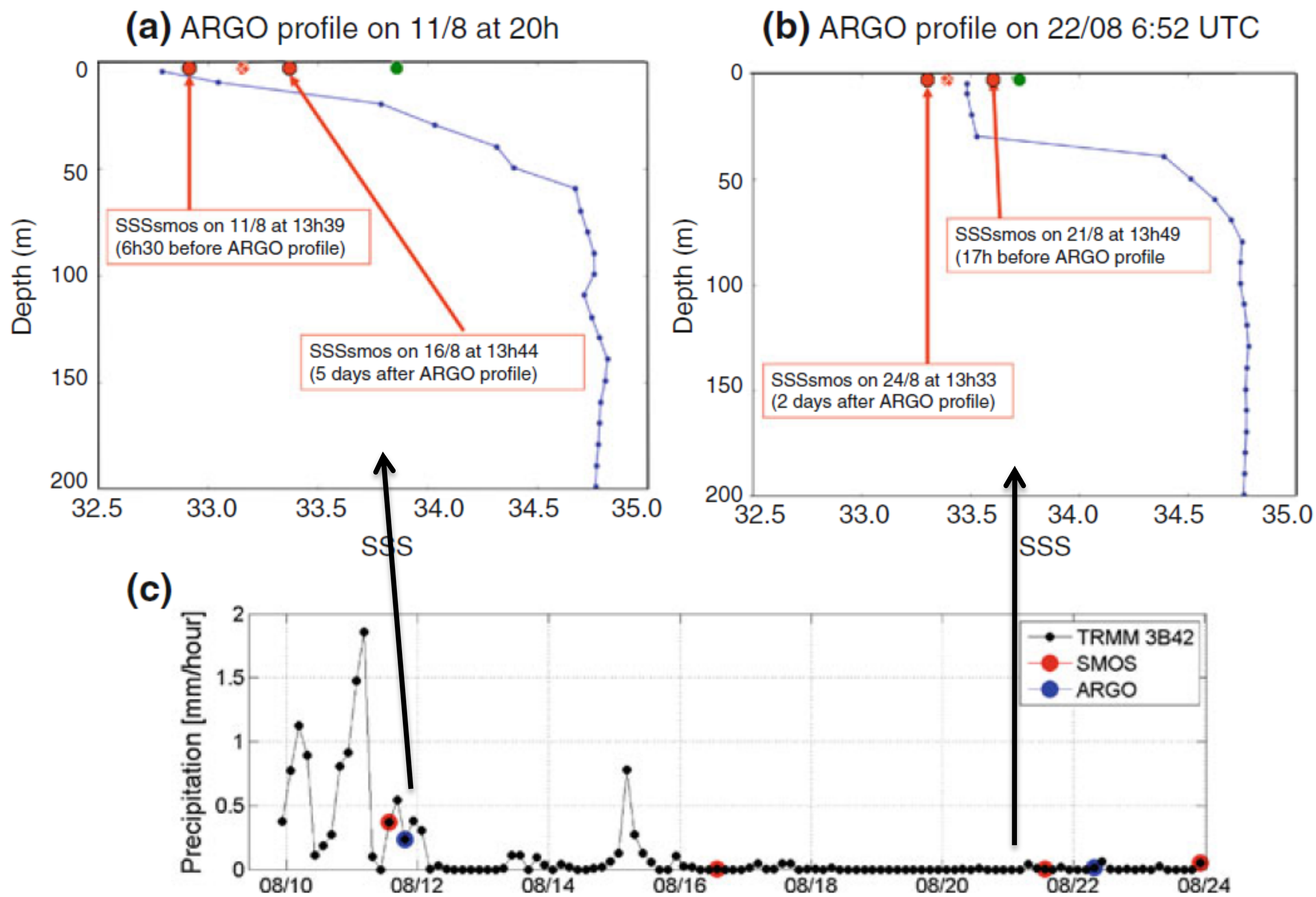

Fig. 13 Two successive Argo profiles taken by float 4900325 (*blue curve*) in the eastern tropical Pacific on **a** 11 August 20:00 UTC (latitude = 12.4°N; longitude = 117.6°W) and **b** 22 August 6:52 UTC (latitude: 12.2°N; longitude: 117.8°W). Mean SMOS SSS collocated within a 5-day window and a radii of 50 km with these profiles are indicated by red dashed point. In each case, two SMOS passes have participated to these collocations: mean SMOS SSS corresponding to each pass is indicated as red filled point. The corresponding ISAS SSS in August is indicated by the green point. The time series of the 3-hourly satellite rain rate from TRMM 3B42 and averaged over (11°–13°N; 116°–118°W) is provided in (**c**). The time at which SMOS and Argo acquired SSS data is indicated by red and *blue dots*, respectively

SMOS (10day-100km) - ARGO in selected regions (Jul-Sep 2010):

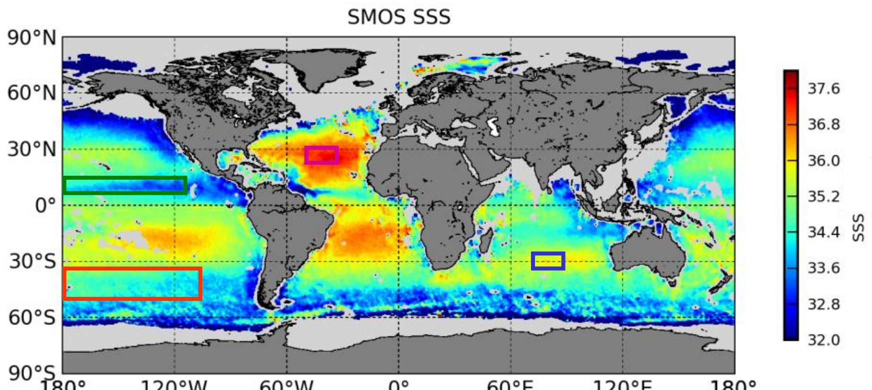

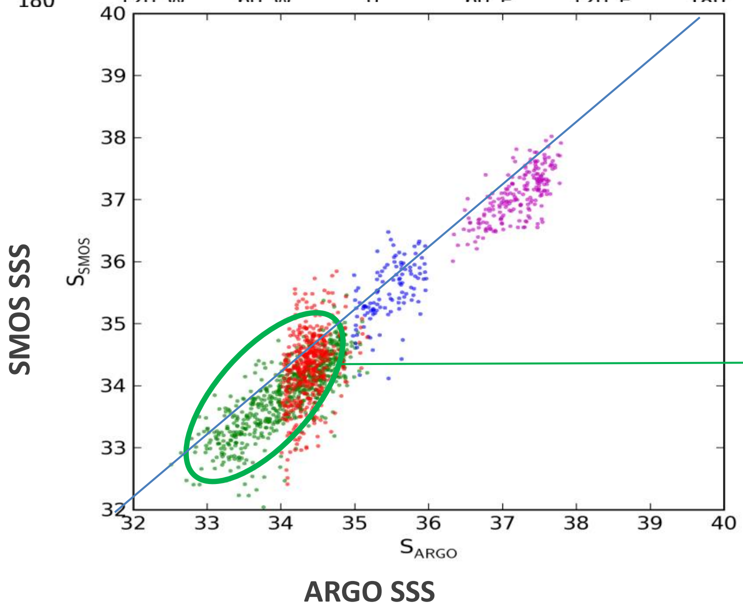

SMOS – ARGO SSS in tropical Pacific 0.1 fresher and noisier than in subtrop Atl: rain?

Mean(std) SMOS(100km-10day mean) -ARGO SSS

-0.13 (0.28) Subtrop. Atlantic
0.04 (0.39) Southern Indian
-0.08 (0.51) Southern Pacific
-0.23 (0.35) Northern Trop. Pacific

Boutin et al., OSD, 2012

February 2011-2010

ISAS 0.5°at 3 m depth

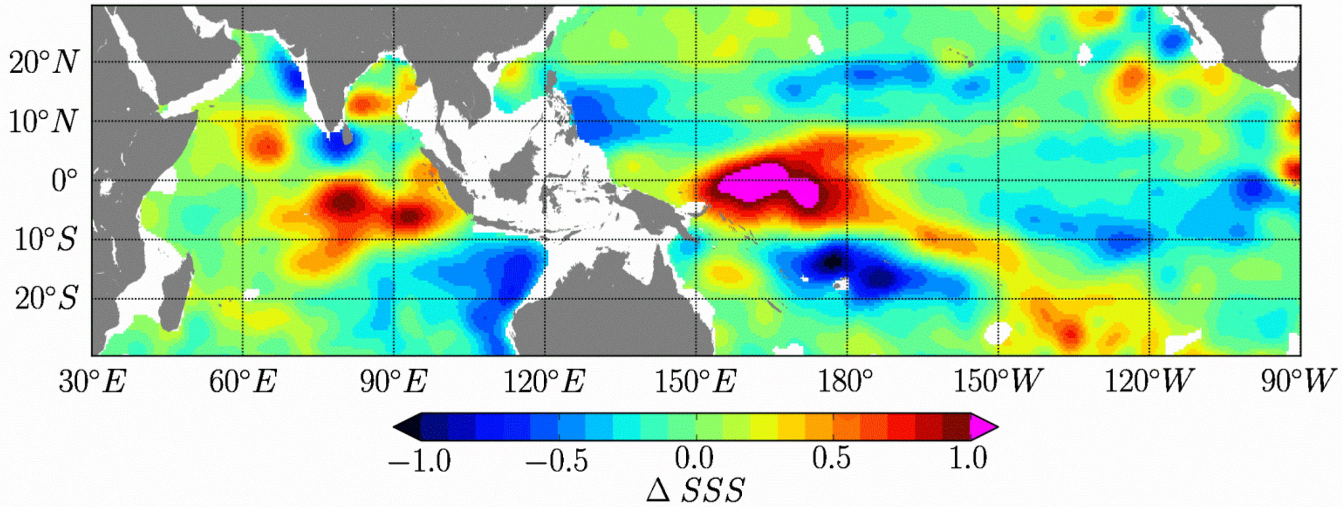

SMOS L3LOCEAN 1° - orbit AD

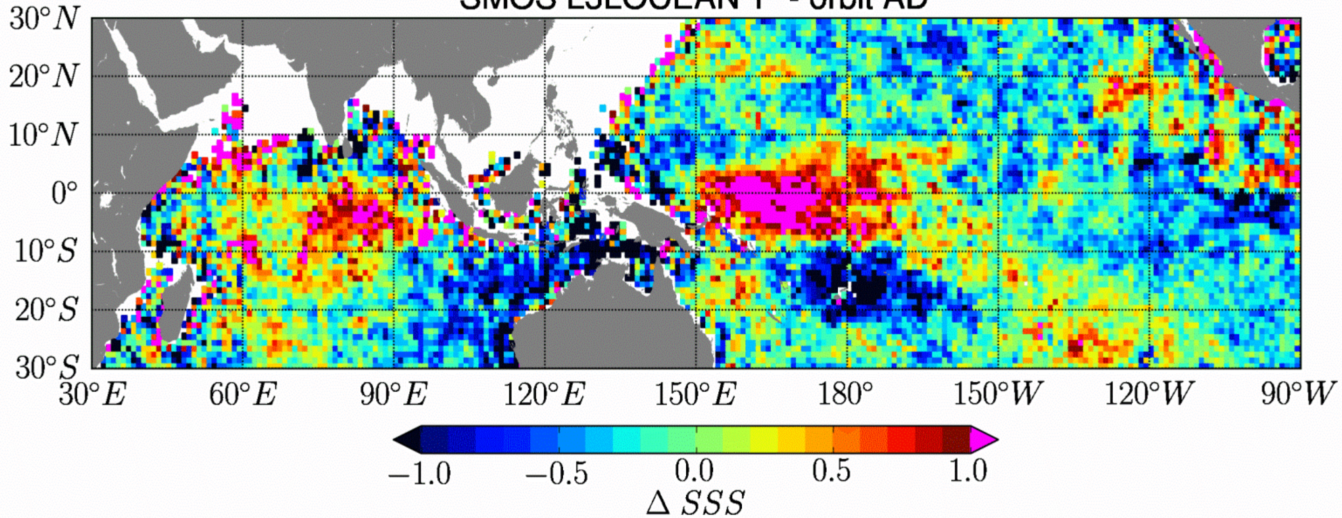

Freshwater interannual balance changes in the Tropics

Changes in SSS and rain rate in between 2011 and 2010

Δrain

ΔSSS

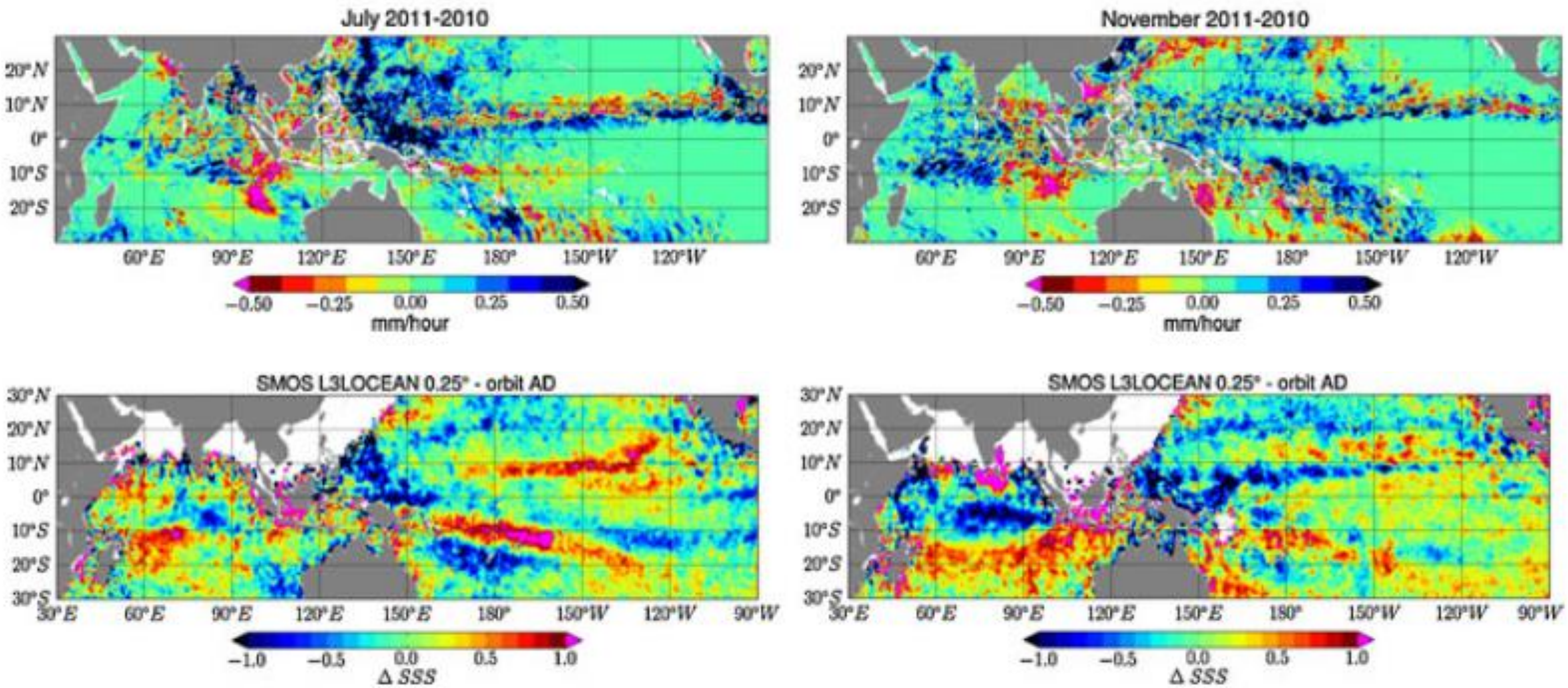

Fig. 20 Differences in the monthly averaged SSS between year 2011 and 2010 for months of July (*left*) and November (*right*). *Top panels* show the $\Delta SSS = SSS_{2011} - SSS_{2010}$ results obtained from in situ OI analysis products ISAS and bottom ones from SMOS data

Salt Conservation in the surface mixed layer

$$\frac{\partial S}{\partial t} = \overbrace{\frac{(E-P-R)S}{h}}^{\text{Atmospheric \& land fluxes}} - \underbrace{\boldsymbol{u}\cdot\nabla S}_{\text{Horizontal advection by currents}} - \overbrace{\Gamma(w_e)\frac{w_e(S-S_d)}{h}}^{\text{Vertical Entrainment by Ekman pumping}} + \underbrace{\kappa\nabla^2 S}_{\text{Turbulent diffusion}}$$

evaporation rate E

precipitations rate P

input by river runoffs R

h is the mixed layer depth

$\boldsymbol{u}$ is the (vertically averaged) current vector,

w_e is the vertical entrainment rate

S.Michel et al., Ocean Science Discuss, 2007

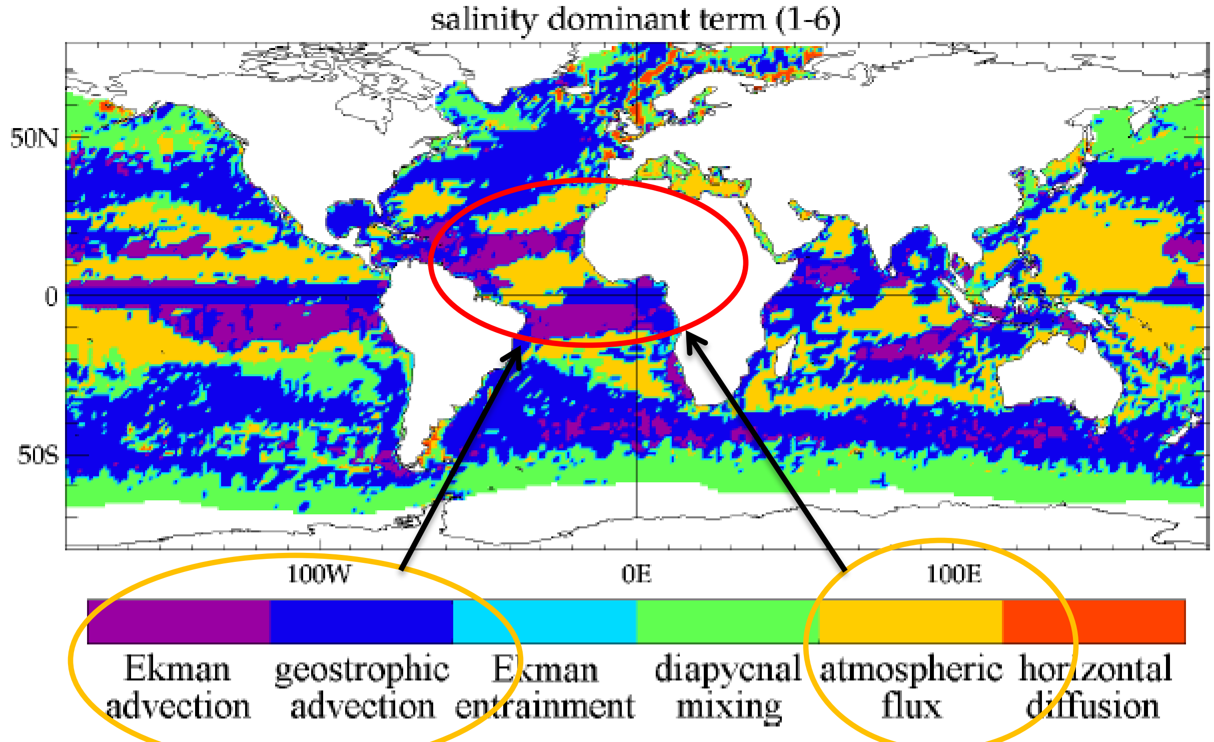

Fig. 11. Dominant term of the mixed layer salinity balance from the simulation. Areas temporarily covered with sea-ice are excluded, as their mean amplitudes are not representative of the annual balance. (See the text for the computation details.)

OAflux TRMM-3B42 OSCAR (Ekman+geostrophic)

$$\frac{\partial S}{\partial t} = \frac{(E - P - R)S}{h} - \boldsymbol{u} \cdot \nabla S$$

smos

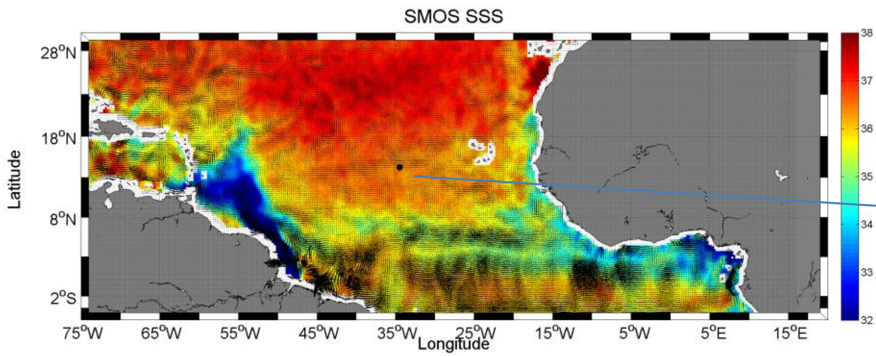
SMOS SSS
Latitude
Longitude
28°N
18°N
8°N
2°S
75°W
65°W
55°W
45°W
35°W
25°W
15°W
5°W
5°E
15°E
38
37
36
35
34
33
32

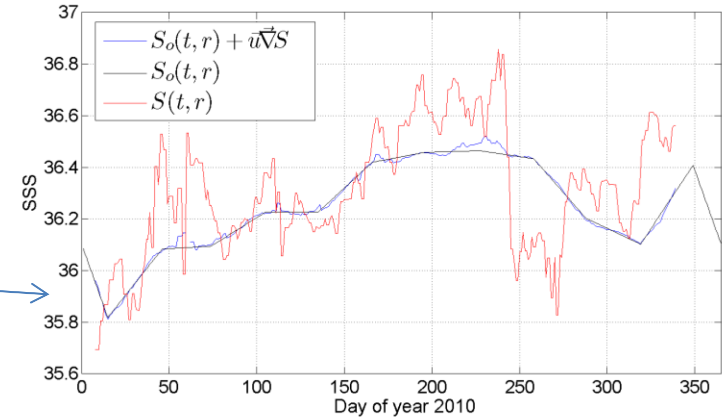
$S_o(t,r) + \vec{u}\vec{\nabla}S$
$S_o(t,r)$
$S(t,r)$
SSS
Day of year 2010

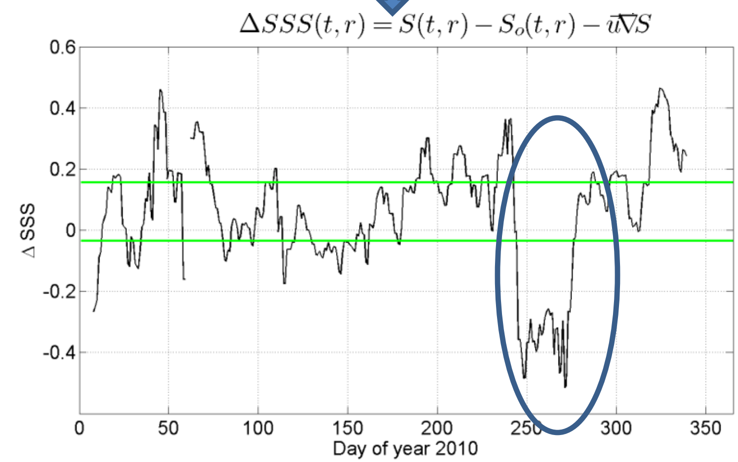
$\Delta SSS(t,r) = S(t,r) - S_o(t,r) - \vec{u}\vec{\nabla}S$
Δ SSS
Day of year 2010

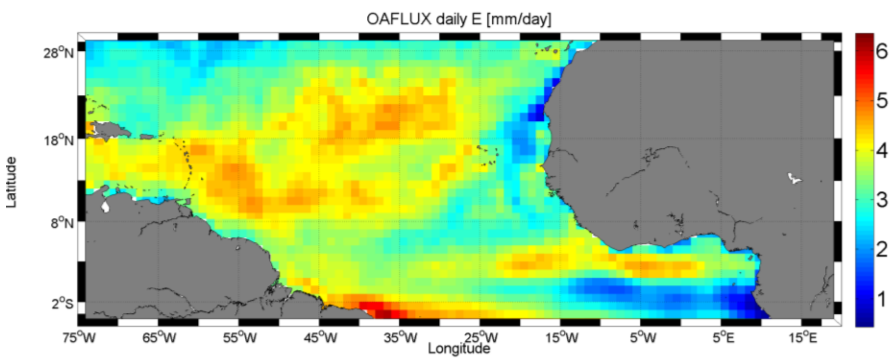
OAFLUX daily E [mm/day]
Latitude
Longitude

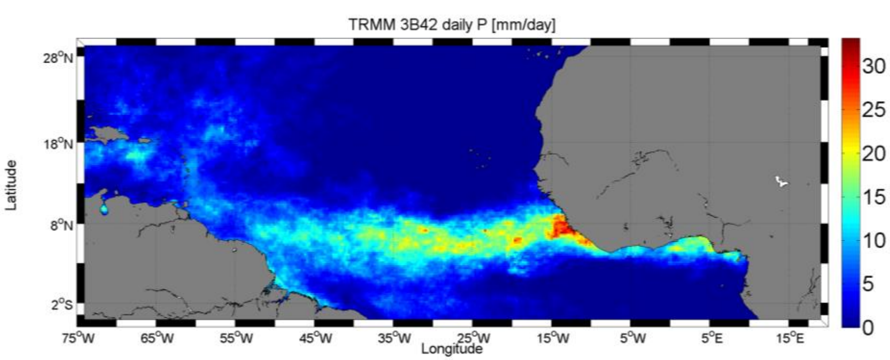
TRMM 3B42 daily P [mm/day]
Latitude
Longitude

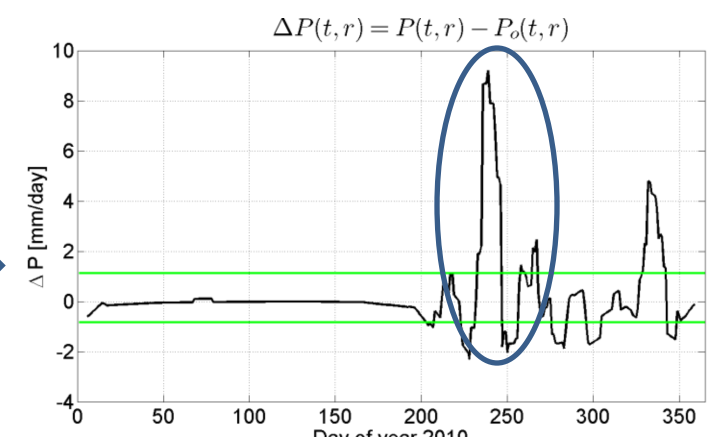
$\Delta P(t,r) = P(t,r) - P_o(t,r)$
Δ P [mm/day]
Day of year 2010

Connection between SSS anomalies and atmospheric fresh water fluxes

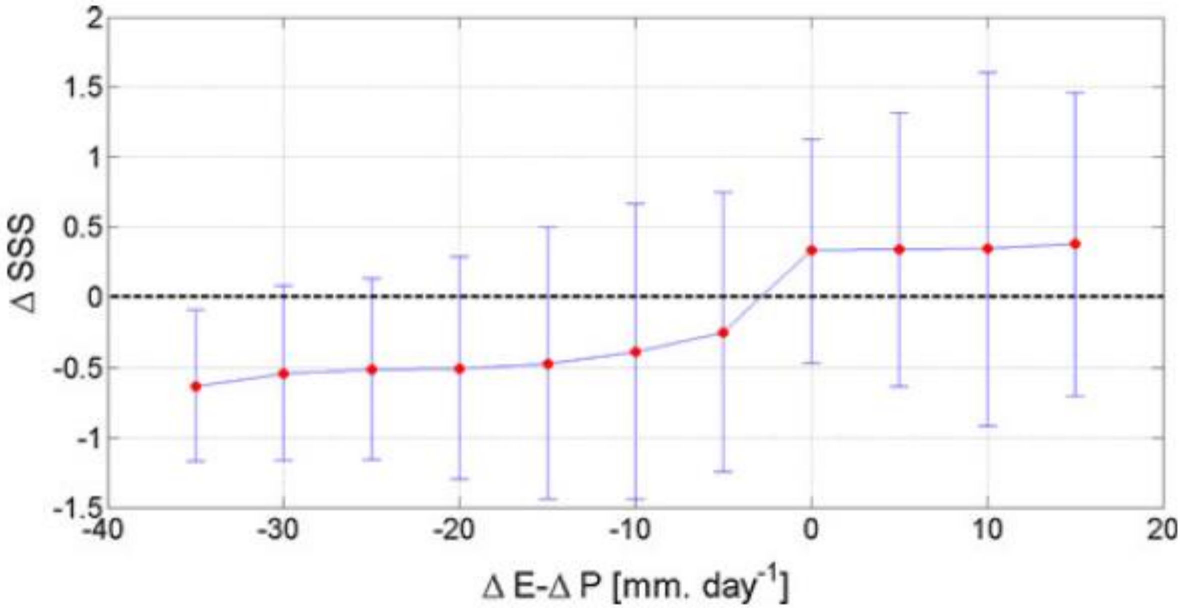

Fig. 18 Average relationship between SMOS SSS anomalies and the net atmospheric freshwater flux anomalies ΔE–ΔP in the tropical Atlantic (defined here by 5°S–20°N;75°W–15°E) over year 2010

Analysis of the SSS variability in the Tropical Atlantic

Tzortzi et al., GRL 2013

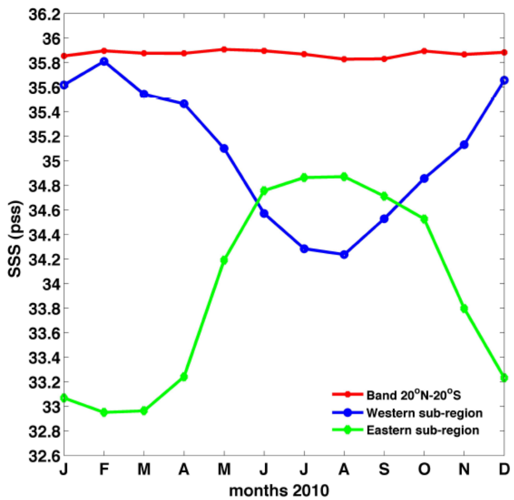

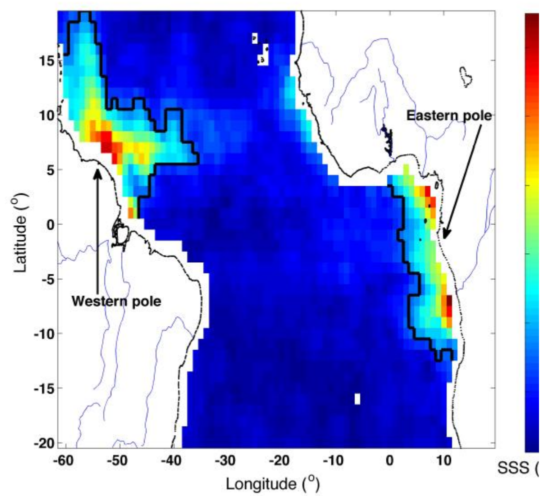

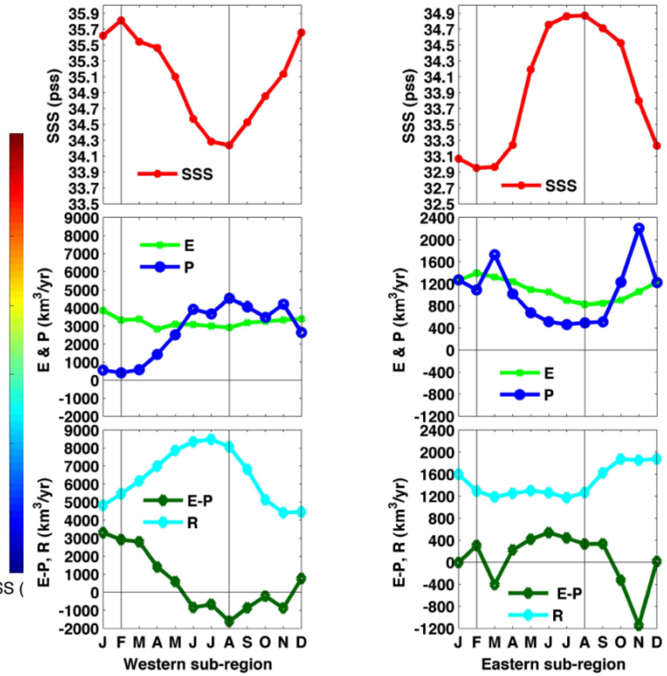

SSS in the western and Eastern Tropical Atlantic show
Out-of-phase (6 months) seasonal variations
And largely compensate each other for the whole Tropical Atlantic

Western Atl: SSS vary in phase with E-P and lag R by 2 months
Eastern Atl: more complex relashionships

Signature of Indian ocean Dipole in SMOS SSS

Durand et al. In press 2013

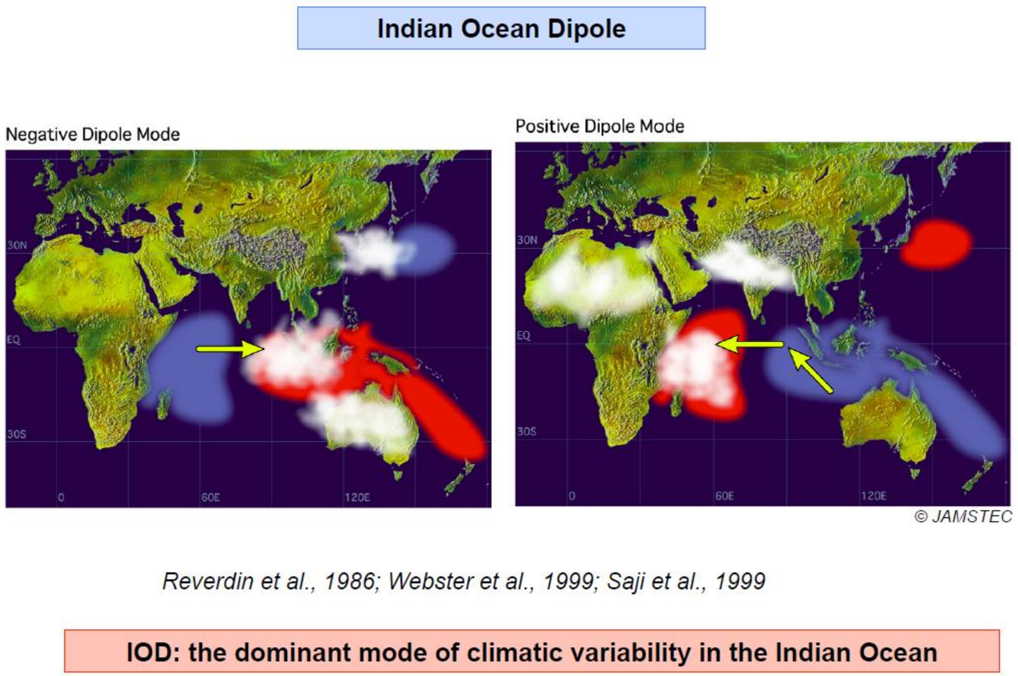

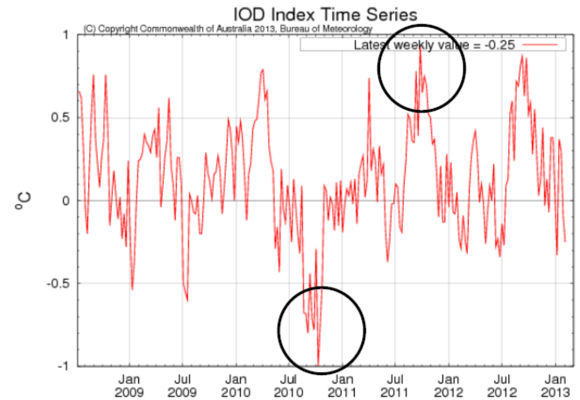

IOD-/IOD+ peaks in november 2010/2011

SSS anomalies: forcing factors ?

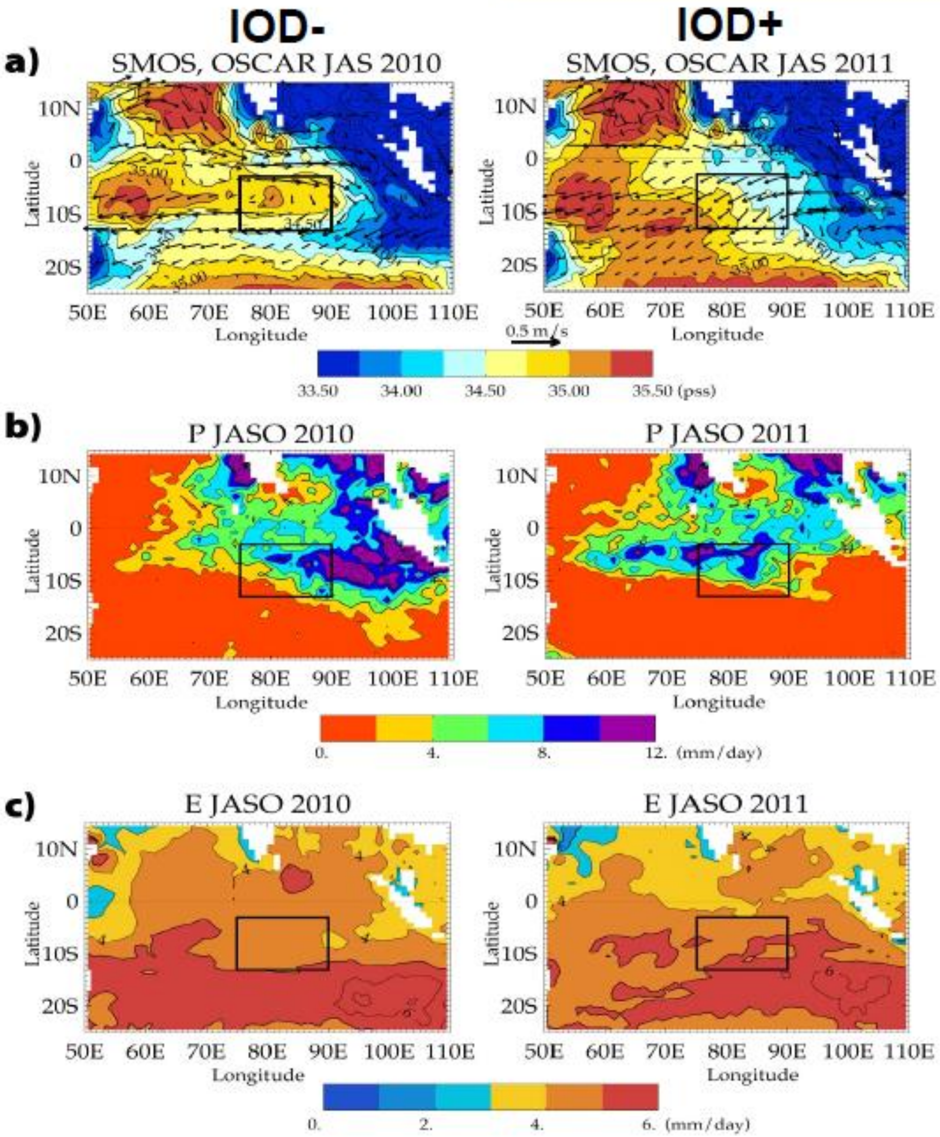

- SMOS SSS (contours) and OSCAR surface current (vectors) averaged during July-September 2010 (left) and during July-September 2011(right).
- TMI precipitation averaged during July-October 2010 (left) and during July-October 2011 (right)
- Same as (b), for OAFLUX evaporation.

One good candidate: horizontal currents

SSS from Space:
a new tool
to monitor the large scale
upwelling systems

Seasonal dynamics of Sea Surface Salinity off Panama : the Far Eastern Pacific Fresh Pool

Gaël Alory, Christophe Maes, Thierry Delcroix, Nicolas Reul, Serena Illig, 2012: **Seasonal dynamics of Sea Surface Salinity off Panama: the Far Eastern Pacific Fresh Pool.** Journal of Geophysical Research, Vol. 117, C04028, doi:10.1029/2011JC007802, 2012.

Why focus on SSS in the the Far Eastern Pacific Fresh Pool?

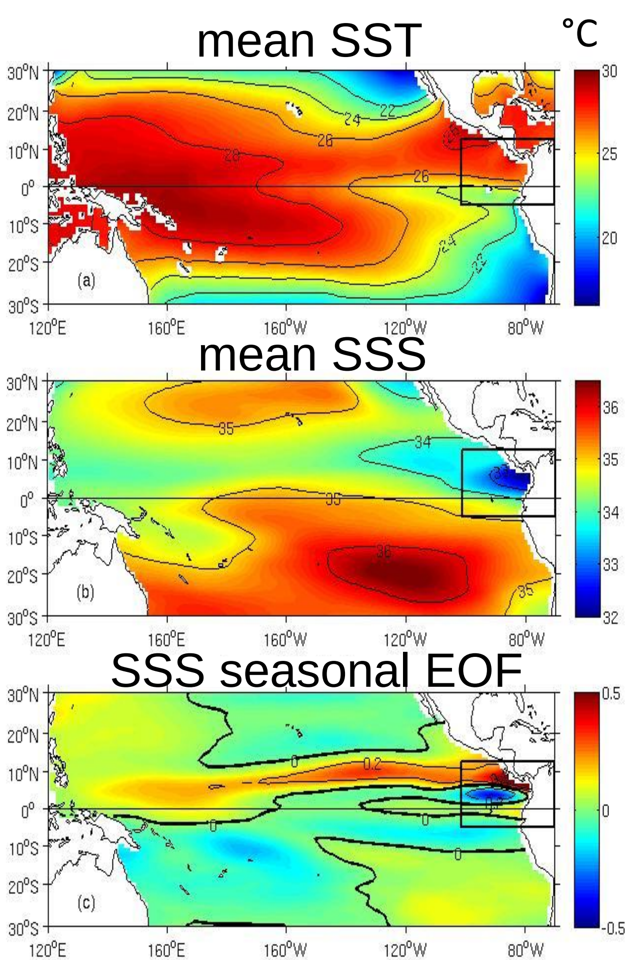

Delcroix et al., 2011

- Between 2 climate relevant features: Eastern Pacific warm pool and equatorial cold tongue
- Minimum in SSS (<33: Far Eastern Pacific Fresh Pool) and maximum seasonal variability
- Strong air-sea-land interactions in this region: monsoon, gap winds... (*e.g. Xie et al. 2005, Fiedler and Talley 2006, Kessler 2006*)
- Potentially active role of salinity stratification on regional climate (*de Boyer Montegut et al. 2007*)
- Good test ground for new SSS satellite products (SMOS, Aquarius)

Main SSS data source: Voluntary Observing Ships

1950-2009 obs. density

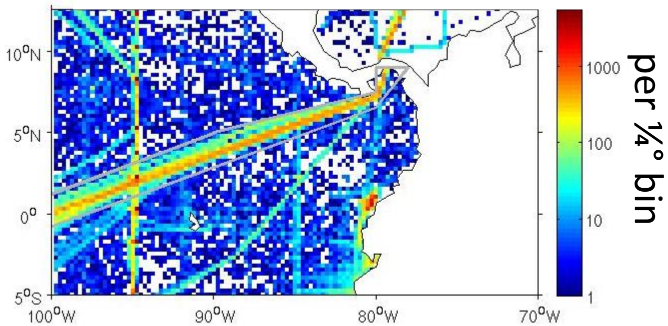

Well-sampled TSG line from Panama canal to Tahiti

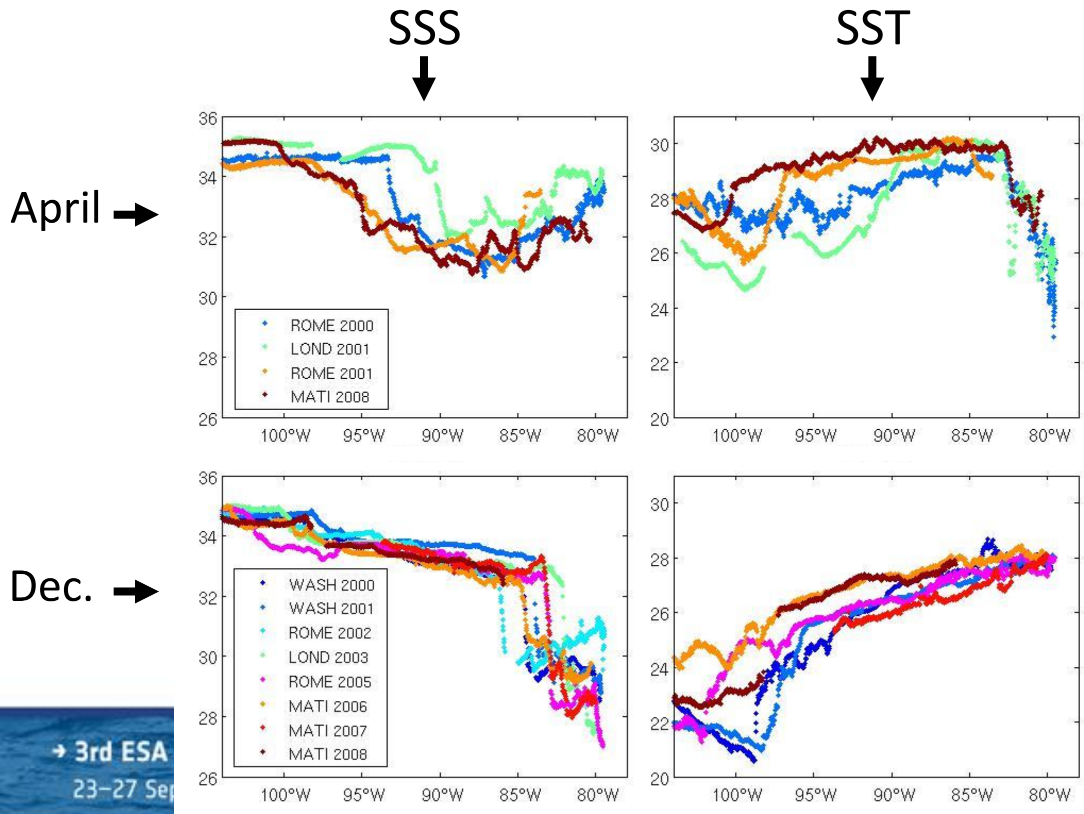

Transect snapshots

- Steep SSS fronts (up to 4 pss/1°) at Fresh Pool west/east boundaries with seasonal displacement >1000 km

- Not always related to SST fronts

SMOS detection of the Upwelling in April 2010

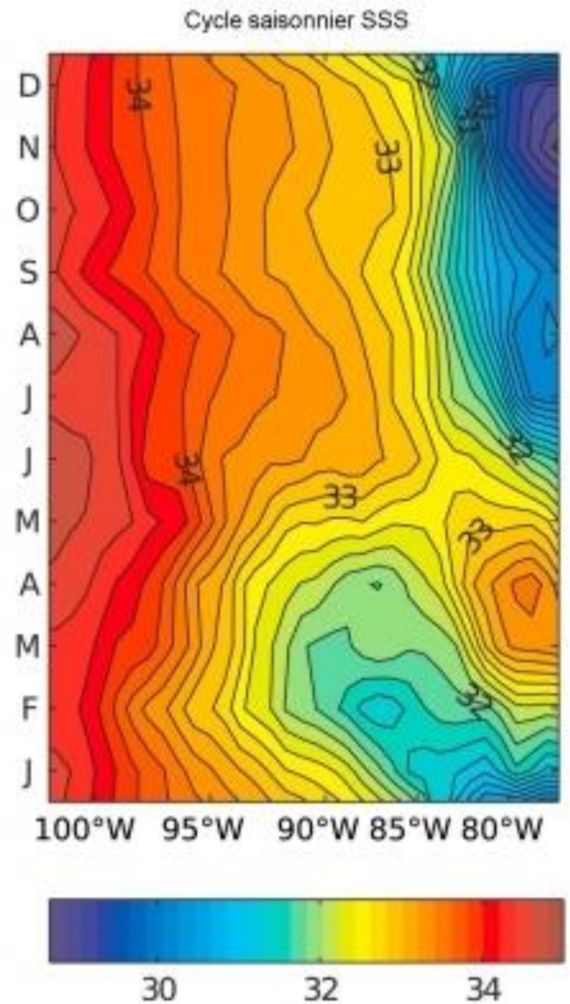

SMOS

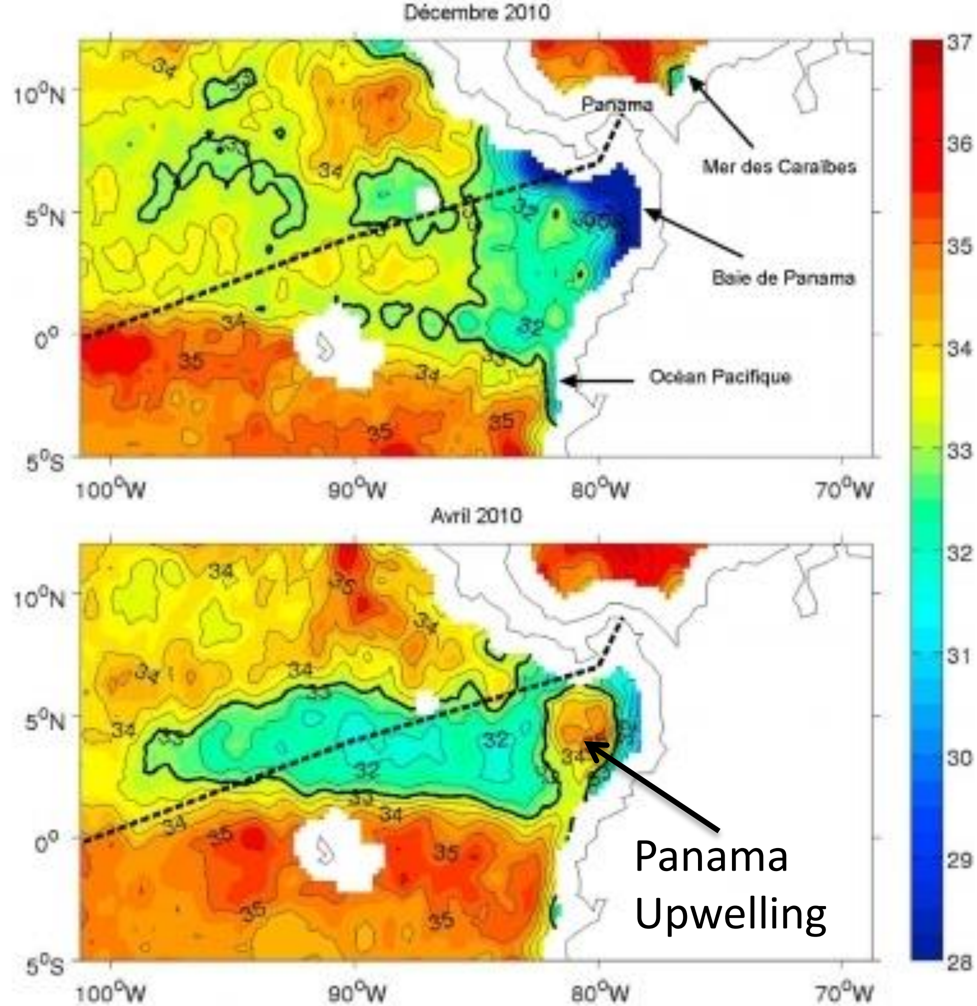

SMOS detection of the Panama Upwelling in 2011

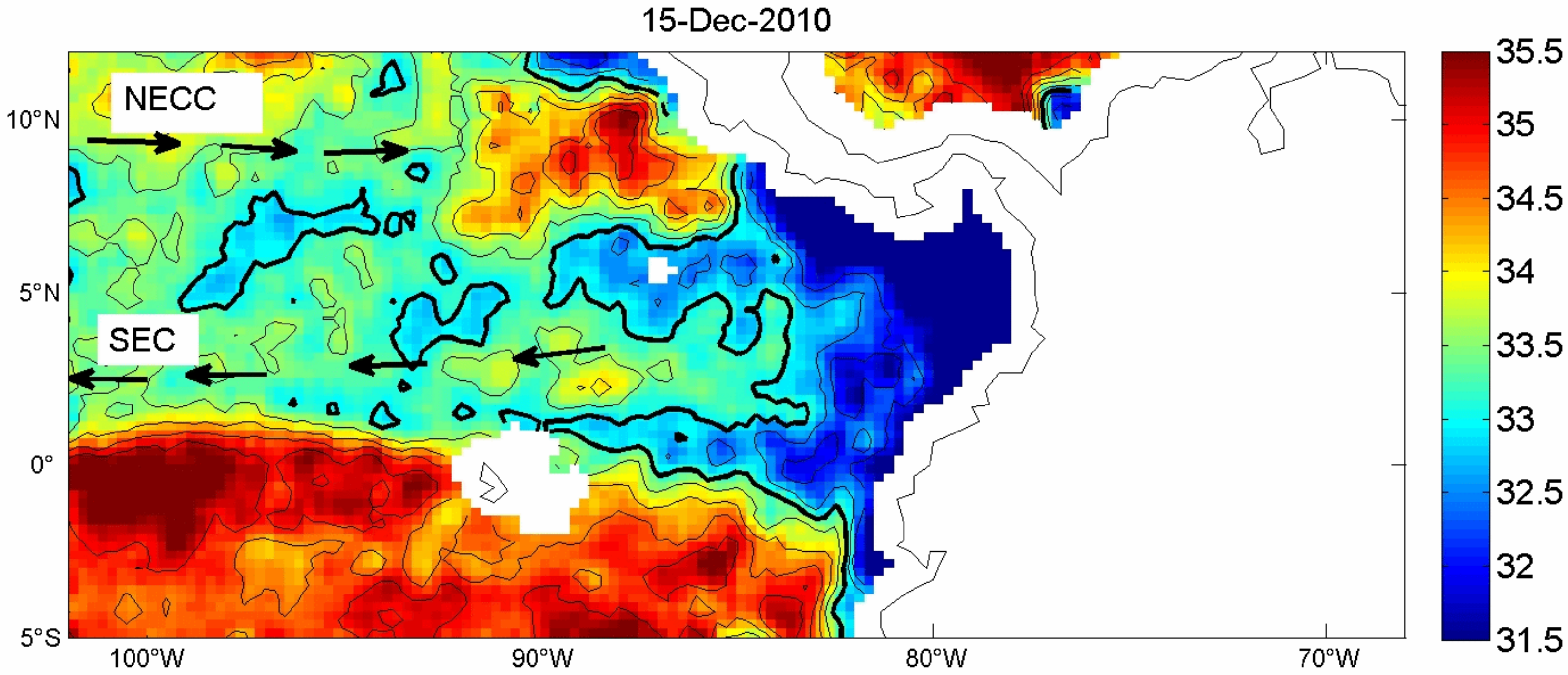

by N. Reul –CATDS products

SMOS detection of the Upwelling in 2012

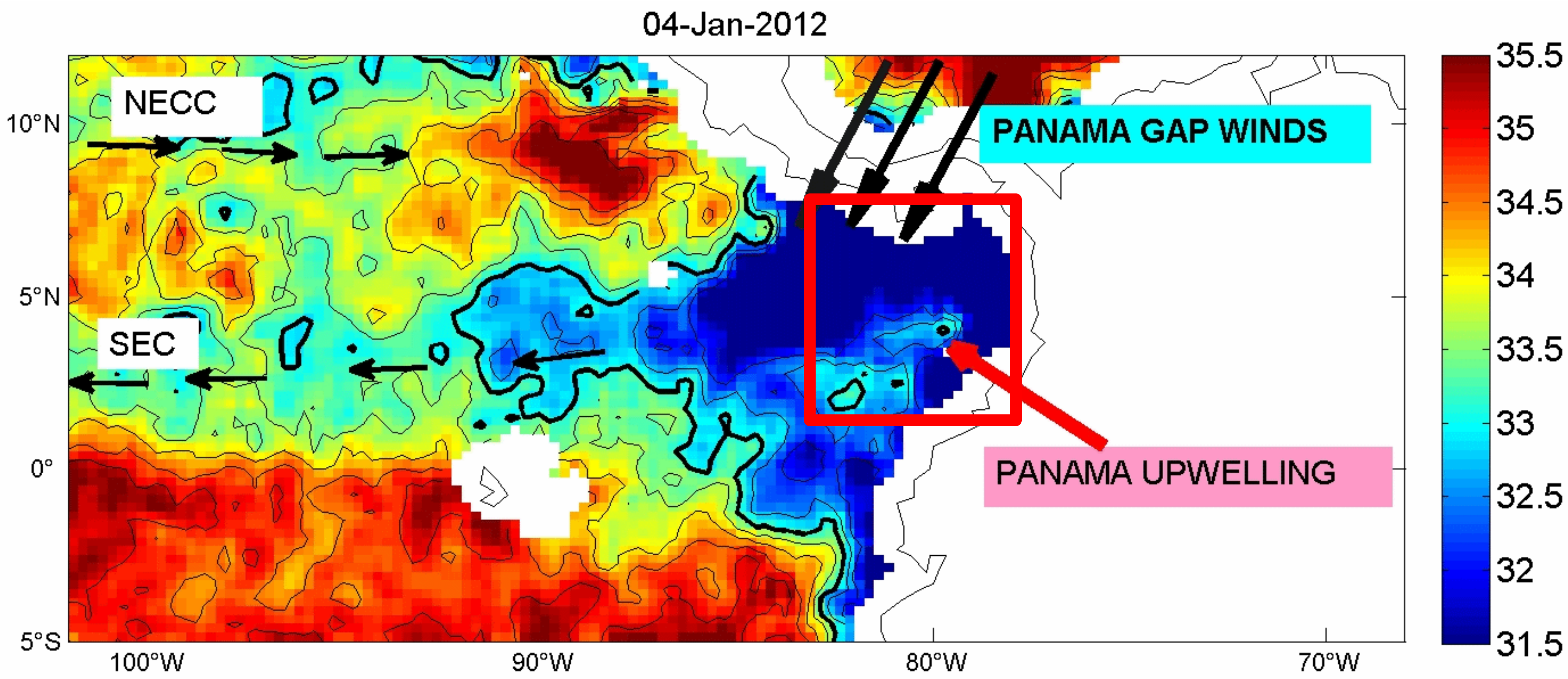

Fresh Pools interactions with wind-driven processes

Far Eastern pacific
Freshpool SSS
Variability

Alory et al., JGR 2012
Reul et al., Surv Geop, 2013

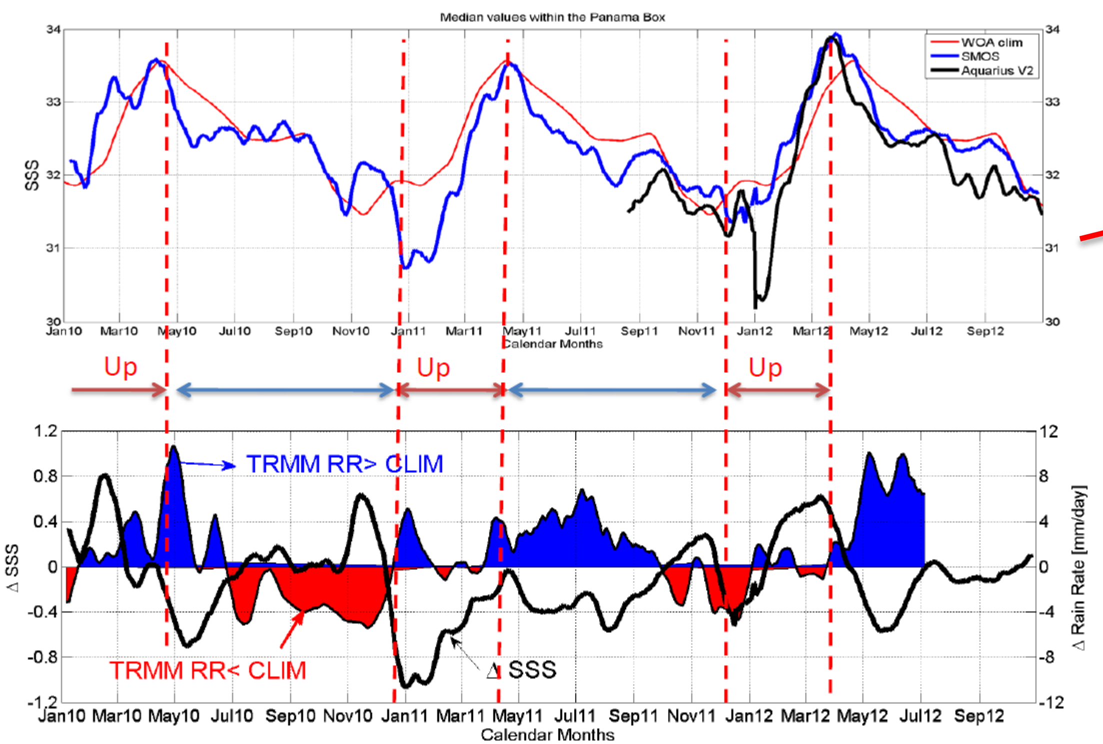

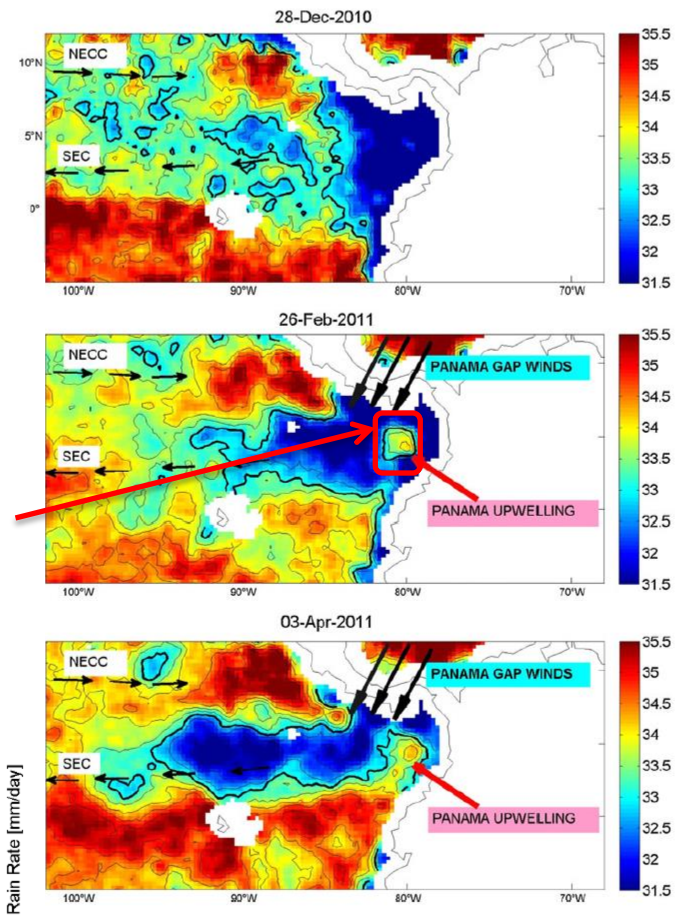

24 10-Day averaged SMOS SSS fields centered on the December 28, 2010 (*top*), February 16, 2011 *dle*), and April 3, 2011 (*bottom*). *Small black arrows* indicate the major surface currents, namely the equatorial current (SEC) and NECC. *Thick black contour* is indicating the 32 pss isohaline

Cross-frontal exchanges of salt in the Gulf-stream area

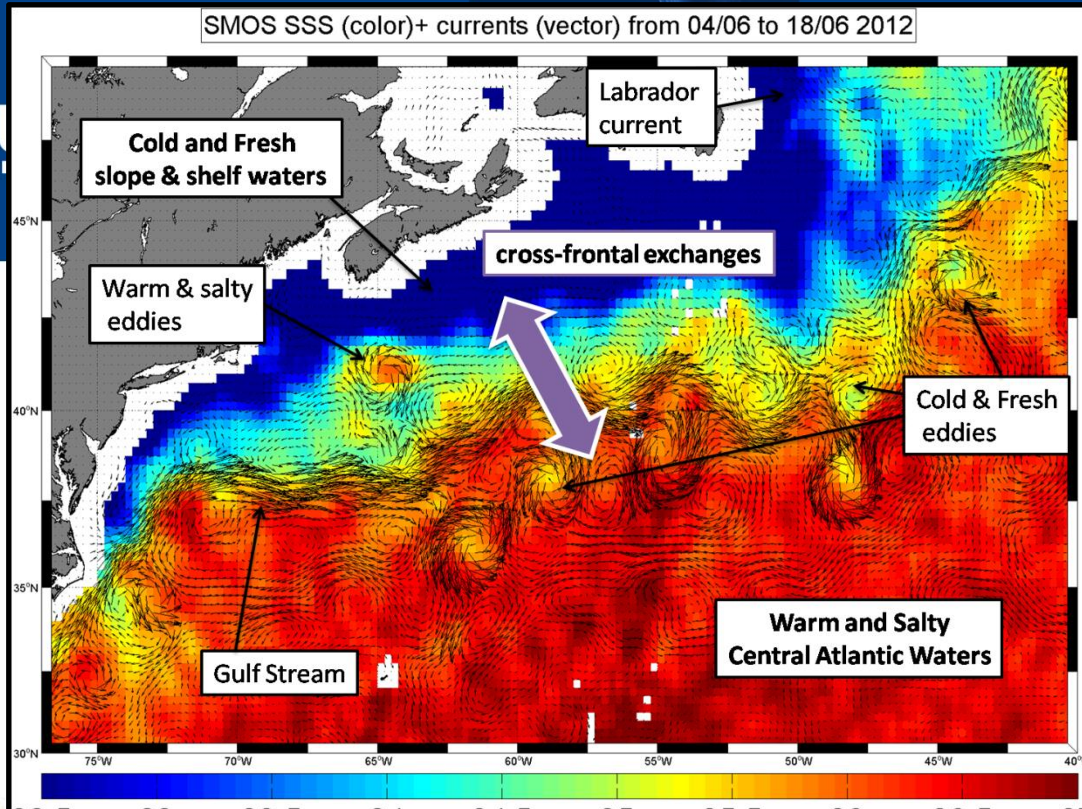

Reul et al., to be submitted to GRL, 2013

Questions:

1) Is SMOS able to track Near-Surface Transport Pathways of salt in the North Atlantic Ocean ?

⇒Looking for Throughput from the Subtropical to the Subpolar Gyre

2) How SMOS data complement SST & SSH informations to better track meso-scale features

3) What accuracy of SMOS products at moderate to low SSTs ?

4) Can SMOS data be used to better monitor biological productivity ?

Cross-frontal exchanges of salt in the Gulf-stream area

RFI context: this area can only be studied starting in 2012 when radar due-line contamination disapeared

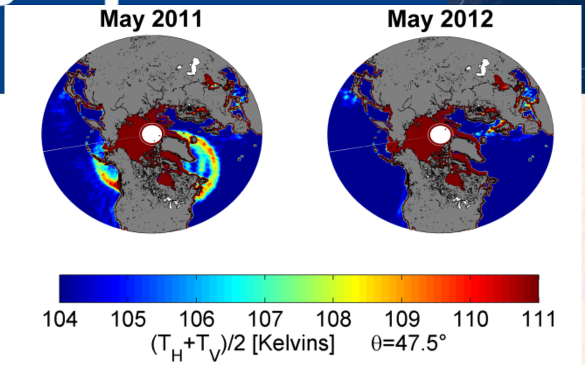

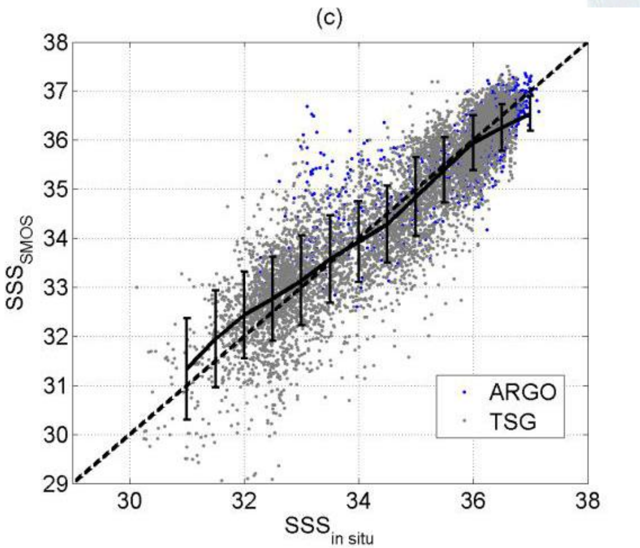

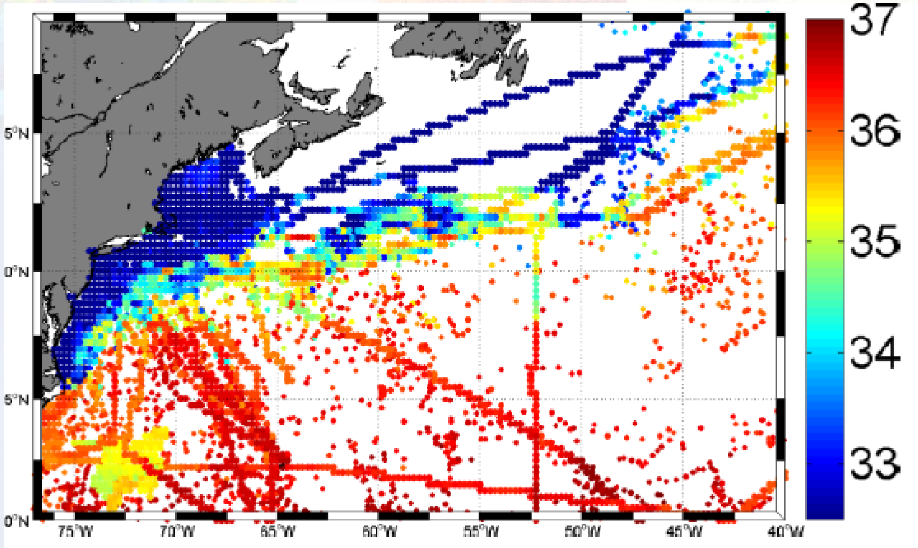

SMOS 25 km res-10 days composite rms diff with in situ ~0.5 psu

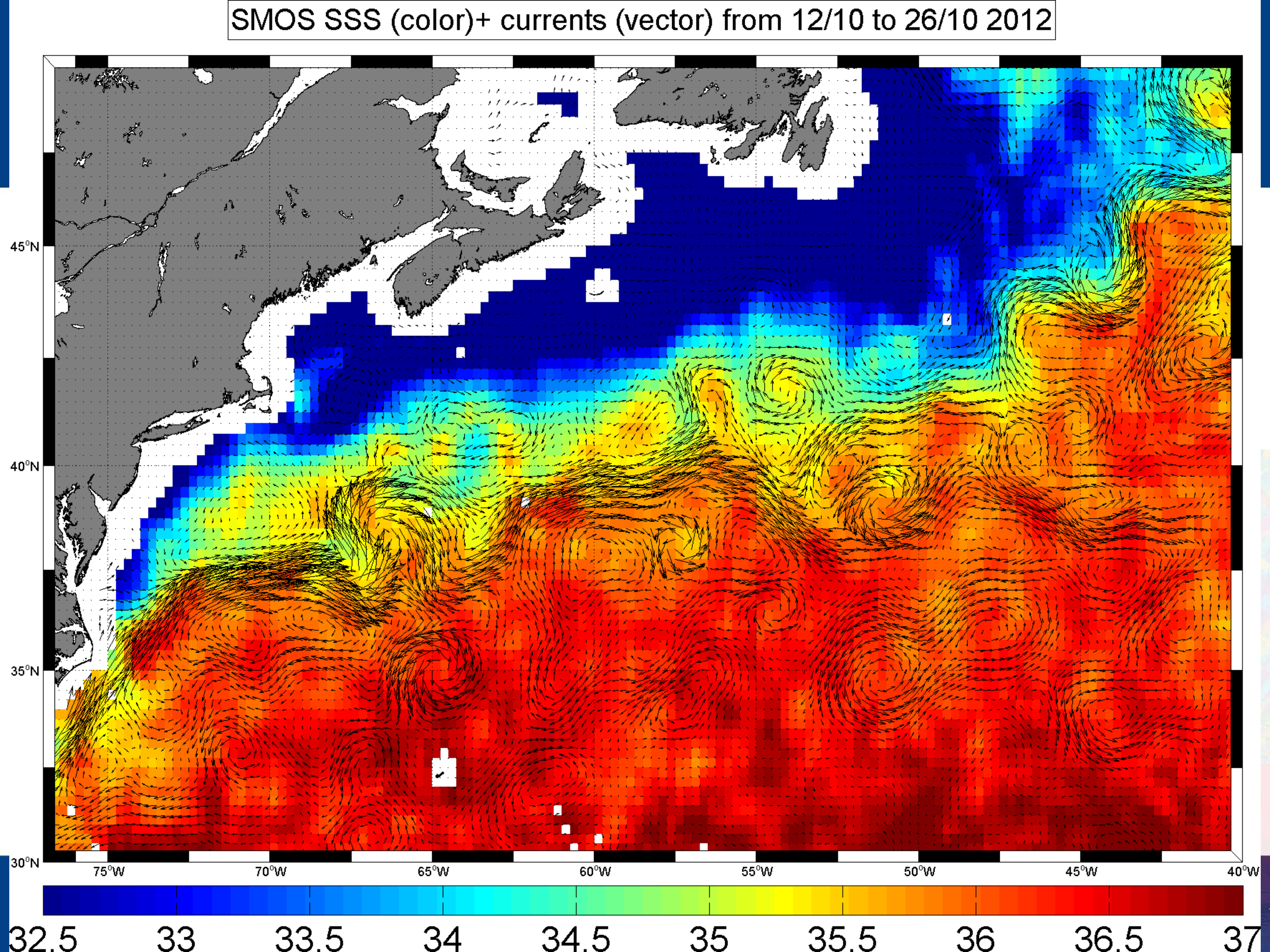
SMOS SSS (color)+ currents (vector) from 12/10 to 26/10 2012
45°N
40°N
35°N
30°N
75°W
70°W
65°W
60°W
55°W
50°W
45°W
40°W
32.5
33
33.5
34
34.5
35
35.5
36
36.5
37

living p

Detection of

Warm & salty core Rings

Cold & Fresh core Rings

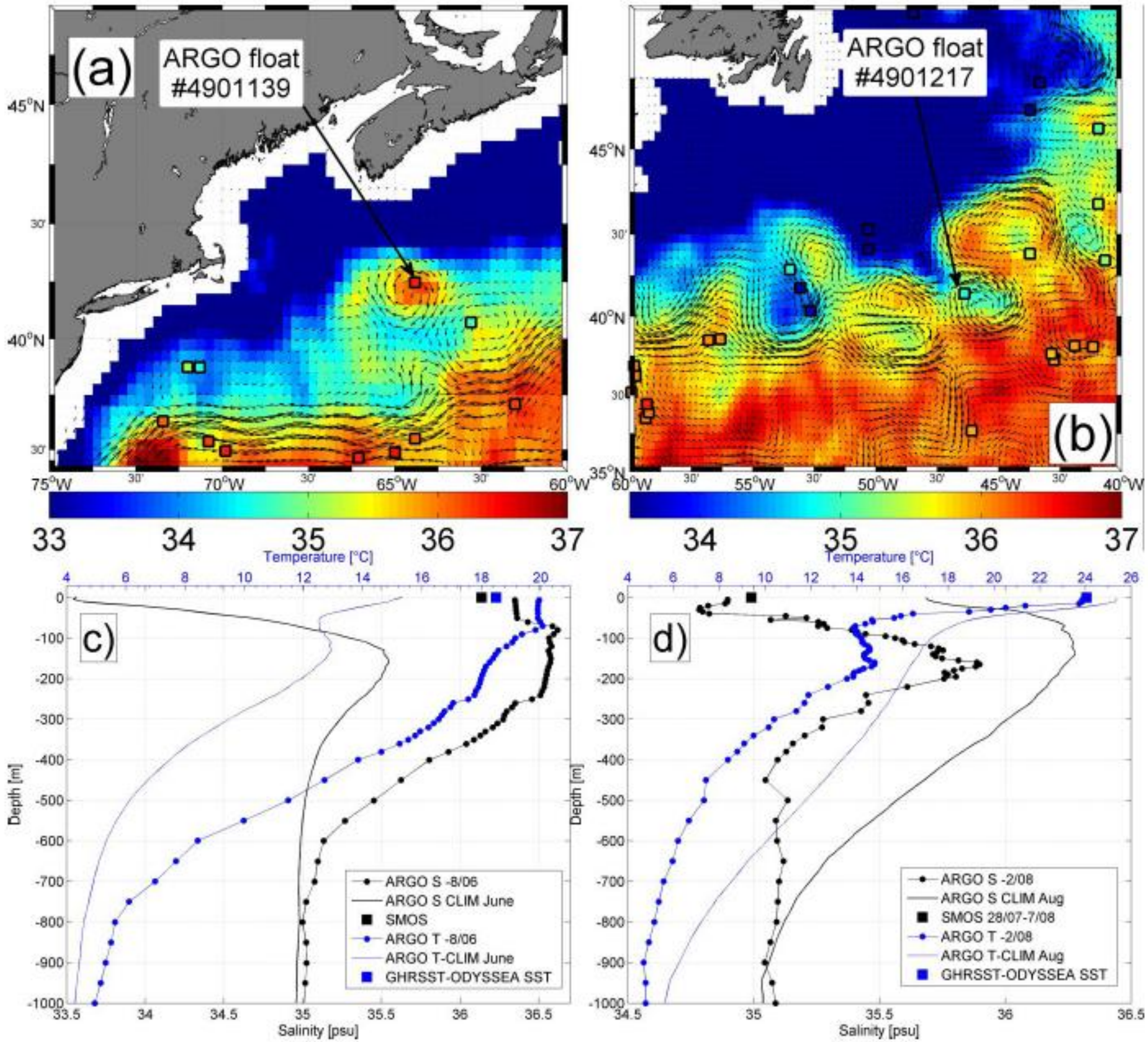

232

$$\rho(S,T) = \rho_o[1 + \beta S - \alpha T]$$

Smos SSS

SST (GHRSST)

Density anomlay fields
(remove LF components)

+Sea Level anomalies from merged altimeter products (Aviso)

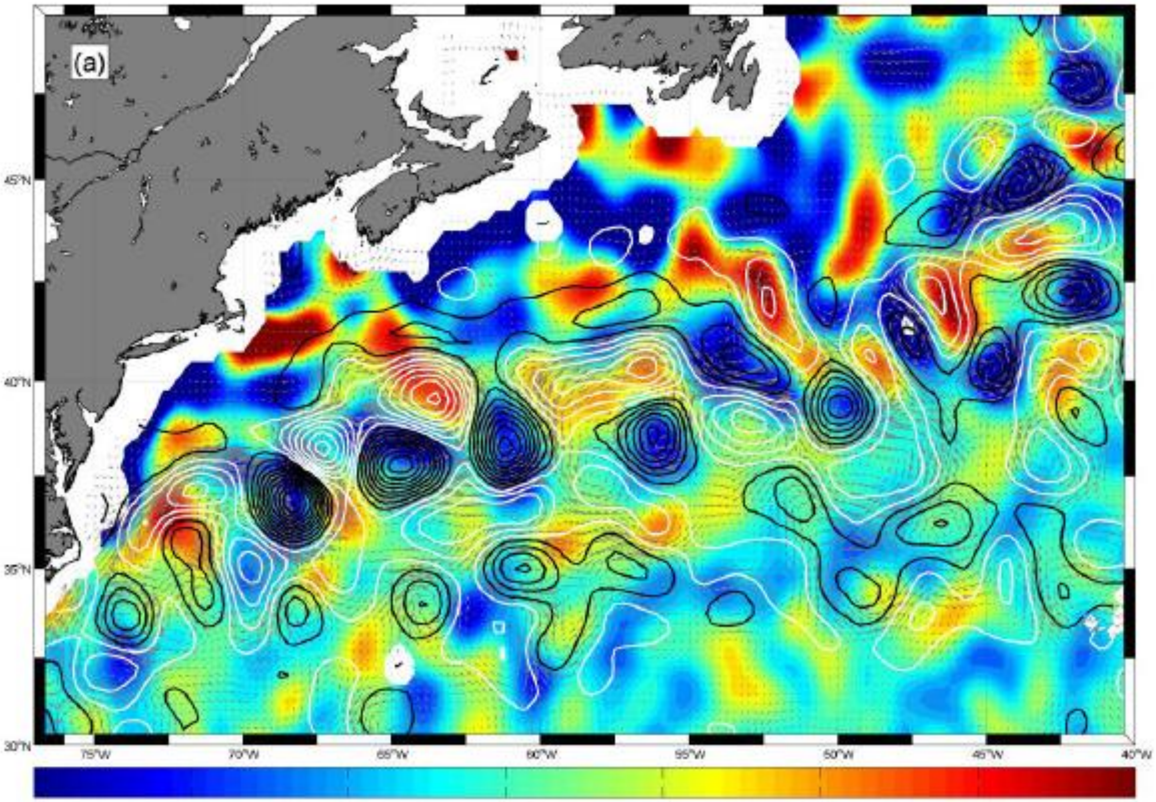

Kg/m3

Contours:

Positive SLA (white)
Negative SLA (black)

$$\widehat{\psi}_{surf}(\vec{k},z) = \frac{\widehat{b}_s(\vec{k})}{Nk} exp\left(\frac{Nkz}{f_o}\right)$$

Surface quasi-geostrophic theory
=> Retrieve surface currents from sat SSS & SST

If one assume SSS=35 and SST given by GHRSST

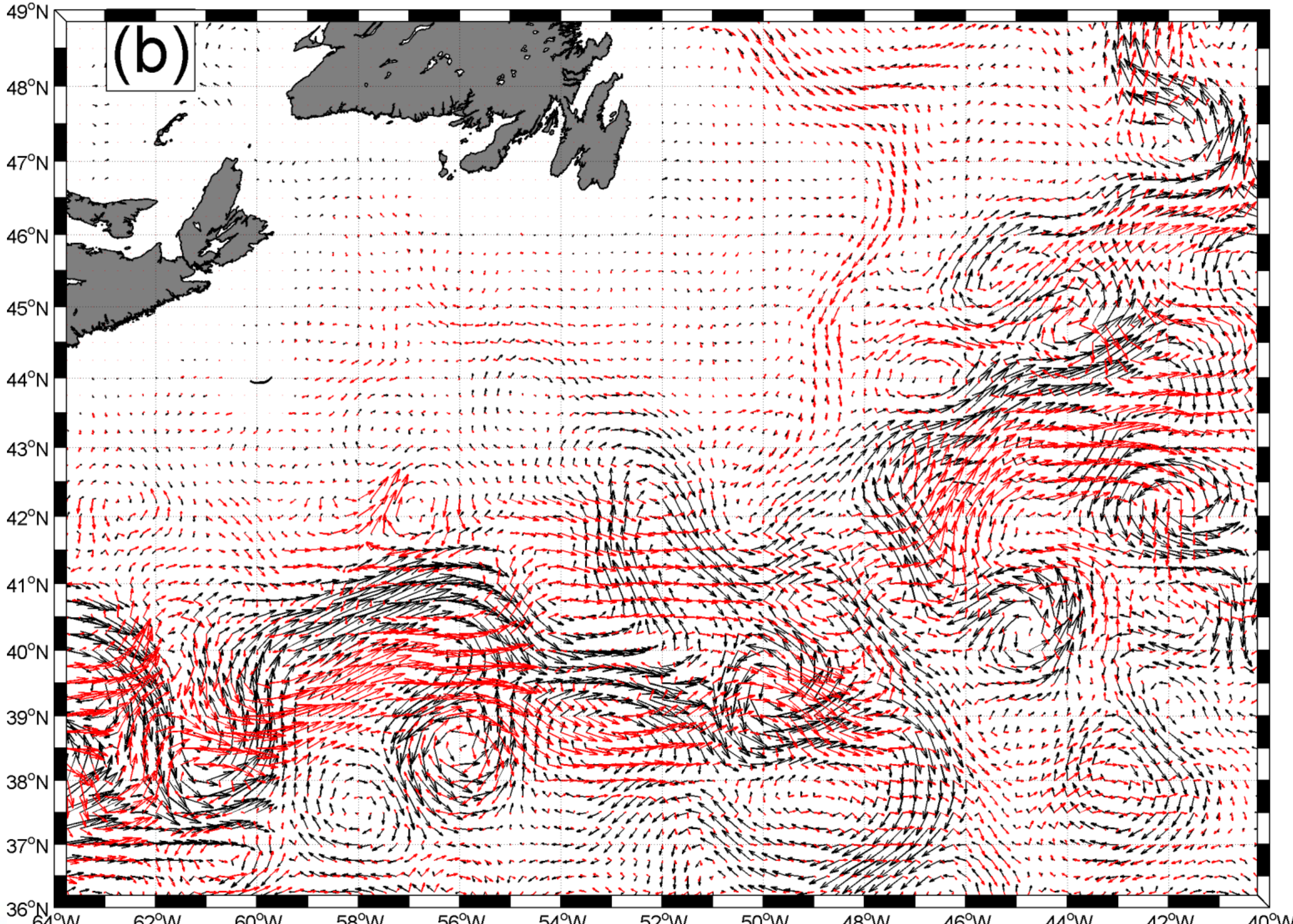

Red are currents from surface density, Black arrows are altimeter derived ones

$$\hat{\psi}_{surf}(\vec{k},z) = \frac{\hat{b}_s(\vec{k})}{Nk} exp\left(\frac{Nkz}{f_o}\right)$$

Surface Quasi-Geostrophy

=> Retrieve surface currents from sat SSS & SST

Now with SSS from SMOS and SST given by GHRSST

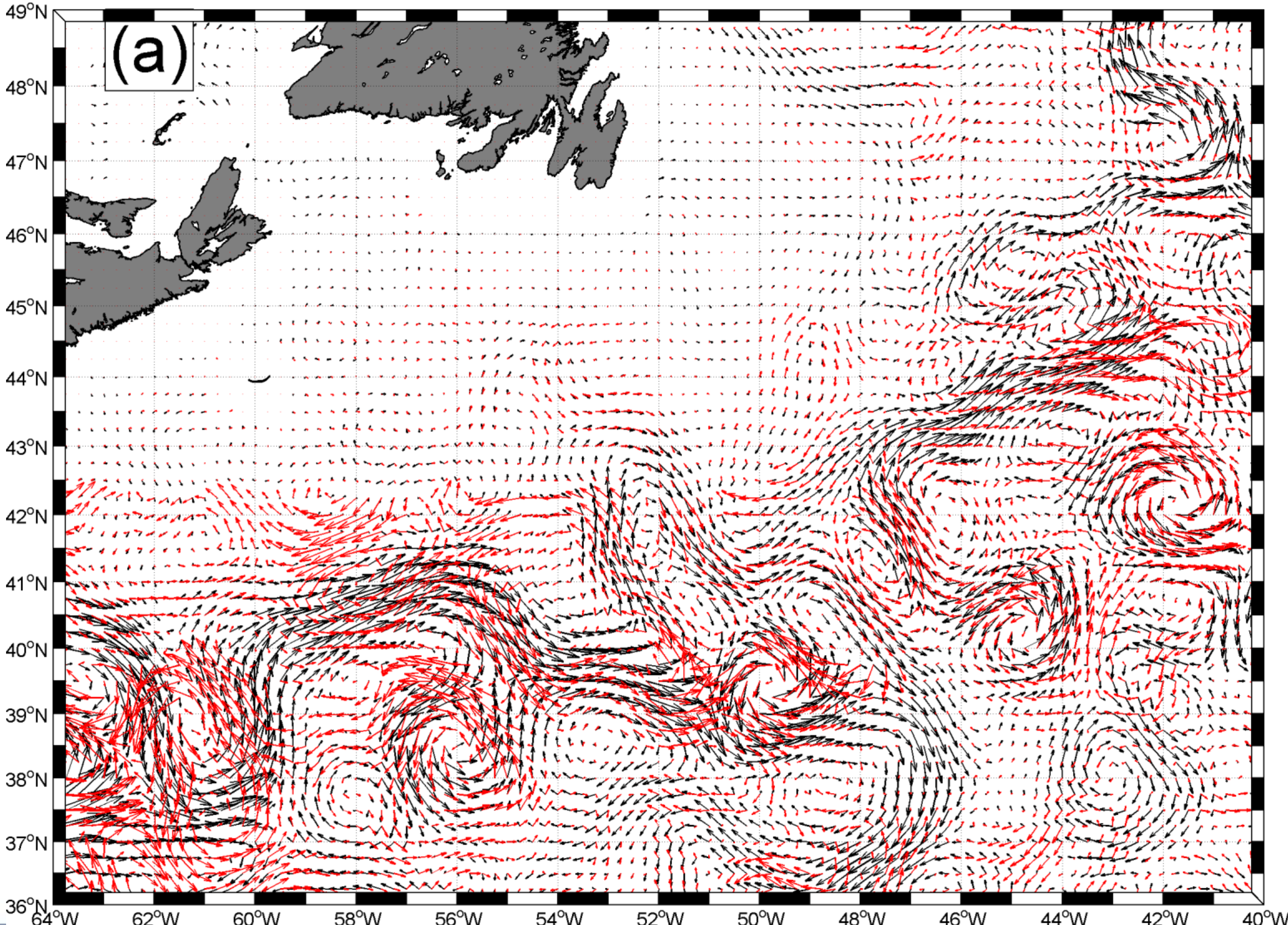

Relashionships between Chlorophylle-A, SSS and SST In the Gulf Stream area

winter

summer

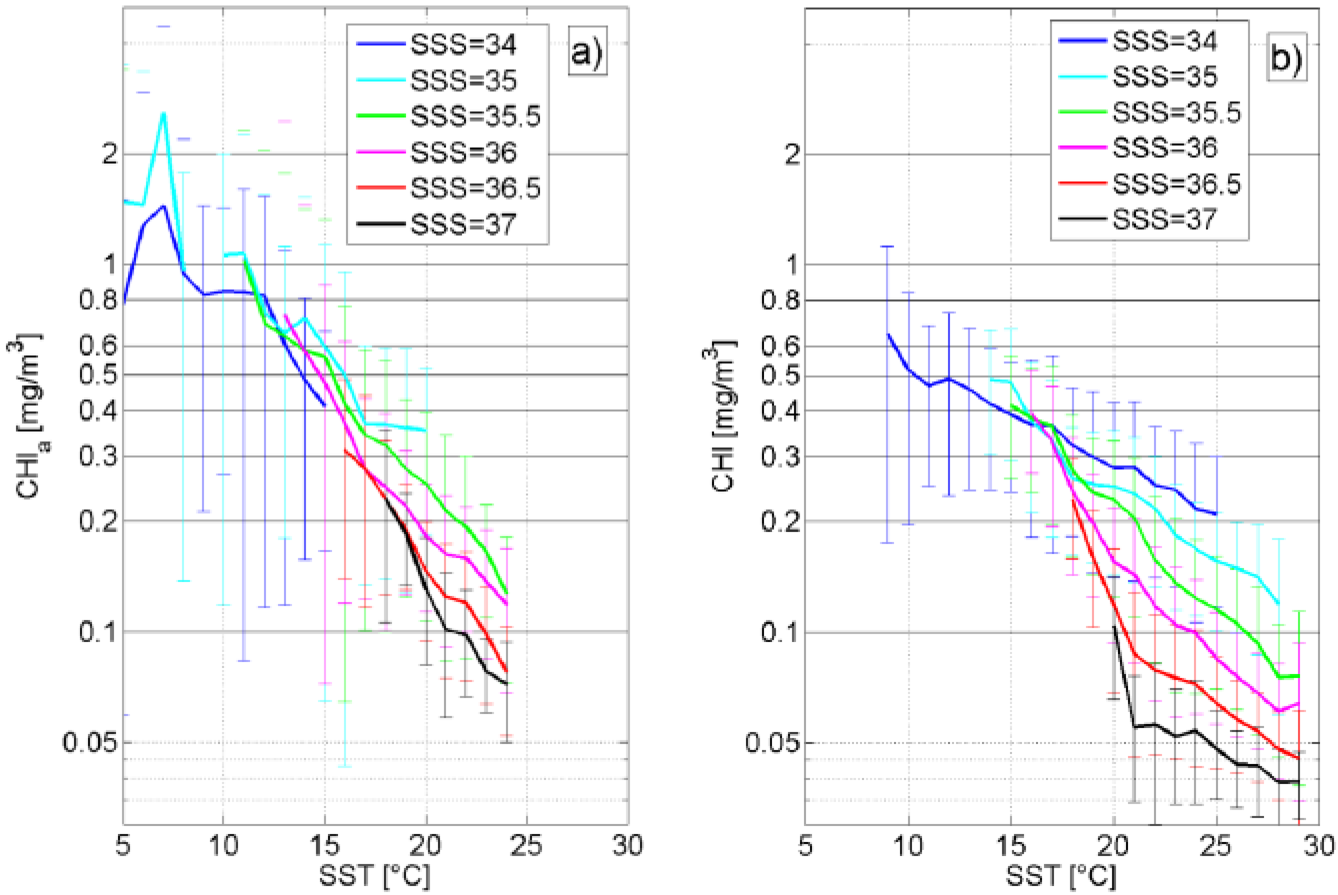

Figure 5: Seasonal variabilty of the Chlorophyll-a concentration from MODIS (a) January to May and (b) bin-averaged dependencies with SST and SSS in the North Atlantic domain [75°W-40°W;30°N-50°N] for year 2012.

Tropical Cyclone Monitoring with SMOS data

smos+
storms
support to science element

- Surface Wind Speed retrievals under hurricanes
- Barrier-Layer effects on Tropical Cyclone Intensification

Reul Nicolas, Tenerelli Joseph, Chapron Bertrand, Vandemark Doug, Quilfen Yves, Kerr Yann (2012). **SMOS satellite L-band radiometer: A new capability for ocean surface remote sensing in hurricanes**. *Journal Of Geophysical Research-oceans*, 117,, 117, C02006

Grodsky, S. A., N. Reul, G. Lagerloef, G. Reverdin, J. A. Carton, B. Chapron, Y. Quilfen, V. N. Kudryavtsev, and H.-Y. Kao (2012), **Haline hurricane wake in the Amazon/Orinoco plume: AQUARIUS/SACD and SMOS observations**, *Geophys. Res. Lett.*, 39, L20603, doi:10.1029/2012GL053335.

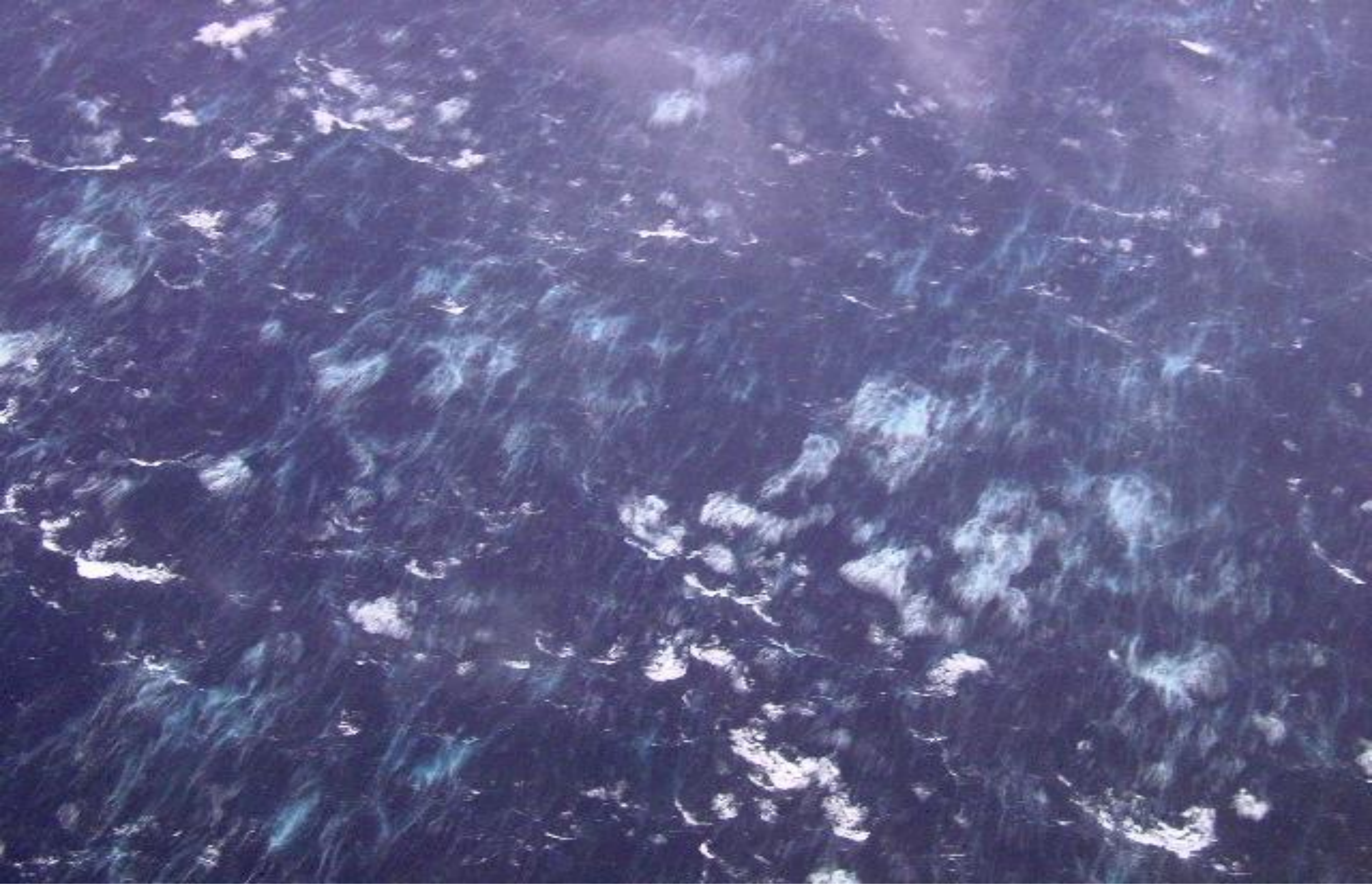

Figure 1: Photograph of the sea surface during a hurricane (Beaufort Force 12) taken from a NOAA ''Hurricane Hunter'' aircraft (Black *et al.*, 1986).

A complex distribution of two-phase oceanic phenomena

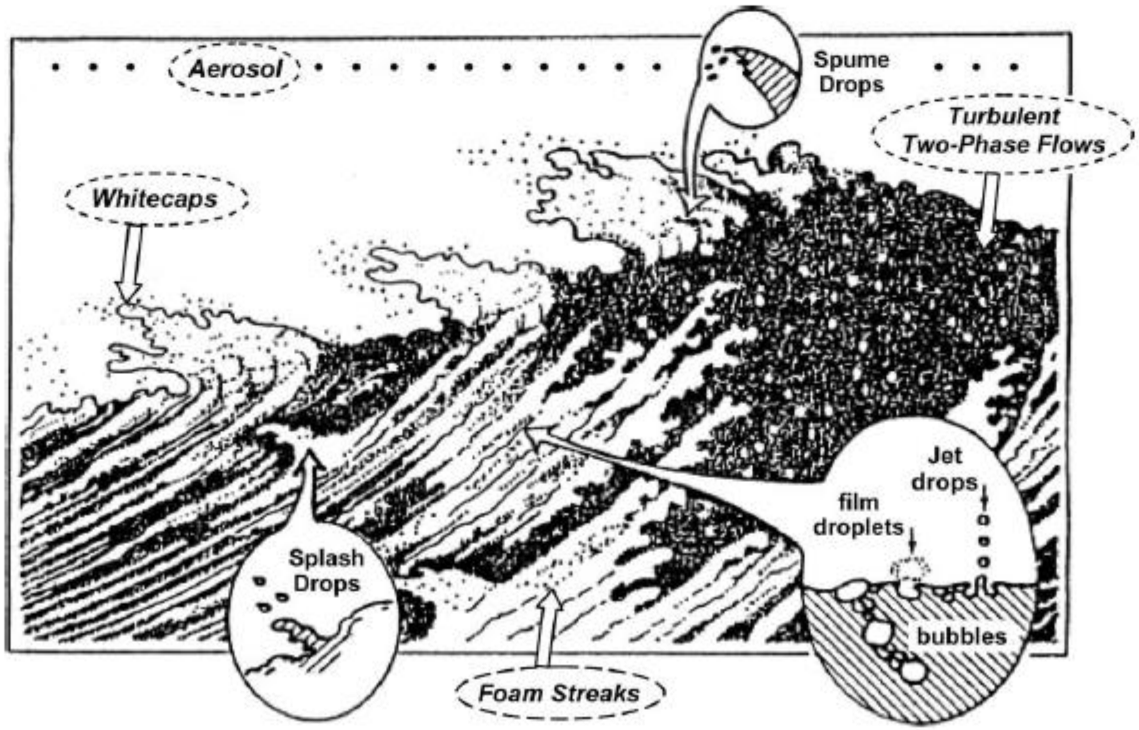

Fig. 1. Classifications of oceanic dispersed media for remote sensing.

Increase of the microwave ocean emissivity
with wind speed ⇔ foam change induce effect

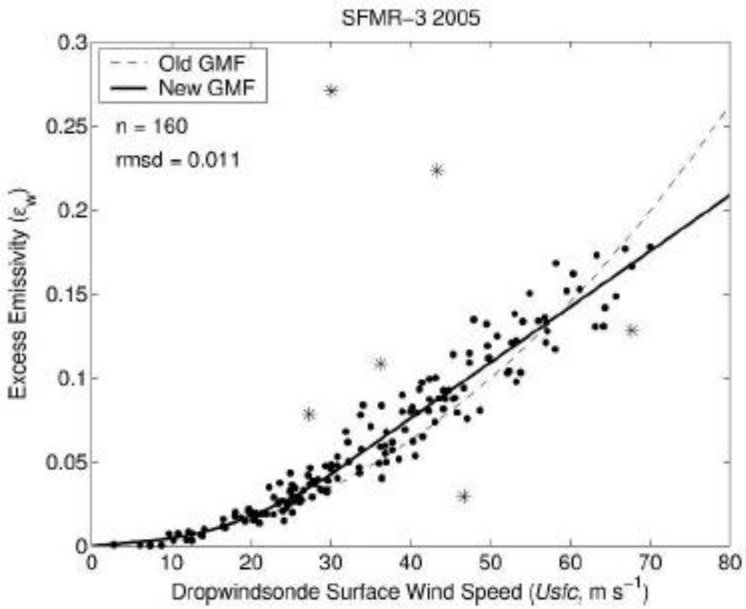

This information can be used to retrieve the surface wind speed in Hurricanes:

Principle of the Step Frequency Microwave Radiometer (SFMR) C-band:

NOAA's primary airborn sensor for measuring Tropical Cyclone surface wind speeds since 30 year (Ulhorn et al., 2003, 2007).

TC signatures in SMOS brightness Temperatures

Hurricane
DANIELLE

25-27 Aug 2010

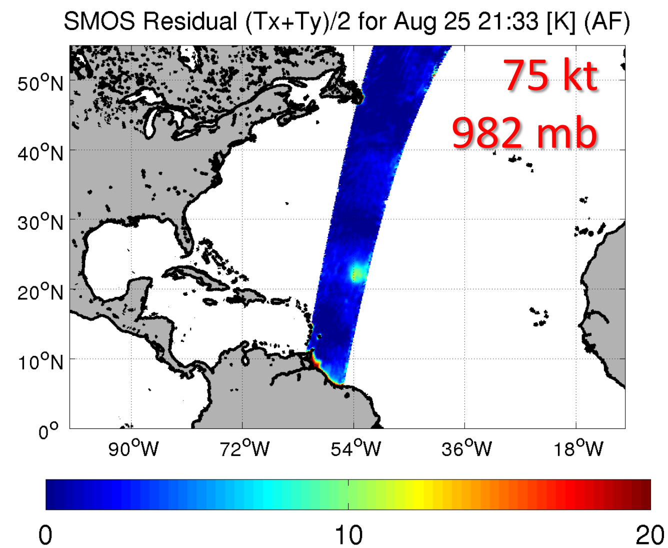

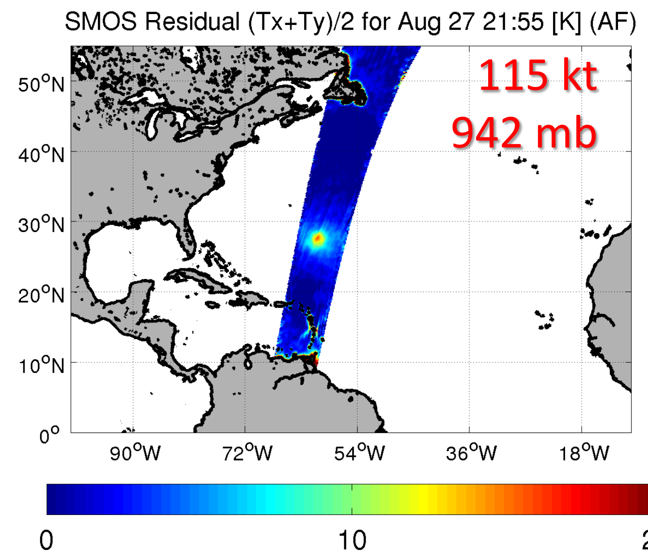

Hurricane
EARL
2-3 Sep
2010

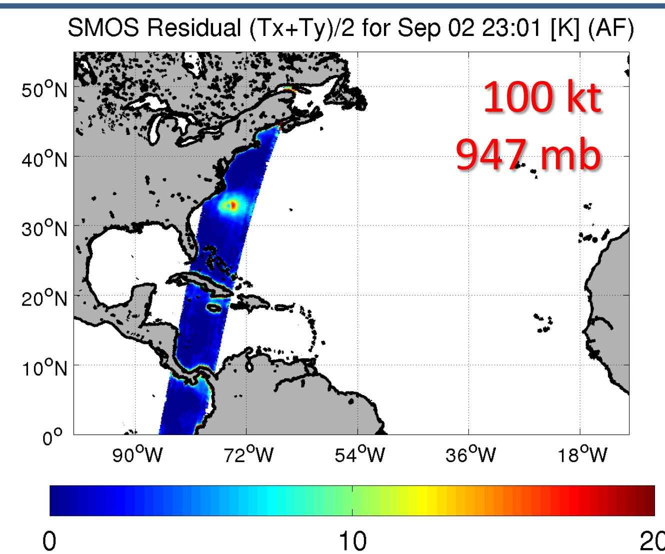

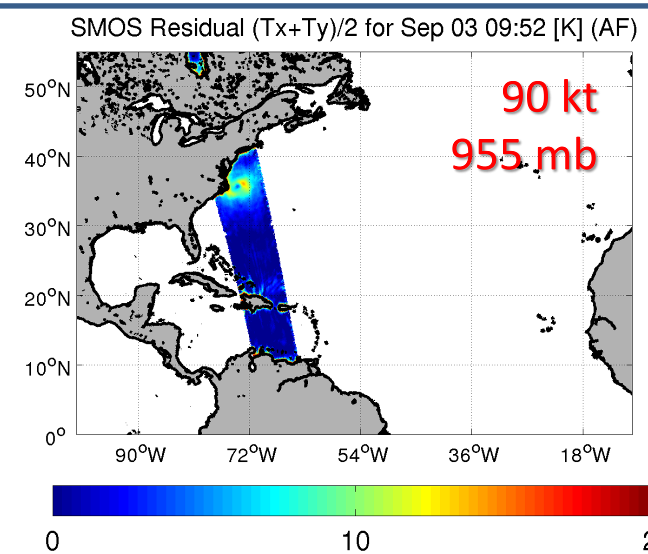

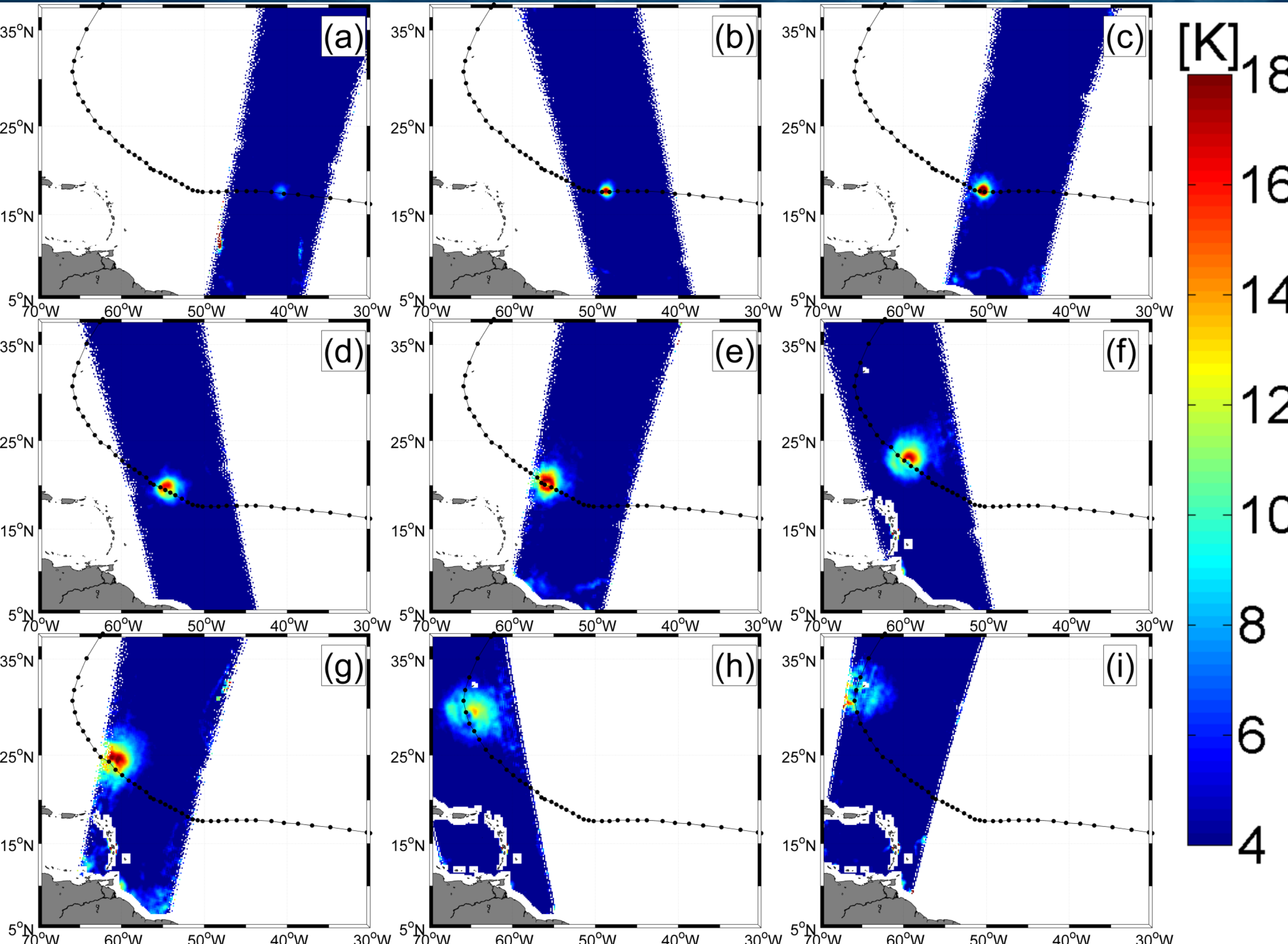
(a)
(b)
(c)
(d)
(e)
(f)
(g)
(h)
(i)
35°N
25°N
15°N
5°N
70°W
60°W
50°W
40°W
30°W
[K]
18
16
14
12
10
8
6
4

Geophysical Model function: Tb=f(wind speed)

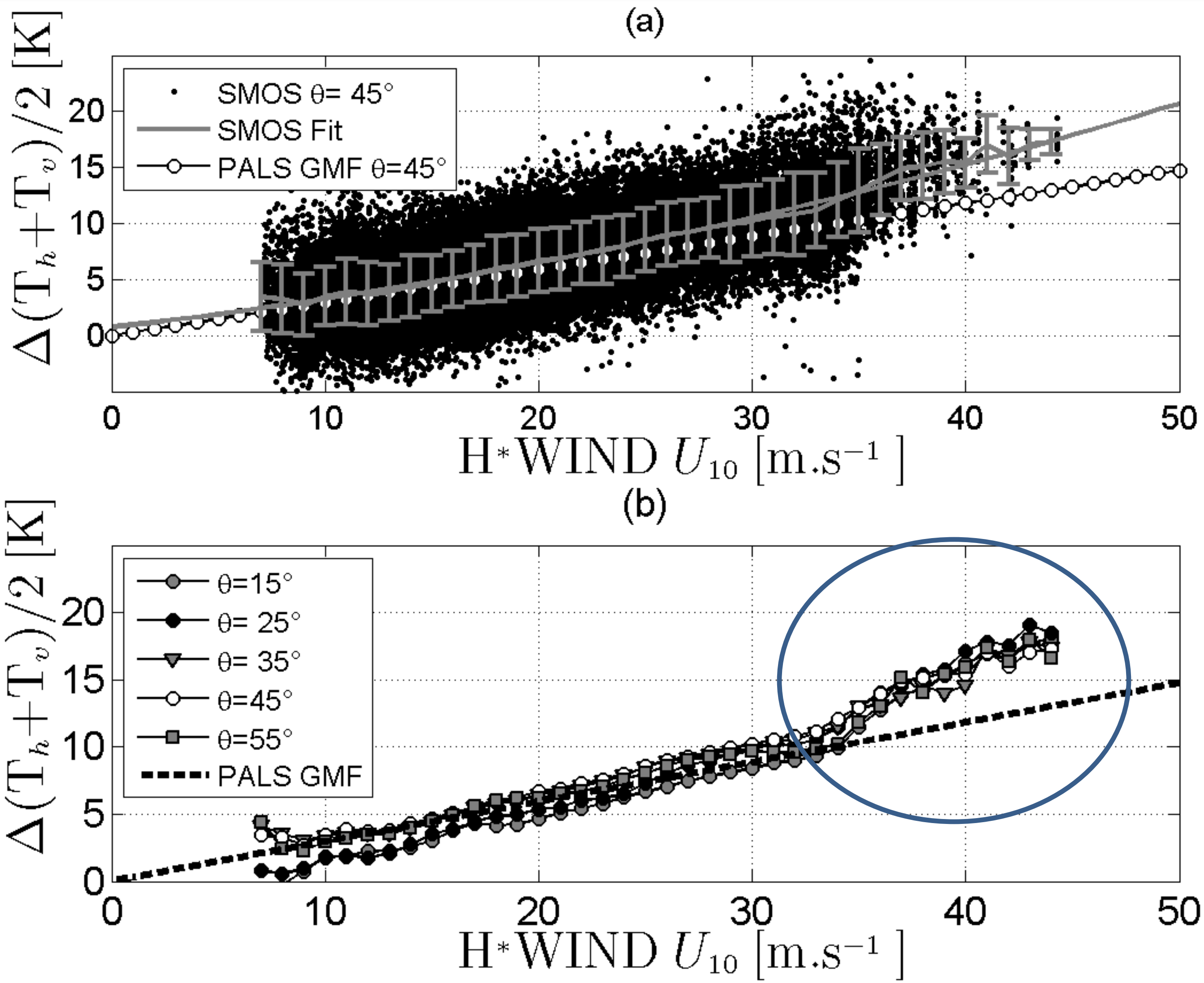

Change of sensitivity at Hurricane wind Force (>33 m/s)

Weak Incidence Angle dependence

SuperStorm Sandy Viewed by SMOS

Hurricane Sandy Oct 2012

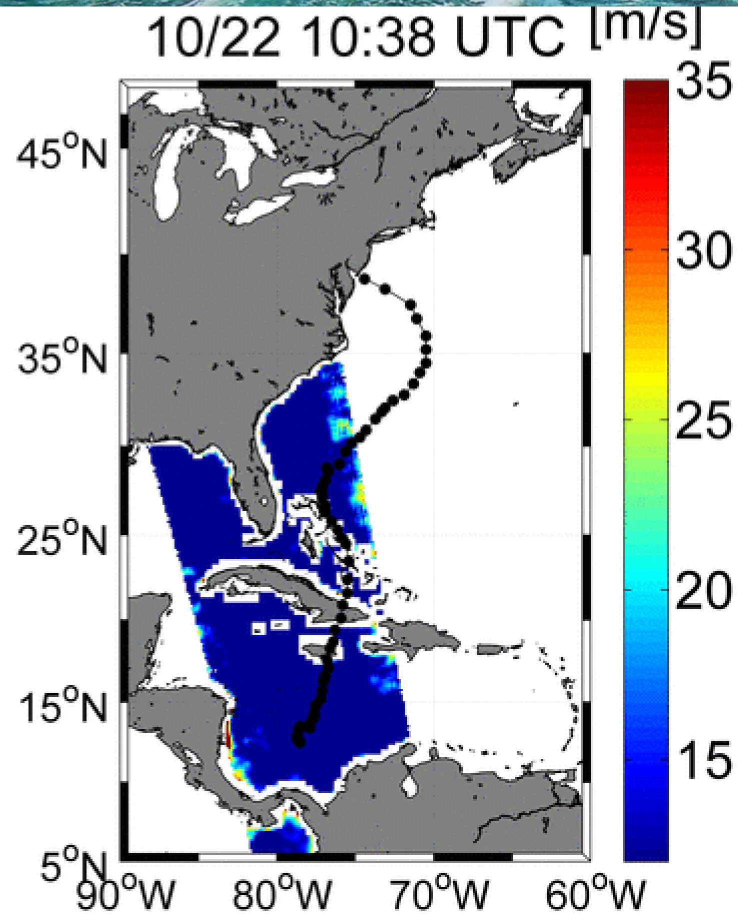

Validation with buoy data

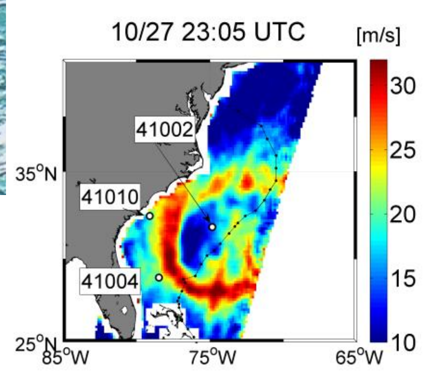

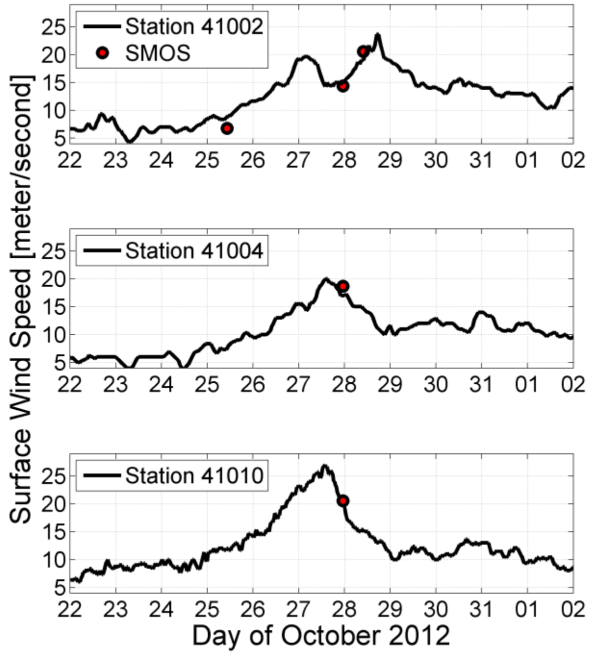

Hurricane Sandy

Validation with NOAA hurricane hunter Aircraft Data (C-band)SFMR

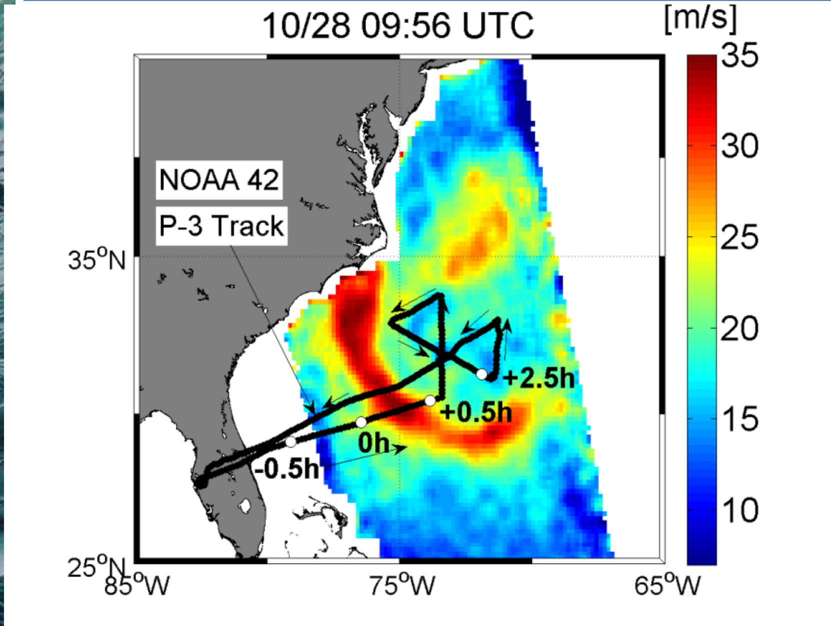

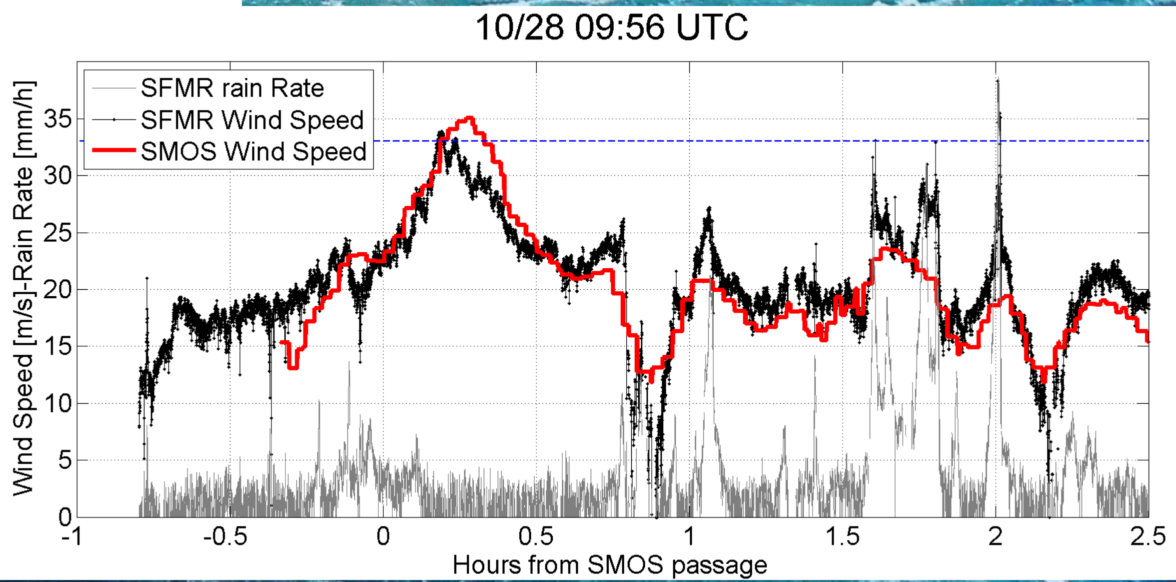

Haline wakes behing hurricanes & Barrier Layer Effect on Tropical Cyclone Intensification

Amazon and Orinoco River Plumes and NBC Rings: Bystanders or Participants in Hurricane Events?

A. FFIELD, J CLIM 2007

Most of the most destructive hurricanes occur in a region where hurricanes interact with the Amazon-orinoco plume

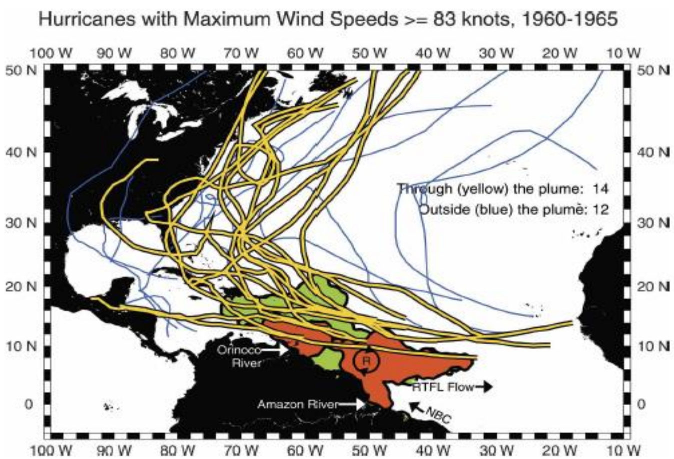

TABLE 1. The distribution of 1960–2000 hurricanes by location. With increasing category (hurricane strength), an increasing (decreasing) percentage of hurricanes pass through (outside) the plume region. For example, for category 5 hurricanes, 68% passed through the plume region, while only 32% passed outside the plume region.

Hurricanes	Through plume		Outside plume		All hurricanes
1960–2000	No.	No./total	No.	No./total	Total
Category 1	17	17%	84	83%	101
Category 2	13	29%	32	71%	45
Category 3	18	45%	22	55%	40
Category 4	18	60%	12	40%	30
Category 5	13	68%	6	32%	19

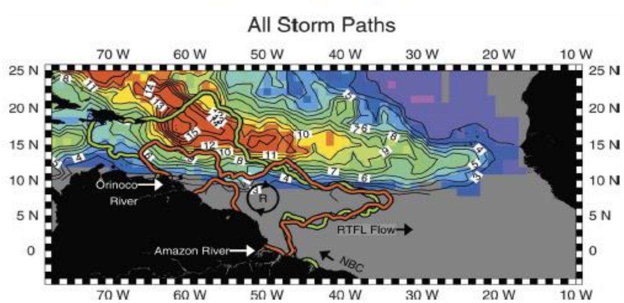

FIG. 3. The number of 1950 through 2003 "best track" tropical storms and hurricanes per one degree square (smoothed by a 3° × 3° block average). The tropical cyclones initially travel westward.

⇒Warm anomaly,
⇒NBC rings &
⇒Freshwater plume Barrier-layer effects

Surface area~ 89000 km^2> Lake Superior, the world largest freshwater lake: a transfer of 1 GTo of Salt in 5 days

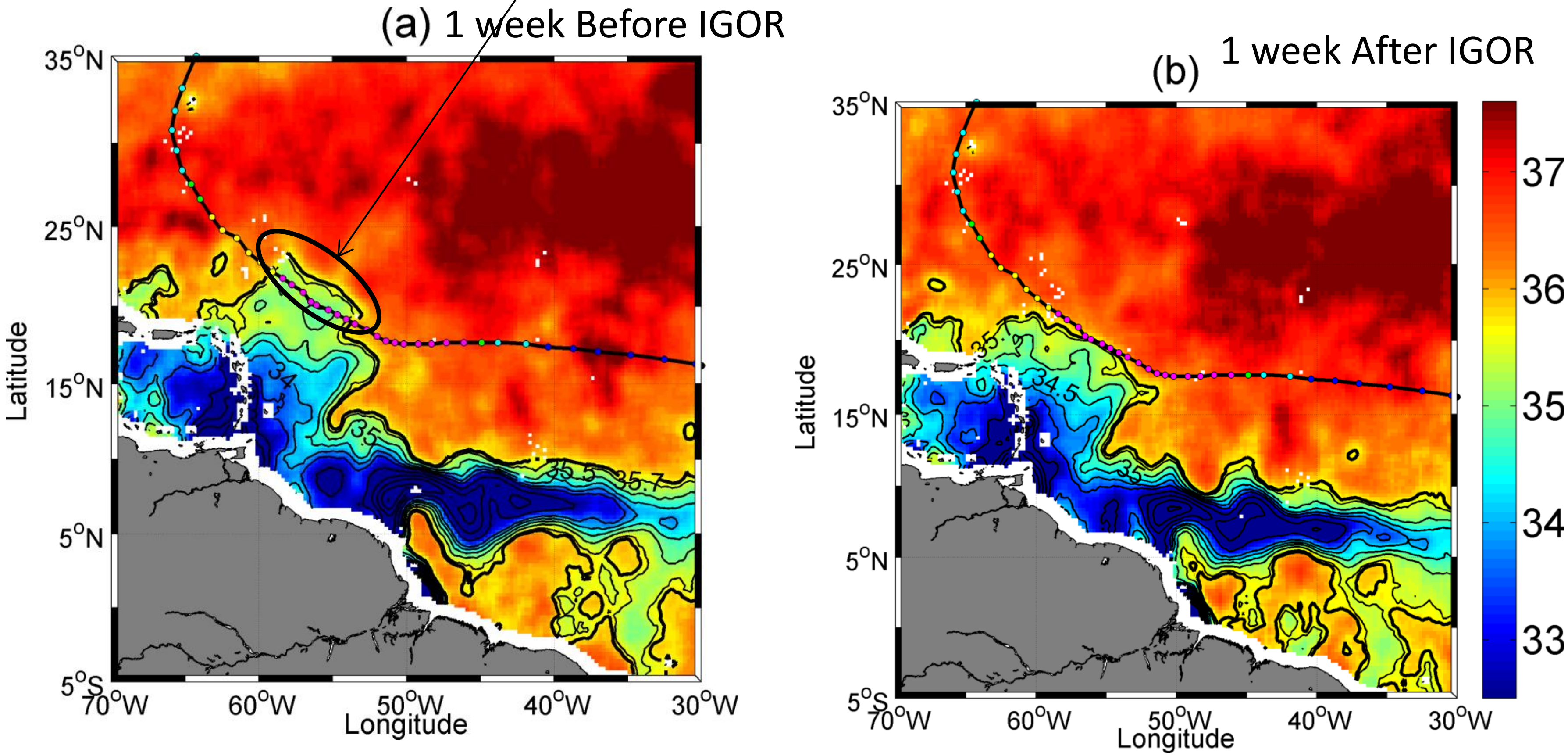

Figure 2: Two SMOS microwave satellite-derived SSS composite images of the Amazon plume region revealing the SSS conditions (a) before and (b) after the passing of Hurricane Igor, a category 5 hurricane that attained wind speeds of 136 knots in September 2010. Color-coded circles mark the successive hurricane eye positions and maximum 1-min sustained wind speed values in knots.
Seven days of data centered on (a) 10 Sep 2010 and (b) 22 Sep 2010 have been averaged to construct the SSS images, which are smoothed by a 1° x 1° block average.

Reul et al=> in preparation 2012

Surface wakes of Igor

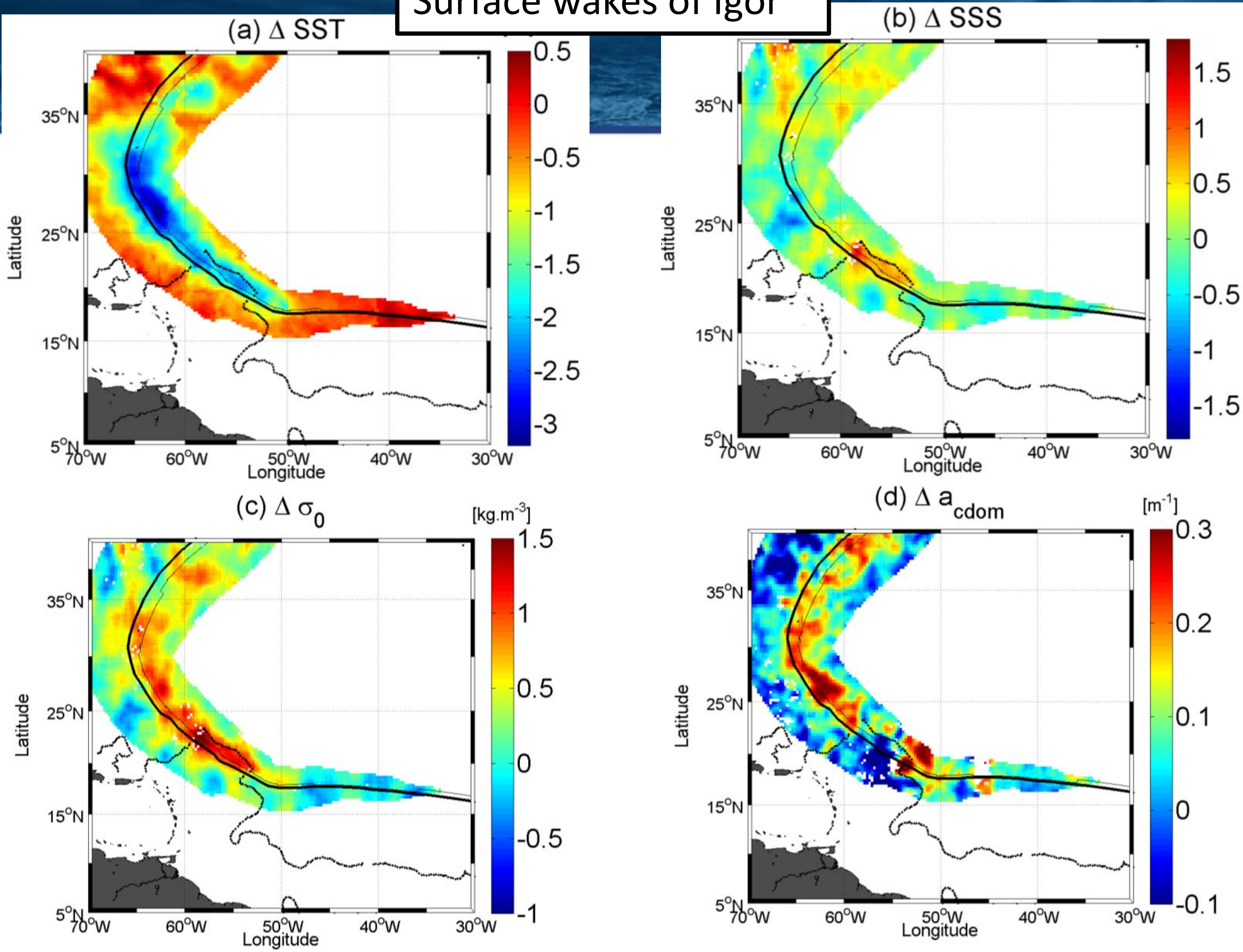

Six days of data centered on t_o–(+) 4 days have been averaged to construct the pre (post)-cyclonic quantities.

Here
$a_{cdom} = a_d + ag$

ag: CDOM (dissolved matter)

ad: non living particulate organic material, bacteria, inorganic material and bubbles

Figure 4: Surface wakes of Hurricane Igor. Post minus Pre-hurricane (a) Sea Surface Temperature (ΔSST) (b) Sea surface Salinity (ΔSSS), (c) Sea Surface Density ($\Delta\sigma_o$) and (d) Sea Surface CDOM absorption coefficient .The thick and thin curves are showing the hurricane eye track and the locii of maximum winds, respectively. The dotted lines is showing the pre-hurricane plume extent. ΔSST, ΔSSS, $\Delta\sigma_o$ wakes were only evaluated at spatial locations around the eye track for which the wind exceeded 34 knots during the passing of the hurricane.

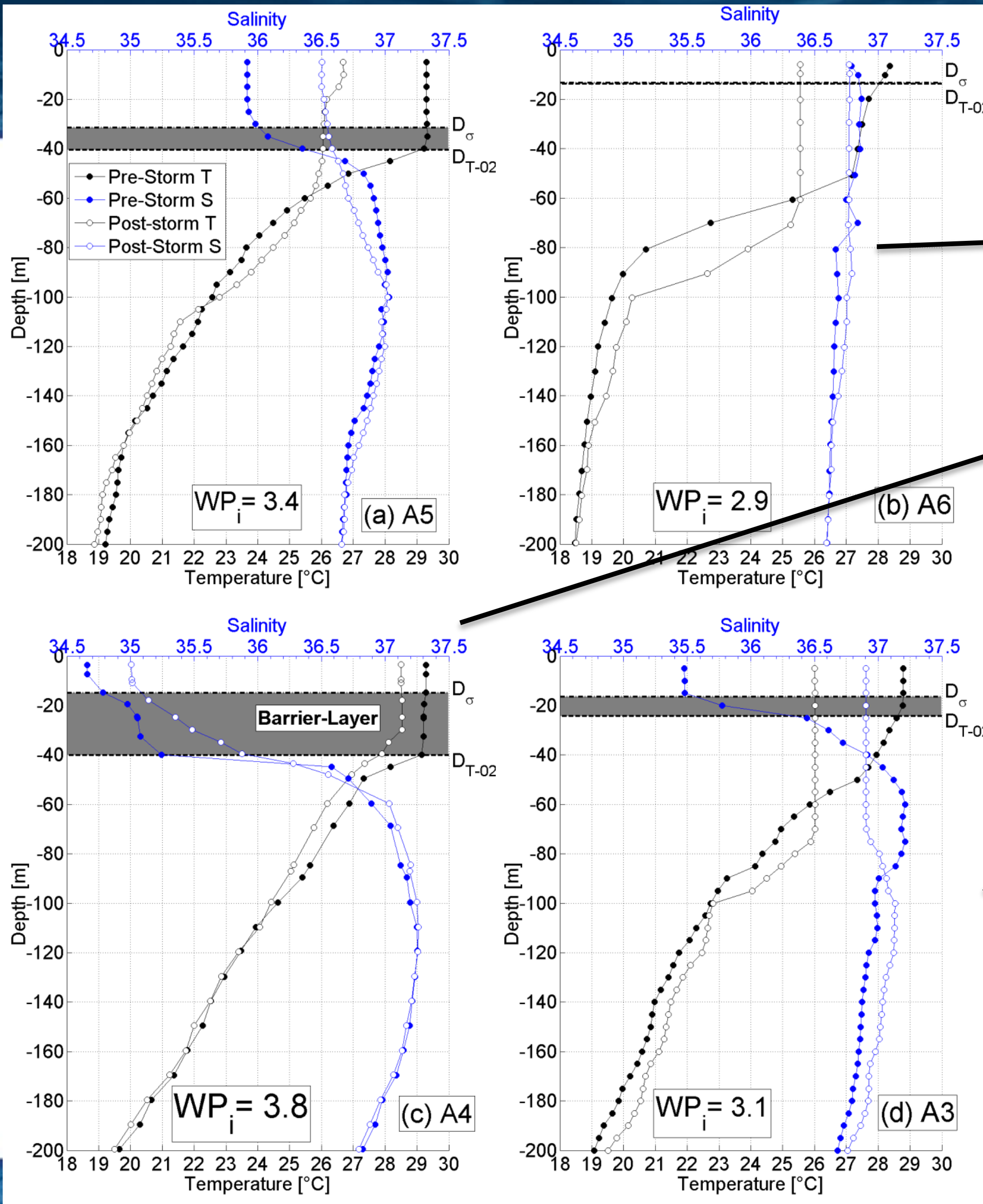

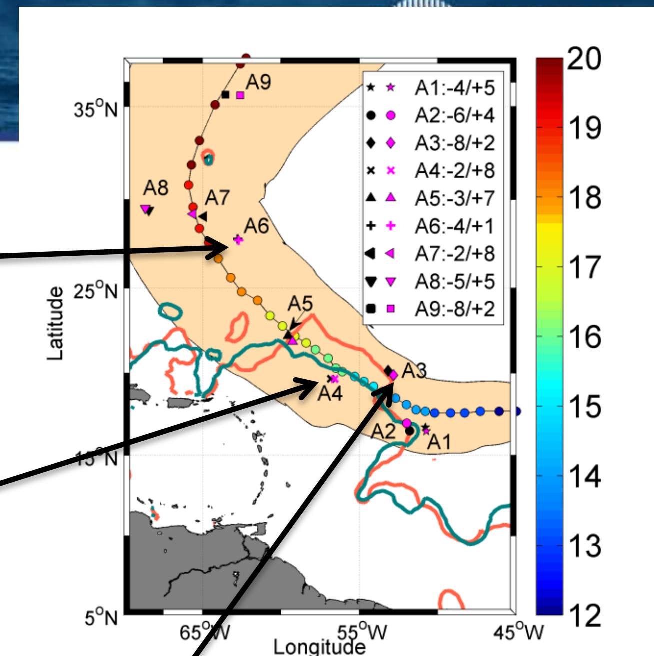

Thick BL>20m=> cooling inhibition
by salt-driven stratification
In the Plume

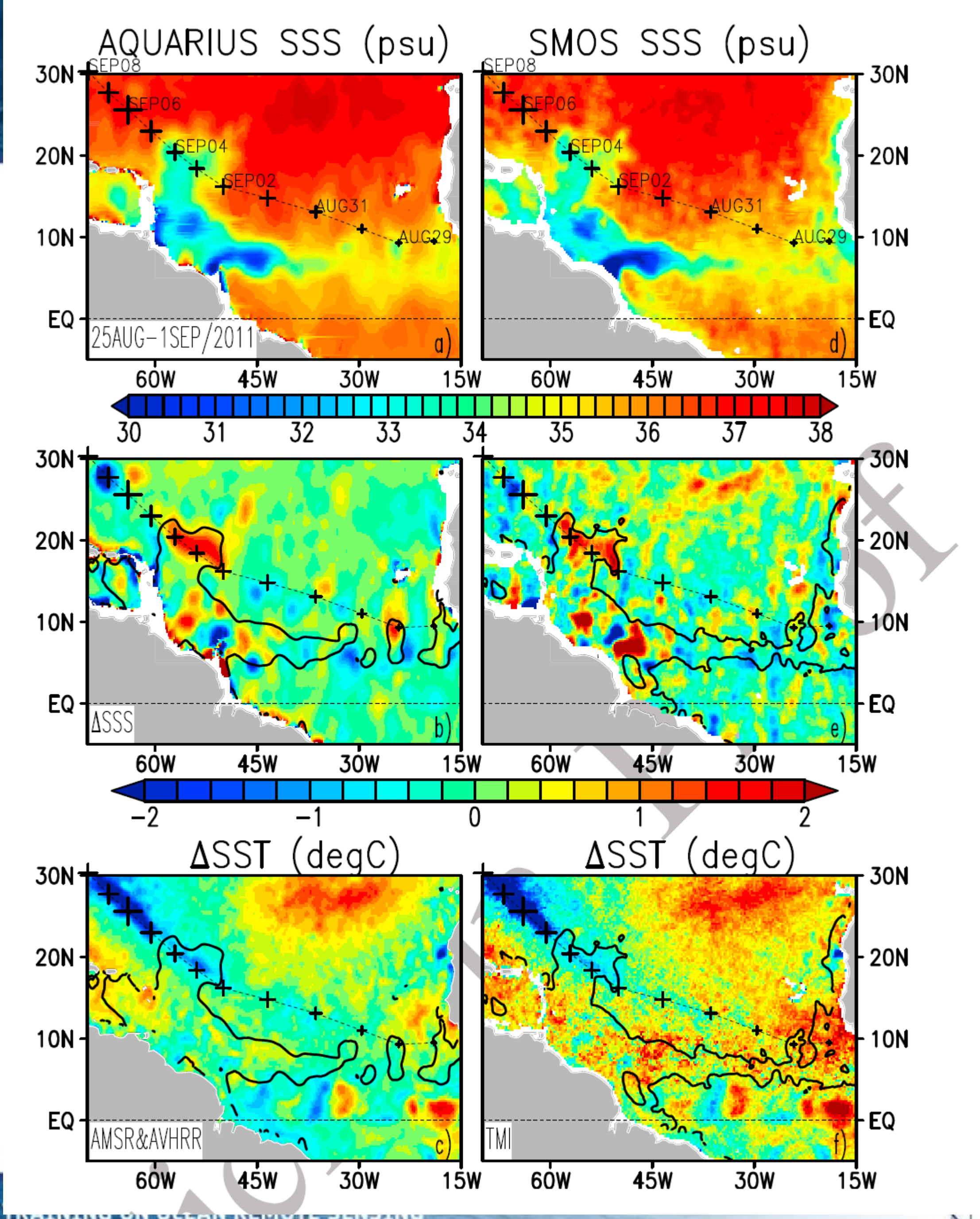

Hurricane Katia 2011

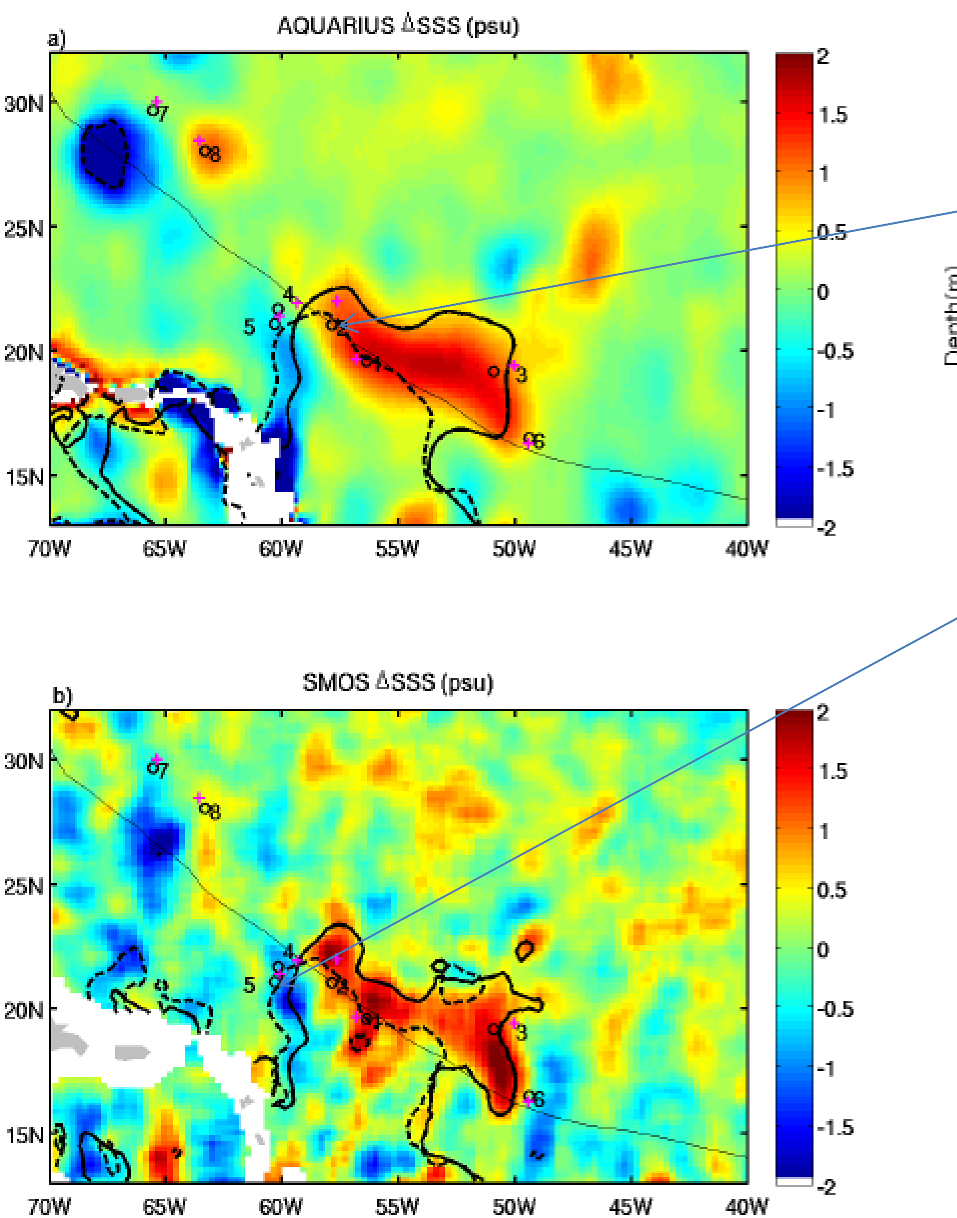

Figure 4. (a) Aquarius and (b) SMOS SSS difference (ΔSSS) between after (5-10 SEP/2011) minus before (25AUG-1SEP/2011) the passage of Katia. Location of Argo profiles before ('o') and after ('+') the passage. Bold solid and dashed are 35psu contour before and after the passage, respectively. Land-contaminated coastal data are blanked.

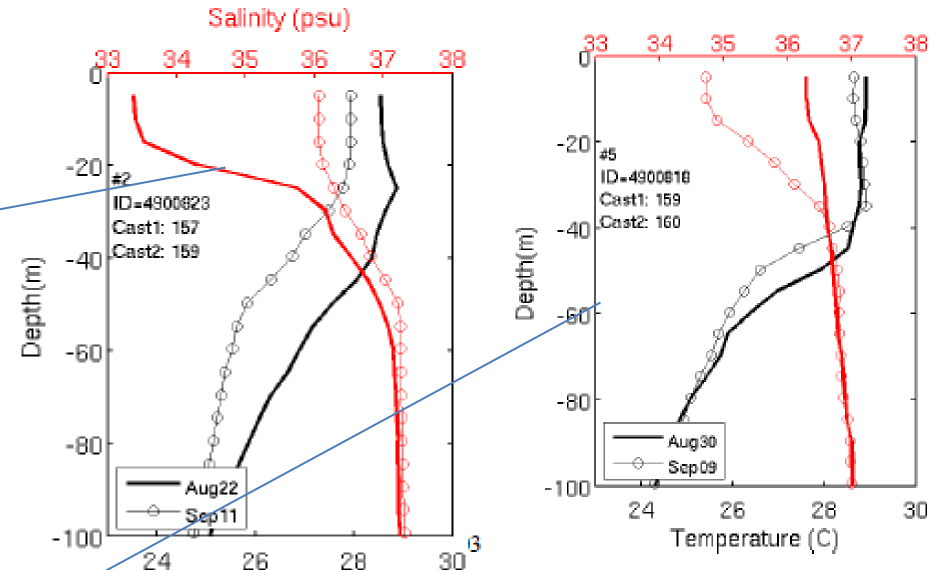

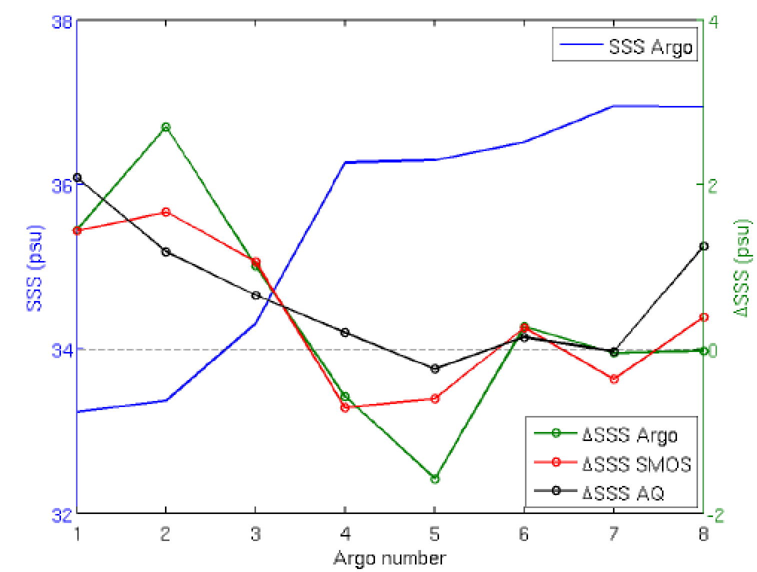

Figure S4. Near surface salinity change ΔSSS from Argo profiles and SMOS and Aquarius SSS change from Figures 4a, 4b. SSS before the passage of Katia is shown in blue.

Better match SMOS/in situ than Aquarius/in situ

Historical Reanlysis

Statisical analysis all tracks 1998-2010

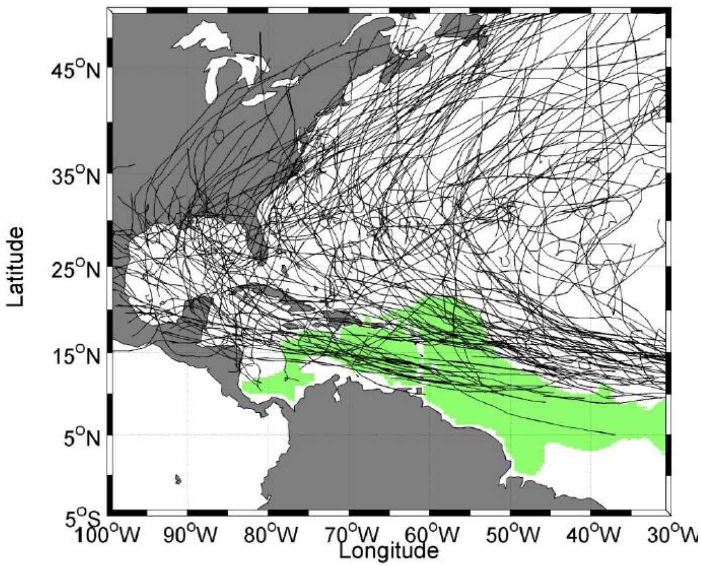

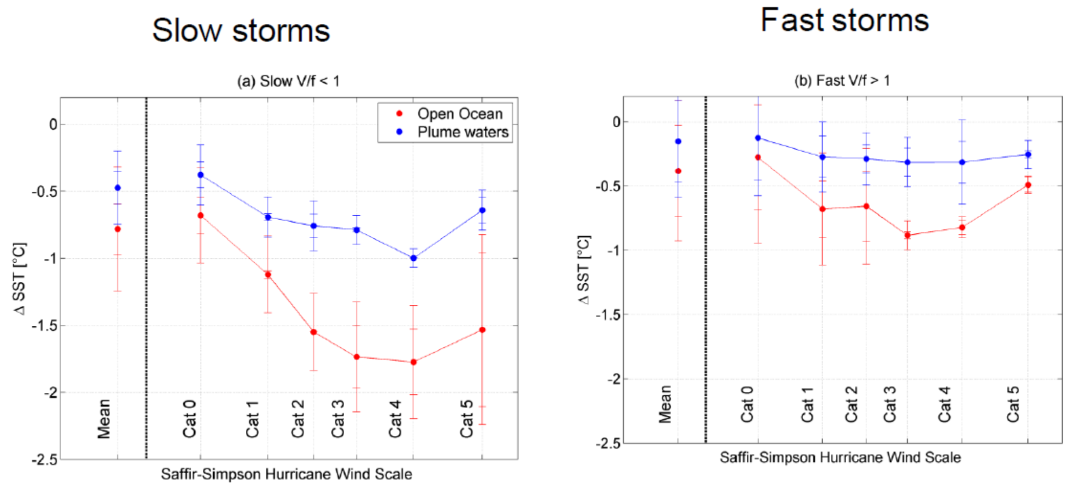

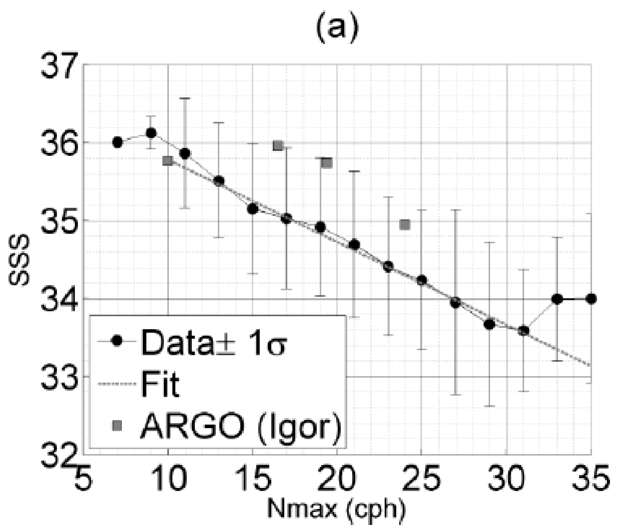

Apparently, SST cooling inhibition in plume waters as observed in Igor Is confirmed by an historical dataset

As expected, the impact is stronger for slow moving storms

SSS can be used as a proxy for vertical density Stratification

=> Usefull for TC intensification monitoring (TCHP)

Conclusions & Perspectives

After 4 years, SMOS data yet do not meet fully the mission requirements objectives in term of accuracy 0.3 (tropics) - 0.5 (Moderate Latitudes) over 10 days/monthly periods

Nevertheless, the:
high temporal repetitivity (3 days)
+ high spatial resolution (40 km) of the instrument sampling
provides a very rich and new information for numerous oceanographic applications:

-Large tropical river plume monitoring (water cycle,land/sea intecations, bio-optical, bio-chemistry)
-Freshwater pool signature of rain/evaporation interannual variability (Barrier Layers)
-Upwelling zones
-Strong air/sea interactions
-Salt exchanges & surface circulation at strong water mass boundaries

⇒SMOS data bring new and usefull information to complement altimetry, SST and lower space/time resolution Aquarius data.